

WORK HARDENING AND DEFORMATION STRUCTURE
IN LITHIUM FLUORIDE SINGLE CRYSTALS

Thesis for the Degree of Ph. D.

MICHIGAN STATE UNIVERSITY

Karatholuvu Narayanasamy Subramanian

1966



This is to certify that the
thesis entitled
**WORK HARDENING AND DEFORMATION STRUCTURE
IN LITHIUM FLUORIDE SINGLE CRYSTALS**
presented by
Karatholuvu Narayanasamy Subramanian
has been accepted towards fulfillment
of the requirements for
Ph.D. degree in Metallurgy

Chuan Tung Wei
Major professor

Date *May 11, 1966*



ABSTRACT

WORK HARDENING AND DEFORMATION STRUCTURE IN LITHIUM FLUORIDE SINGLE CRYSTALS

By Karatholuvu Narayanasamy Subramanian

Lithium fluoride crystals having a dislocation density of approximately 10^4 lines per square centimeter were successfully grown by using the Czochralski method at the rate of 1/4 to 3 inches per hour utilizing off-centering and necking techniques. The deformation studies of such crystals showed that in combined fatigue and latent hardening experiments, the yield strength of the specimen in the latent slip systems was as high as thirty fold compared with the yield strength of the crystal in the as grown condition provided the specimen underwent a complete reversal of the resolved shear stresses acting in the primary slip systems in the fatigue cycles. The growth of the slip bands during deformation and the stress pattern in the deformed crystals were investigated with polarized light microscopy. A band-like structure, which might be called deformation bands, was observed to develop in the slip planes usually in a direction perpendicular to the slip direction. There were few instances where they were parallel to the line of intersection of the primary slip planes with the non-conjugate slip planes. These bands were of constant width of approximately 20 microns. Bulk specimens work hardened rapidly during deformation and developed such band

structures whereas thin specimens did not develop the band structure during deformation and were not work hardened. A theory of deformation band formation based on interactions of dislocation loops originated from randomly distributed sources is proposed. The various hardening phenomena observed in lithium fluoride single crystals are explained in terms of the relative orientation of the slip planes and the slip directions with respect to that of the deformation bands developed.

WORK HARDENING AND DEFORMATION STRUCTURE
IN LITHIUM FLUORIDE SINGLE CRYSTALS

By

Karatholuvu Narayanasamy Subramanian

A THESIS

Submitted to
Michigan State University
in partial fulfillment of the requirements
for the degree of

DOCTOR OF PHILOSOPHY

Department of
Metallurgy, Mechanics and Materials Science

1966

640794
11-15-66

ACKNOWLEDGEMENTS

The author wishes to express gratitude to Dr. C. T. Wei for the guidance in this work. The helpful suggestions and encouragements given by Dr. A. J. Smith, Dr. T. Triffet and Dr. J. T. Pindera are also gratefully acknowledged. The entire staff of the Department of Metallurgy, Mechanics and Materials Science are thanked for their assistance and helpful discussions. Finally, he would like to thank the Atomic Energy Commission for the financial help granted under the contract no. AT (11-1)-1042.

TABLE OF CONTENTS

	Page
INTRODUCTION	1
EXPERIMENTAL TECHNIQUES	16
RESULTS	25
DISCUSSION	57
I. Crystal growth	57
II. Principles of polarized light microscopy	62
III. Slip distribution and work hardening	71
IV. Theory of band formation	73
V. Relation between deformation structure and work hardening	105
CONCLUSIONS	114
REFERENCES	116

LIST OF FIGURES

Figure		Page
1	Projection of $\{110\}$ slip planes onto (001) surface	15
2	Czochralski furnace for growing LiF single crystals	23
3	Arrangement for polarized light microscopy . .	24
4	Dislocation distribution in crystals grown by Bridgman method: (a) Cleaved specimen, (b) Acid-saw cut specimen.	34
5	(a), (b) Sub-grain boundary distribution in a crystal grown by Czochralski method (c) A region of low dislocation density in a crystal grown by Czochralski method.	35
6	Effect of off-centering on sub-boundary distribution: (a) Before off-centering, (b) After off-centering.	36
7	Divergent beam X-ray picture of LiF crystal grown by Czochralski method (using off-centering principles)	37
8	A typical stress-strain curve for a fatigue-latent hardening experiment	40
9	Orthogonal slip bands on (100) surface as observed at various orientations of the slip vector with the direction of polarization in dark field: (a) Direction of polarization vertical, (b) Direction of polarization 30° to the vertical, (c) Direction of polarization 50° to the vertical, (d) Direction of polarization 70° to the vertical.	41
10	Slip band growth observed on (100) plane during unreversed cyclic loading (a) After the first cycle, (b) After the second cycle.	42

LIST OF FIGURES (continued)

Figure		Page
11	Slip band growth observed on (100) plane during reversed cyclic loading (a) After the first half of first cycle, (b) After the second half of the first cycle with reversed shear in the same slip planes deformed in the first half cycle.	43
12	Slip distribution observed on a (100) plane of a crystal deformed in the latent direction . . .	44
13	Orthogonal slip bands on the (100) surface of a specimen prepared for the observation of damage in the (011) slip plane	45
14	Band structure observed in the slip plane of the specimen shown in figure 13, linearly polarized light dark field observations: (a) Direction of polarization vertical, (b) Direction of polarization 30° to the vertical, (c) Direction of polarization 45° to the vertical, (d) Direction of polarization 65° to the vertical.	46
15	Polarized light observations of the bands in the slip plane: (a) Bands making 10° to the direction of polarization, (b) Bands making 15° to the direction of polarization, (c) Bands making 20° to the direction of polarization, (d) Bands making 25° to the direction of polarization, (e) Bands making 30° to the direction of polarization, (f) Bands making 35° to the direction of polarization, (g) Bands making 40° to the direction of polarization, (h) Bands making 45° to the direction of polarization.	47 and 48
16	Band structure at various stages of deformation in three-point bending; Burgers vector parallel to the direction of polarization	49
17	Band structure at various stages of deformation in three-point bending; Burgers vector making 50° to the direction of polarization.	50

LIST OF FIGURES (continued)

Figure		Page
18	Network observed in a lithium fluoride crystal	51
19	Band structure observed along non-orthogonal slip plane intersections in a thick specimen deformed in three-point bending; Burgers vector making 20° to the direction of polarization . . .	52
20	Band structure in a thick sodium chloride specimen deformed in uniaxial compression; direction of polarization vertical (a) and (b) are two different orientations of the Burgers vector with respect to the direction of polarization.	53
21	Band structure in the sodium chloride specimen observed in figure 20 after thinning down (a) and (b) reveal loops in these bands, (c) and (d) reveal the stress concentration caused by non-orthogonal slip band intersections.	54
22	Transmission electron micrographs of an MgO single crystal fatigued in cantilever bending at room temperature	55
23	Edge dislocation dipoles and debris observed in transmission electron micrographs of fatigued MgO specimens	56
24	Dependence of contrast on the orientation of the slip vector with respect to the direction of polarization	70
25	General mechanism of band formation	95
26	Model for formation of screw-lock	96
27	Stability of screw-lock	97
28	Forces associated with the formation of screw-lock	98
29	Model for the force field at the central portion of the screw-lock	99

LIST OF FIGURES (continued)

Figure		Page
30	Interaction of two rows of edge dislocations	100
31	Interaction of edge dislocation arrays in nearby slip planes	101
32	Stability of interacting dislocation loops	102
33	Total strain energy of a dipole of unit length making various angles with the Burgers vector . .	103
34	Mechanism of band formation due to intersecting slip	104
35	Conjugate slip intersection	112
36	Non-conjugate slip intersection	113

INTRODUCTION

Work hardening in materials remains one of the basic problems in plastic deformation. This phenomenon depends on many variables such as chemical composition, crystal structure, elastic properties, history of the specimen and imperfections. Experimental observations on the hardening behavior of materials with different crystal structures and under various conditions have shown the complexity of this problem. For a particular, chemically pure, and nearly perfect single crystal the dislocation structure appears to be the most important single factor.

The purpose of this work was to grow reasonably pure lithium fluoride single crystals having low dislocation density and to study their deformation behavior. The deformation studies were directed towards the advancement of the understanding of work hardening. Although there has been a large amount of research done on ionic crystals, the overall picture of work hardening in this type of crystal as well as in other materials is yet far from being clearly understood.

Theories of Work Hardening

Various theories have been advanced to explain the work hardening of materials. According to Taylor's theory of work hardening, slip commences at many position throughout a crystal by the multiplication of positive and negative dislocations.¹

These dislocations stop within the crystal due to the interaction of their stress fields, and thus build up a 'superlattice' array of dislocations of both signs. At any given strain, the stress field associated with such an array opposes the movement of other dislocations so that the stress has to be increased to produce further plastic flow. This theory gives a parabolic relationship between stress and strain.

Mott's theory of work hardening is an extension of Taylor's theory.^{2,3} He proposes that dislocations generated from a Frank-Read source in a slip plane may pile up against sessile dislocations in the same slip plane. The dislocation pile-up so formed at an obstacle consists of dislocations of the same sign. Due to the stress field around the piled up groups of dislocations sessile dislocations are formed between the edge parts of the dislocations in a group and the edge parts of the dislocation loops generated from sources in some other slip systems. As a result, when the stress is removed, the dislocations in the piled up groups are prevented from being forced back to their sources by the back stress from the pile-up. According to this mechanism hardening is due to the stresses around the piled up groups which may be regarded as 'super-dislocations' of strength $n\vec{b}$, where n is the number of dislocations in a pile-up, and \vec{b} is the Burgers vector. Mott's theory differs from Taylor's in suggesting that the piled up groups are locked in position and have n times as much strength as those considered by Taylor. However, this theory also gives a parabolic relationship between stress and strain.

The results of experiments with single crystals of face centered cubic metals have shown evidence of three stages of hardening under specific conditions.⁶⁻¹⁴ In order to explain this many theories have been advanced. Mott has suggested that during stage I, also known as easy glide, most dislocations originated from Frank-Read sources leave the crystal.² The fact that the dislocations of the first operative slip system have to cut through the dislocations of the Frank net intersecting the slip plane has in itself been considered as a cause of hardening by Mott, Cottrell, and Friedel.^{3, 4, 5} Koehler's view is that easy glide is an exhaustion hardening process, by which he means that, at first, the longest Frank-Read sources come into operation and as the dislocations generated from these are held up by the obstacles in the slip plane, shorter and shorter sources are activated.⁶

The following theories have been proposed for face centered cubic materials to explain the stage II hardening, also known as rapid hardening or linear hardening. Friedel ascribes the rapid rate of work hardening in stage II to a particular distribution of Lomer-Cottrell sessile dislocations formed by the interaction of dislocations of the primary slip system with those of the secondary systems.⁷ He propounds that Lomer-Cottrell sessile dislocations are formed around each active source in at least two directions in the primary slip plane. The piling up of dislocations against these Lomer-Cottrell barriers

surrounding each source increases the stress necessary to operate the source. New sources begin to operate and are in turn blocked by the formation of sessile dislocations. This theory, therefore, assumes the operation of at least two secondary systems at the beginning of stage II. He suggests that, as the piled up groups in neighboring slip planes are closer to a particular source than those in its own slip plane, and, as a result, a loop traversing the primary slip plane has to overcome the variations of stress produced by the neighboring groups, it is the neighboring groups which are responsible for the hardening. Seeger assumes that a continued formation of Lomer-Cottrell barriers throughout stage II leads to a decrease of the slip distance with increasing strain and to smaller dislocation groups of essentially constant size, which are piled up against the barriers and more or less randomly distributed.^{8, 9, 10} Mott considers the secondary slip to be responsible for most of the network of dislocations observed in cold worked materials.¹¹ This network accounts for a considerable part of the flow stress. The secondary slip also hardens the sources by forming glissile and non-glissile jogs; when the source is stressed hard enough, the dislocations annihilate each other, thus unlocking the source. The dislocations move until the jog density becomes high.

The stage III hardening is generally attributed to cross-slip. Seeger et al have suggested that stress relief in the piled up groups is caused by dislocations leaking out of the pile-ups by cross-slip.^{8, 9, 10} It is suggested that the stress necessary to cause the

screw components of these piled up dislocations to slip on the cross-slip plane is less than that required for the dislocations to break through the barrier. Friedel suggests that the leakage of dislocations by cross-slip results in a relief of the stress in the pile-ups and in the annihilation of dislocations by those of the opposite sign from the neighboring pile-ups.⁷ With further slip there is still some hardening because the edge dislocations may continue to pile up.

Basinski's hypothesis is that the internal stress varying over distances longer than the separation between successive dislocations emitted from the source will not contribute appreciably to hardening and that the most important source of hardening is the resistance encountered by the dislocations in cutting through the dislocation forests.¹² He suggests that strain hardening is primarily due to local interactions of intersecting dislocations. Mitra and Dorn have shown that both the long range stress fields and the short range stress fields contribute to the work hardening of face centered cubic metals.¹³ They reason that the long range stresses due to piled up dislocation arrays account for the low hardening rate in easy glide. Both the long range and localized stress fields at the intersections of dislocation arrays contribute to stage II hardening.

Kuhlman-Wilsdorf has suggested a work hardening mechanism which is applicable to a wide variety of materials irrespective of the type of their dislocation substructure.¹⁴ According to this mechanism, in the easy glide stage, dislocations multiply in a number of restricted

areas and penetrate from there into crystal regions still considerably free of glide dislocations. This continues until a quasi-uniform dislocation distribution is established. The cause of work hardening in easy glide is primarily due to the accumulation of jogs on the dislocations and the interaction between point defects and dislocations. When there are no more areas left into which newly formed dislocations have not yet penetrated rapid hardening ensues. Irrespective of how the dislocations are arranged at the end of easy glide, the stress necessary to overcome the line tension of the dislocation segments must increase, because as the dislocation density increases the average free dislocation length decreases. The increase in the stress necessary to cause the dislocation segments to bow out into loops is responsible for the major part of work hardening in stage II. Cross-slip and conservative climb are the dominating factors in stage III.

Gilman has proposed a debris mechanism of strain hardening based on the observations made on lithium fluoride and magnesium oxide single crystals.¹⁵ According to this mechanism damage in the form of edge dislocation dipoles continuously builds up in proportion to the strain. These dipoles have the metastability needed to account for the plastic strain. The debris, composed of small dislocation loops, acts as sources of internal stresses. A considerable part of cross-slip which causes dislocation multiplication and hardening is initiated at the surface. Nabarro et al suggest that the quantity of debris produced is proportional to the

number of dislocations already trapped in the crystal and hence the density of debris is proportional to the square of the strain.¹⁶

Work Hardening Due to Deformation Bands

It has been suggested that deformation bands can cause work hardening. Mott proposes that the increase of applied stress required to form stabilized loops, when the deformation bands become more and more tightly packed with dislocations, manifests itself in the form of work hardening.¹⁷ According to Doris Kuhlman, deformation bands formed by the locking of unlike dislocations act as strong obstacles against the movement of dislocations, thus become the source of work hardening.¹⁸

Review of Deformation Bands

Deformation bands have been observed in various metals like iron, aluminum, zinc, etc.¹⁹⁻²⁴ The main features of these bands are the following: (1) each band is a thin sheet running through the crystal and, at small strains, is almost a plane and perpendicular to the active slip direction; (2) their width is approximately constant; (3) they start being formed during the early stages of deformation; (4) slip bands formed in the early stages bend themselves to follow the curvature of the lattice and cross the deformation bands without interruption, but those formed later do not penetrate the deformation bands at all.²⁵

According to Mott, deformation bands are formed by walls of positive dislocations on one side and negative dislocations on the

other.² In a deformation band locking of dislocations results from slips in intersecting planes. When some dislocations are locked due to the dislocations in an intersecting plane, the resulting stress field acts as a barrier against dislocations moving in nearby planes and stops their motion. The dislocations so stopped act in a similar manner to stop other dislocations in their neighboring planes. Wei's mechanism of band formation in zinc single crystals makes use of sources in parallel slip planes.²⁴ The interaction through screw components of the dislocation loops makes them line up in a direction perpendicular to the slip vector and stabilizes the structure.

Experimental Limitations

Work hardening experiments are usually conducted by deforming bulk crystals under uniaxial loading. The dislocation structure of these crystals is mostly studied either at the surface by using an etch-pit technique or by observing thin sections made out of these deformed crystals under an electron microscope. Thus one is limited to either the surface or a thin section of the bulk. These methods give only a partial picture of the dislocation structure. To understand the work hardening behavior of materials, it is necessary to know the three dimensional dislocation structure in deformed bulk crystals. Polarized light microscopy of transparent crystals, therefore, appears to be a suitable technique. Lithium fluoride is a transparent crystal and is suitable for studies under a polarized light microscope. Besides, it has several other advantages as described below.

Advantages of Lithium Fluoride

Lithium fluoride is an ionic crystal and has the NaCl structure. The slip systems are one of the simplest. The primary slip planes are the $\{110\}$ type planes and the secondary slip planes are the $\{001\}$ type. The slip directions are $\langle 1\bar{1}0 \rangle$ in both cases. The projection of the six $\{110\}$ planes onto the (001) plane is shown in figure 1. There is only one $\langle 1\bar{1}0 \rangle$ direction in each $\{110\}$ slip plane. The slip bands due to slip in planes perpendicular to the $\{100\}$ plane are known as 90° bands or orthogonal slip bands. On the other hand, the slip in planes which are at an angle of 45° to the $\{100\}$ surface and intersect along $\langle 001 \rangle$ gives parallel slip bands or 45° bands. There can be only one kind of mobile dislocation in each active slip plane and hence the complication of dislocations with different Burgers vectors to be found in the same slip plane can be avoided. Initiation of secondary slip is difficult due to the high stresses needed for moving dislocations in the secondary slip planes.^{26, 27} In the NaCl structure no two primary slip planes have the same Burgers vector, and hence cross-slip at room temperature is improbable.

Lithium fluoride crystals having fairly low dislocation density can be grown easily. The grown-in dislocations in these crystals are reportedly pinned by precipitates.^{28, 29} The pinning points are so close that these dislocations do not act as active sources, but they may play an indirect role in the multiplication

process in these materials.³⁰ Specimens having $\{100\}$ bounding surfaces can be cleaved easily and the damage introduced during fast cleavage is not severe.^{31, 32} The damage introduced is mainly on or near the surface and, therefore, can be polished off.

Besides the transmission electron microscopy and the etch-pit method and their limitations mentioned previously a decoration technique can be used to obtain a three-dimensional picture of the dislocation structure in ionic crystals when the density of dislocations is low.³⁶ However, its usefulness is limited to small deformations, and no further testing can be done once the crystals are decorated, because the dislocations are pinned by impurities. The decoration technique is, therefore, not suitable for studying the dislocation substructure during various stages of loading. X-ray techniques are non-destructive, but the low magnification obtainable does not give enough information about the dislocation structure of heavily deformed crystals.³⁷

A polarized light microscopy study of the slip band growth in a transparent bulk crystal can give a three-dimensional slip distribution.³⁸⁻⁴¹ This method provides a magnification of the order obtainable by the etch-pit or decoration technique and is free from the limitation of the pinning of dislocations. However, its limitations are not apparent without a knowledge of the nature of polarized light and its relation with the stress field in the crystal. These will be discussed in a later section.

Deformation Behavior of Ionic Crystals

Deformation studies of ionic crystals have been helpful in understanding the dislocation behavior in lithium fluoride.^{28, 44-46} The yield strength of lithium fluoride depends sensitively on the impurity content.⁴⁷ A variation of 15 to 85 parts per million of a divalent impurity like magnesium may increase the yield strength by a factor of ten. Gilman has suggested a cross-slip mechanism for dislocation multiplication in lithium fluoride crystals.^{48, 49} Another possible multiplication mechanism is based on the formation of jogs in screw dislocations.^{28, 50} According to this, there are two possible ways of multiplication depending on whether the jog is large or small.

Cyclic stressing of lithium fluoride has shown that the dislocations do not return to their original positions when the stress is released.⁵¹ Hardening in cyclic stressing is similar in many respects to hardening in unidirectional stressing.⁵² The damage produced in the slip bands in fatigue stressed and unidirectionally loaded magnesium oxide crystals is predominantly edge dislocation dipoles. However, in the fatigue stressed specimens the density of the debris is lower compared to the unidirectionally stressed specimens for comparable total strains.⁵³ The dislocation density in a slip plane is independent of the number of fatigue cycles indicating that slip in new planes is preferable to an increase in the dislocation population within the same slip plane. Unlike materials which fatigue harden in the early stages of fatigue deformation and soften on further cycling, the materials, in which cross-slip is

difficult, fatigue harden continuously up to a certain limit.^{54, 55} The dynamic recovery of these materials on cyclic stressing is suppressed by the absence of easy cross-slip, thus the materials become stronger and stronger.⁵⁶ Consequently, if the material does not fail during the first cycle at a particular stress level, it would never fail at this stress level even after an infinite number of cycles. Failure of the material occurs only during the increase of the load but not during the fatiguing of the specimen at any part of the test if the load remains within a limit.^{55, 57} This behavior is exhibited by lithium fluoride, sodium chloride and magnesium oxide single crystals. Zinc also exhibits this phenomenon at low temperatures.⁵⁸ The increase in the fatigue strength of copper by the addition of zinc has been explained by the reduction of the tendency to cross slip.⁵⁹ The necessity of cross-slip for fatigue failure seems to favor Mott's mechanism rather than a mechanism proposed by Cottrell and Hull based on intersecting slips for its explanation.⁶⁰⁻⁶²

McEvily Jr. and Machlin have demonstrated the necessity of cross-slip for fatigue failure.⁵⁵ Later Coronet and Gorum obtained a conventional stress versus number of cycles curve for magnesium oxide and, contrary to the above-mentioned observations, it showed fatigue failure.⁶³ McEvily Jr. and Machlin showed that the fatigue failure of magnesium oxide suggested by Coronet and Gorum was due to microcracks near the surface introduced by cleavage that were not removed by polishing.⁶⁴ The author's investigation of fatigue damage in magnesium oxide crystals favors

the original proposal that there is no fatigue failure in these ionic crystals.⁵³ Alden's work verifies and strongly supports the same view.^{65, 66} Experiments with zinc and cadmium also show the necessity of cross-slip for fatigue failure.⁶⁷⁻⁶⁹ Of these two, cadmium is susceptible to fatigue failure because the primary and secondary slip planes have a common Burgers vector and consequently cross-slip is possible, whereas in zinc, cross-slip as well as fatigue failure is absent. This method of "fatigue hardening" can increase the strength of ionic crystals five to six times after millions of cycles with stepwise increase in load.⁶⁶ FATIGUE may be defined as the tendency of a material to break under conditions of repeated cyclic stressing considerably below the ultimate tensile strength.⁷⁰ It appears that this definition is not appropriate for ionic crystals and other materials which do not have an endurance limit. So, in this article, the term fatigue will be used in the sense of cyclic loading.

Uniaxial loading of a lithium fluoride crystal along a $\langle 100 \rangle$ direction usually causes slip on one set of conjugate slip planes only, in spite of the fact that the resolved shear stresses on two such sets of planes are equal.^{42, 43} If the direction of loading is changed after the original deformation to the direction perpendicular to the plane containing the orthogonal slip bands, the crystal yields at a much higher resolved shear stress.⁷¹ This direction is known as the latent direction or the hard direction. The hardening observed in the latent direction depends on the plastic strain in the original direction, and this phenomenon is called latent hardening. On the

other hand, if the crystal is stressed in the other remaining $\langle 001 \rangle$ direction perpendicular to the plane containing the parallel slip bands, the material deforms easily. This direction is known as the soft direction. Zinc crystals also exhibit the latent hardening property.

Purpose

In the present work, the combined effects of fatigue and latent hardening in lithium fluoride crystals are investigated. Besides, the effect of a complete reversal of the stress in the fatigue cycles is checked against the predictions of the debris mechanism of hardening, according to which there should be no difference in the behavior of the lithium fluoride crystals subjected to a cyclic loading whether there is a complete reversal of stress in each cycle or not.⁶⁴ The increase in yield strength in the latent direction, which depends on the mechanical treatment given before the testing in the latent direction, is compared with the yield strength of the initial slip systems of the same crystal. A study of the deformation structure, specifically the dislocation configuration in the slip plane, is carried out and the theoretical basis for the development of such a structure is discussed. The main objective of this work is to correlate the dislocation structure with the work hardening behavior of lithium fluoride crystals in the hope that the results may shed some new light on the theory of work hardening in general.

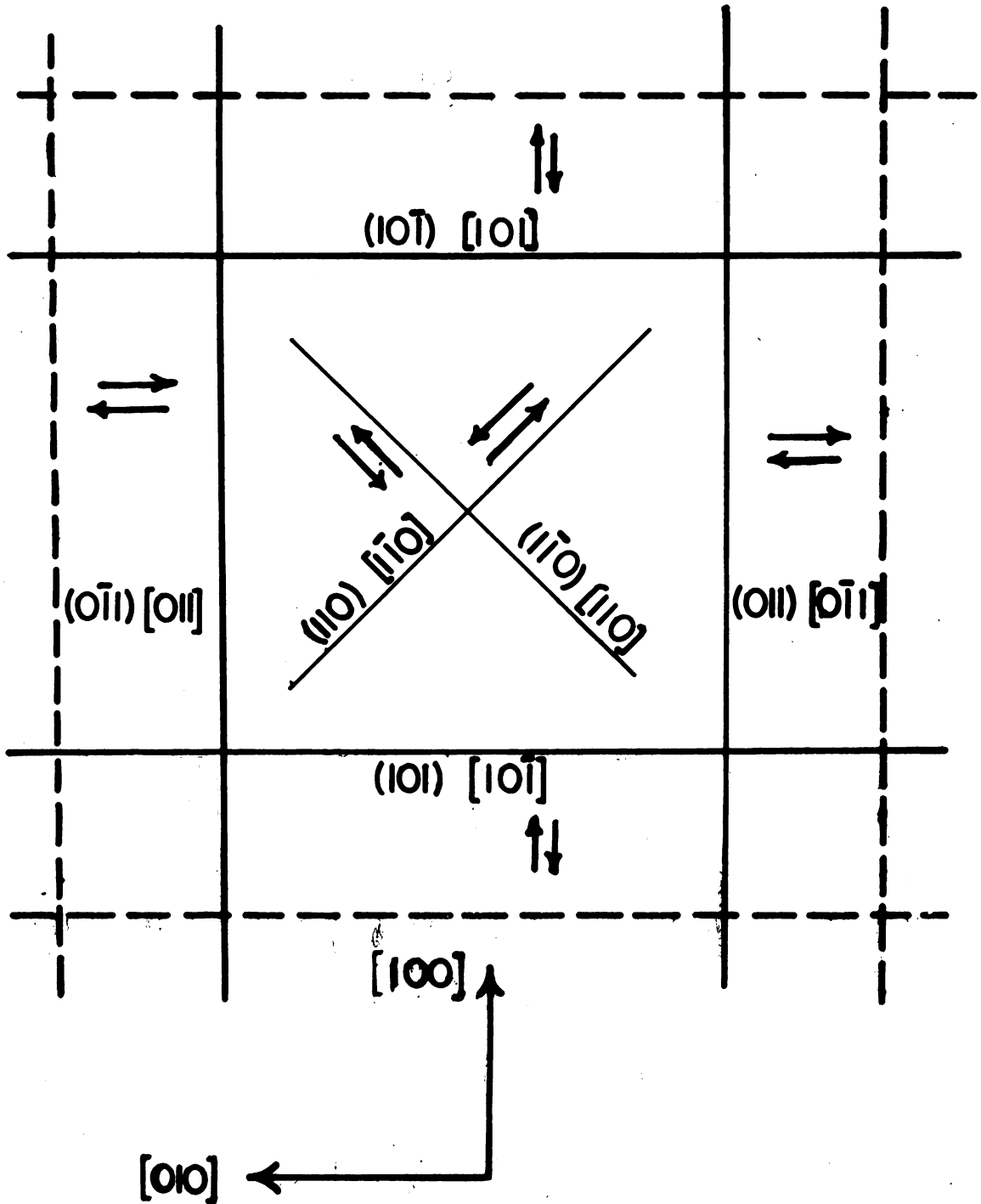


Fig. No. 1

Projection of $\{110\}$ Slip Planes onto (001) Surface

EXPERIMENTAL TECHNIQUES

Lithium fluoride crystals were initially grown by the Birdgman method using a sharp tipped high density graphite crucible. Lithium fluoride powder, obtained from Kawecki Chemical Company, was used as the starting material and had the chemical composition given in Table 1. The crystals were grown at the rate of one millimeter per hour. The graphite crucible was fitted with a refractory sleeve to smooth out the temperature gradient. Some of the crystals grown by this method had approximately $[100]$ as the direction of growth and these were cleaved and used as seeds in a Czochralski furnace shown in figure 2. All the crystals used in mechanical testing were grown by the Czochralski method under the conditions and improvisations described below for achieving faster growth rates and lower dislocation densities. The high density graphite crucible, holding the melt, and the seed were rotated in opposite directions at the rate of approximately one to two revolutions per minute to obtain a homogeneous melt and a planar solid-liquid interface. The furnace was water-cooled. The rod holding the seed was also water-cooled to maintain a necessary longitudinal temperature gradient. The heating element was made of graphite. Two chromel-alumel thermocouples were placed at diametrically opposite points and a potential divider circuit was used to find the average thermo-emf. This emf was fed to a

Minneapolis Honeywell controller to maintain the temperature of the melt within $\pm 2^{\circ}\text{F}$ of the set temperature which was usually 10° to 20°F above the melting point of lithium fluoride. Nitrogen, helium and argon were used to provide an inert furnace atmosphere. When nitrogen was used it was passed through a purification train containing alkaline pyrogallol, glass beads and phosphorous pentoxide to eliminate oxygen and water vapor. A small positive pressure of this atmosphere was maintained in the furnace when it was in operation. A graphite sleeve having a half inch diameter hole in the center was allowed to float on the top of the melt to reduce sudden temperature fluctuations during the growth of the crystals. A secondary heating element was also used to reduce the radial temperature gradient. The crystals were grown at the rate of $1/4''$ to $3''$ per hour.

To avoid sub-boundaries propagating from the seed during the growth process off-centering and necking methods were employed. The growth prefers to follow the common axis of rotation, thereby introducing an initial curved growth immediately next to the seed if the seed is made in contact with the melt at a point away from the axis of rotation. This is called the off-centering. In the necking technique, the crystals were at first pulled out much faster than the normal growth rate. This made the crystals grow as thin as needles. After some time, the growth rate was decreased and the temperature of the melt reduced in order to obtain crystals of the required size. The formation of a

neck between the seed and the growing crystal prevented most of the sub-boundaries in the seed from propagating into the grown crystal.

Fluoboric acid was used for rough polishing and distilled water, for fine polishing. The etchant used was a very dilute solution (approximately 10^{-4} molal solution) of ferric chloride in distilled water. The dislocation etch-pits were counted using a Baush and Lomb metallograph. For dislocation density studies, the crystals were cleaved or cut with an acid-saw using fluoboric acid.

The crystals were homogenized before testing by first packing them with graphite powder in zirconia tubes and then heating at 900°F for four days in an atmosphere of dry nitrogen. After the heat-treatment, the furnace was cooled approximately at the rate of 40°F per hour down to 200°F and thereafter cooled at a very slow rate. Specimens (approximately 0.5 cm cubes) were cleaved out of this stock and first rough polished with fluoboric acid and then fine polished with distilled water. The polished crystals were sprinkled with alundum powder to introduce fresh dislocations which acted as active sources. The testing was always performed under compression with an Instron testing machine using petroleum vaseline as the lubricant.

The deformation studies were focused on (i) the slip band growth in the early stages of fatigue, with or without the reversal of shear stresses in the fatigue cycles, and (ii) the effect of the shear stress and strain in the initial slip systems, with or without reversal, on the strength in the latent direction. The yield strength

of a lithium fluoride crystal is considerably affected by the divalent impurities present in it.⁴⁷ Even specimens prepared from the same single crystal gave scattered results. In order to avoid this complication, the increase of strength of a specimen in the latent direction after a particular mechanical treatment was compared with the yield strength of the initial slip systems of the same specimen. The reversal of the resolved shear stress in the initial slip systems was achieved in the following way. The crystals were compressed along an $[100]$ direction and then turned around and compressed in the soft direction instead of performing alternate tension and compression experiments on the same specimen. The latter would pose difficult grip problems. The growth of the slip bands on the $\{100\}$ planes was studied with linearly polarized light in a dark field. Detailed observations of the damage in the slip bands were made with monochromatic light (mercury green) in a photoelastic set up and also with a modified petrographic microscope.

In the slip plane the stress fields of the dislocations are such that they can be observed with polarized light. In the dark field observations, where the directions of polarization of the polarizer and the analyzer are perpendicular to each other, the stress fields due to dislocations appear as bright lines provided that the slip vector has a certain orientation relationship with the direction of polarization. Fairly thin specimens were used since the depth of focus was critical. The thin specimens were prepared from bulk crystals, previously deformed in compression along the

[100] direction, by grinding them with emery paper so that the broad surfaces were parallel to one of the slip planes active during the deformation of the bulk crystal. The thin crystals were subsequently polished with a metallographic polishing wheel and then chemically polished with fluoboric acid at least for an hour. Fluoboric acid polishes at a rate of approximately 20 microns per minute, thus at least one millimeter of the crystal was removed from each side. This prolonged chemical polishing ensured the removal of the damage introduced during the grinding and mechanical polishing. Finally the specimens were polished with distilled water to obtain smooth surfaces. The thickness of the specimens after the above treatments was of the order of one thousandth of an inch. A petrographic microscope was used for studying the damage in the slip plane. Observations were made with linearly and circularly polarized monochromatic light in both bright and dark fields. The microscope stage on which the specimen was mounted was rotated to obtain various relative orientations of the slip vector with respect to the direction of polarization. Long photographic exposures were required due to the extremely low intensity of the lines observed in the slip plane.

Lithium fluoride specimens having $\{110\}$ planes as the planes of observation were also deformed in three-point simple bending to study the formation of a possible band-like structure. The jig employed for bending the specimens was mounted on the stage of the petrographic microscope. Pictures were taken at

the successive stages of deformation using polarized light in the dark field. The bending jig and the specimen were rotated together to study the relationship between the direction of polarization and the slip vector and its effect on the patterns. An optical condensing system was used to enhance the light intensity in the field of observation in order to reduce the exposure time for photographing. The arrangement used for this purpose is shown in figure 3.

Table 1

Lithium fluoride	99.200%
H ₂ O	0.700%
S O ₄	0.050%
Acidity as HF	< 0.040%
Fe ₂ O ₃	< 0.020%
Na	< 0.005%

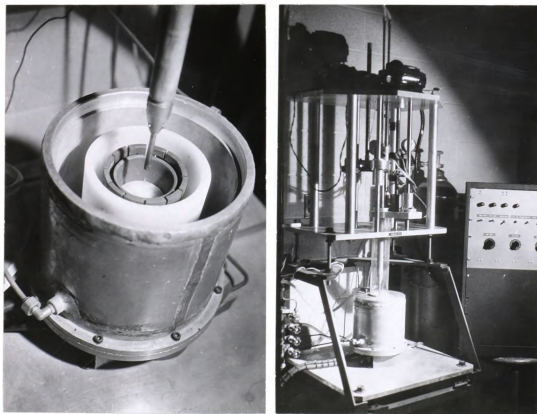


Fig. 2. Czochralski furnace for growing LiF single crystals.

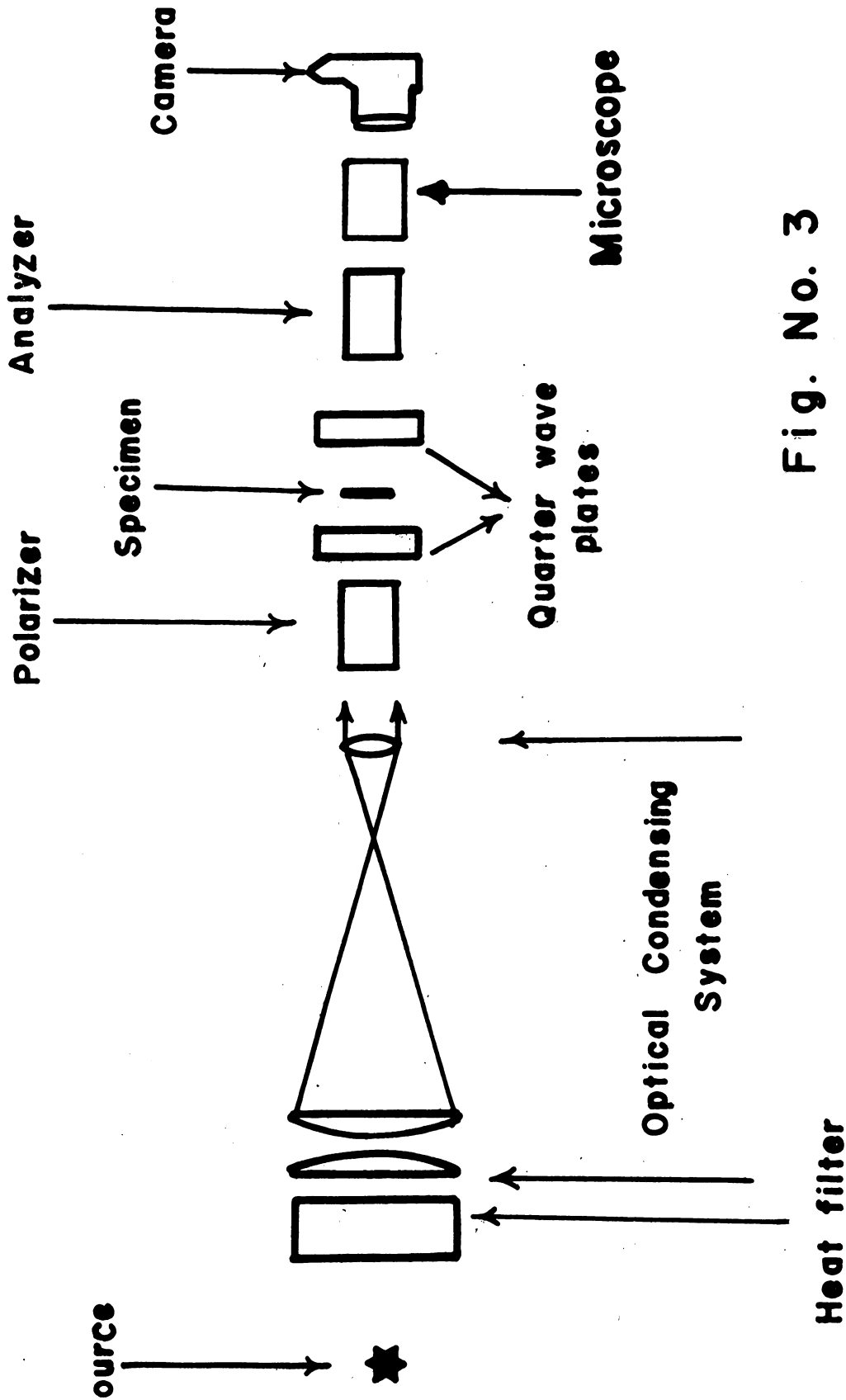


Fig. No. 3

Arrangement for polarized light microscopy

RESULTS

A comparison of the etch-pit patterns of the surfaces of the acid-saw cut and the cleaved crystals grown by the Bridgman method showed that even a fast cleavage had increased the dislocation density. Figures 4 (a) and (b) show the typical dislocation etch-pit patterns observed in cleaved and acid-saw cut crystals respectively. The cleaved crystals always had comparatively more sub-grain boundaries and a larger number of dislocations between the boundaries than the acid-saw cut crystals. The average dislocation density in the cleaved crystals was of the order of 5.4×10^4 lines per square centimeter, and that in the acid-saw cut crystals was of the order of 2.5×10^4 lines per square centimeter. Thus cleaving increased the dislocation density by a factor of two.

The typical dislocation distribution in crystals grown by the Czochralski method is shown in figures 5 (a), (b) and (c). The sub-boundary distribution is shown in (a) and (b), whereas an area of low dislocation density is shown in (c). These crystals were cut with the acid-saw and polished with fluoboric acid to obtain smooth surfaces. The ridges seen in these pictures are due to the localized unevenness of the fluoboric acid polishing.

The necking and off-centering techniques were found to be effective in eliminating the sub-boundaries propagating from the seed. Figure 6 (a) shows the distribution of sub-boundaries grown

from the seed without using the off-centering method. The absence of sub-boundaries after using the off-centering method is shown in figure 6 (b). The ridges in both these pictures are again due to prolonged rough polishing with fluoboric acid. A pseudo Kossel back reflection pattern of one such crystal taken with a micro-focus X-ray unit is shown in figure 7. The absence of any visible breaks in the lines observed in this pattern indicates that sub-boundaries having $O^{\circ}1'$ or greater disorientation were not present in that crystal.

The results of the fatigue-latent hardening experiments are tabulated in Table 2. A comparison of the yield stress in the latent slip systems with the yield stress in the initial slip systems of the crystals used in the fatigue-latent hardening experiments showed that the fatigue cycles with reversed shear were more effective in increasing the strength than the unreversed fatigue cycles. As this table shows, crystals fatigued under the unreversed shear show an increase in strength in the latent direction by a factor of four or five. A typical stress-strain curve for the fatigue-latent hardening experiment with reversed fatigue cycles is given in figure 8. It can be seen that in this particular crystal the yield stress in the latent direction showed a remarkable increase by a factor of approximately ten.

Polarized light observations of the slip bands on the $\{100\}$ surfaces in the early stages of deformation are shown in figure 9. The specimen used in this case was not etched. The series of

pictures in figure 9 were taken with a camera using a small aperture. The polarizer and the analyzer were crossed and rotated together clockwise as viewed from the camera. There was complete extinction of the slip bands when the direction of polarization was either parallel or perpendicular to the Burgers vector. When the slip vector made an angle of 45° with the direction of polarization the slip bands were most distinctly visible. With the polarized light microscopy only the growth of the orthogonal slip bands but not the parallel slip bands on the $\{100\}$ surfaces can be observed.

The slip band growth in a specimen subjected to an unreversed cyclic loading is shown in figure 10. Pictures (a) and (b) show respectively the slip band distribution as observed on the $\{100\}$ plane after the first and second cycles. It was observed that during the second cycle, very few new slip bands were formed. Figures 11 (a) and (b) show the slip band distribution in a specimen subjected to reversed cyclic loading after the first and second half cycles respectively. In this case the directions of the shear stresses, in the operating slip systems, during the second half cycle were opposite to those during the first half cycle. Contrary to the former case a large number of new slip bands were formed. Figure 12 shows the $[100]$ observation of a crystal deformed in the latent direction after being fatigued by the reversed shear. It appears that the new slip bands have difficulty propagating through the existing barriers.

Figure 13 shows the orthogonal slip bands in the (100) plane of one of the specimens prepared for the [110] observations. The four pictures in figure 14 show the effect of the orientation of the direction of polarization with respect to the Burgers vector. In figure 14 (a) the direction of polarization is perpendicular to the Burgers vector whereas the direction of the analyzer is parallel to it. This picture shows the regions of stress concentration within the slip plane, indicating that the slip is not uniform. But it does not reveal any further details. More details of the stress concentration areas were obtained as the polarizer and the analyzer were rotated together successively. In (b), (c) and (d), a band-like structure becomes visible when the direction of polarization makes an angle with the Burgers vector from 30° to 65° , and can be best seen when this angle is 45° . However, the resolution was poor because the specimen was too thick.

More details of these band formations in one of the stress concentration regions of figure 14 were revealed by reducing the thickness of the specimen and by studying it with a petrographic microscope using the plane polarized light. The results are shown in figures 15 (a) - (h). The crystal was mounted on the microscope stage and rotated successively while the polarizer and the analyzer were kept fixed to obtain different orientations of the Burgers vector with respect to the direction of polarization. The parallel set of bright lines in these pictures are due to the slip in the slip planes which are the conjugate of the slip plane under observation. The conjugate slip bands appear to be spaced more or less evenly. The

striking feature of this set of pictures is the band structure along the direction A'A'' in each picture. These bands represent a certain stress pattern and are in the plane of observation. They are different from the parallel set of bright lines due to the intersecting slip planes. Each of these bands appear to be made up of loops that have lined up in a direction perpendicular to the slip vector. These loops become prominent only when the orientation of the Burgers vector is in the range of 20° to 30° with respect to the direction of polarization.

Thin specimens were found to be extremely ductile when deformed by using a three-point bending jig. No apparent hardening was observed in them and no band structure was detected either. In thick specimens, because of a complicated stress distribution, slip took place not only in the plane under observation and its conjugate but also in planes non-conjugate to it. This facilitated the study of the role of the intersecting slip in the formation of these bands and the interaction of non-conjugate slip with the band structure. Figures 16 and 17 are plane polarized monochromatic light dark field pictures of a region of the specimen at various stages of progressive deformation designated as I, II and III. Two sets of figures are presented in order to show the dependence of the contrast of the band structure on the orientation of the Burgers vector with respect to the direction of polarization. The band structure is not at all visible in figure 16, where the Burgers vector is parallel to the direction of polarization. The band structure is visible in figure 17 where the direction of

polarization is inclined at 50° with the slip vector. In figure 17-II the bands just begin to form and the stress birefringence shows high stress concentration. In figure 17-III the bands are well-developed and further deformation of the specimen is difficult. The pictures in these two sets and figure 15 indicate that these bands are of approximately constant width of 20 microns. They are evenly spaced and are usually perpendicular to the slip vector. Figure 18 shows an enlarged portion of the left side of figure 17-III. The interesting feature revealed by this picture is the alignment of the loops along directions which deviate gradually by approximately 20° on both sides of the direction of growth.

In a few instances the loops lined up along the line of intersection of the slip plane under observation with various other primary slip planes as shown in figure 19 where the bands BB' are along the line of intersection of a non-conjugate slip plane with the slip plane under observation. These bands are not well-developed, and give a lower contrast than the bands formed along the direction perpendicular to the Burgers vector, i. e. the line of intersection between the conjugate slip system and the system under observation. The specimen used in this particular case was about 2.5 mm thick, and the knife edges through which the bending load was applied were close together. As a result the stress pattern in the specimen became very complicated. The slight curvature of the band structure perpendicular to the slip vector is due to the curvature of the top surface of the specimen caused by the lateral compressive stresses along the axis of bending, resulted from the complicated stress pattern in such a thick specimen.

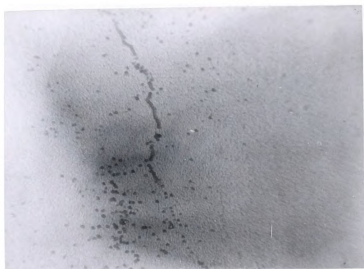
The band structure in the active slip plane of a sodium chloride crystal deformed under compression along $[100]$ direction is shown in figure 20. This specimen was 2.4 mm thick and not thin enough for a clear observation. The band structure in the same specimen after thinning is shown in figures 21 (a) and (b) which reveal the loops associated with these bands. Figures 21 (c) and (d) show the stress concentration due to the intersection of non-conjugate slip with this band structure.

The essential features of the band structure observed in the slip plane are summarized as following:

- (1) The bands were usually perpendicular to the slip vector.
- (2) There was some evidence of bands developing along the line of intersection between the non-conjugate slip planes and the slip plane under observation.
- (3) The bands were typically of constant width of approximately 20 microns.
- (4) They were made up of loops usually interlinked by segments parallel to the slip vector.
- (5) They were distributed non-uniformly throughout the slip planes.
- (6) They did not develop in thin specimens which did not work harden.
- (7) The existing bands in a direction perpendicular to the slip vector acted as strong barriers for non-conjugate slip.

Although lithium fluoride is well suited for studies using the etch-pit, polarized light, X-ray and decoration techniques, a direct observation of the dislocations in lithium fluoride using electron transmission microscopy is difficult if not impossible, because of its poor thermal conductivity and low melting point. Vibration of the specimens due to electrostatic charges is also a problem. On the other hand, magnesium oxide, which has the same crystal structure as lithium fluoride and exhibits a behavior similar to lithium fluoride in fatigue and latent hardening, is well suited for transmission electron microscopy. Figures 21 and 22 are electron transmission micrographs of magnesium oxide single crystals deformed in fatigue at room temperature. The damage in the slip bands, which happen to be the parallel slip bands in all these pictures, consists predominantly of edge dislocation dipoles in the shape of elongated loops. Some of the observations made in these micrographs are summarized below. The points A, B, C and D whereat there are sharp bends on the dislocation lines, are collinear in figure 22 (a). The top and bottom segments of the dislocations at B, C and D are respectively more or less parallel to each other. The same details can also be seen at points A and B in figure 22 (b). Figure 23 (a) shows five dislocations A - E which are approximately parallel to one another. From the geometry of these dislocation lines they appear to have been generated by a single source. The center portion of the dislocation CC' bends around an elongated dislocation loop. At point E there is a dipole of approximately edge orientation and at point E' a dipole of approximately

screw orientation. Both these dipoles are partly made of the same dislocation EE' . Figure 23 (b) gives a much clearer picture of the formation of these dipoles. At points X and Y there are edge and screw dipoles respectively. It appears that these dipoles are formed as a result of the interaction of the loops AA' , BB' and CC' . These dipoles need not always be edge dipoles or close to the edge orientation. As this picture shows they can be of various orientations. Figure 23 (c) shows edge dislocation dipoles which appear to be formed by the interaction of two dislocations from one source with two from another. Figure 23 (d) shows the interaction of two dislocations of predominantly edge orientation.



100x

(b)



100x

(a)

Fig. 4. Dislocation distribution in crystals grown by Bridgman method:
(a) Cleaved specimen (b) Acid-saw cut specimen

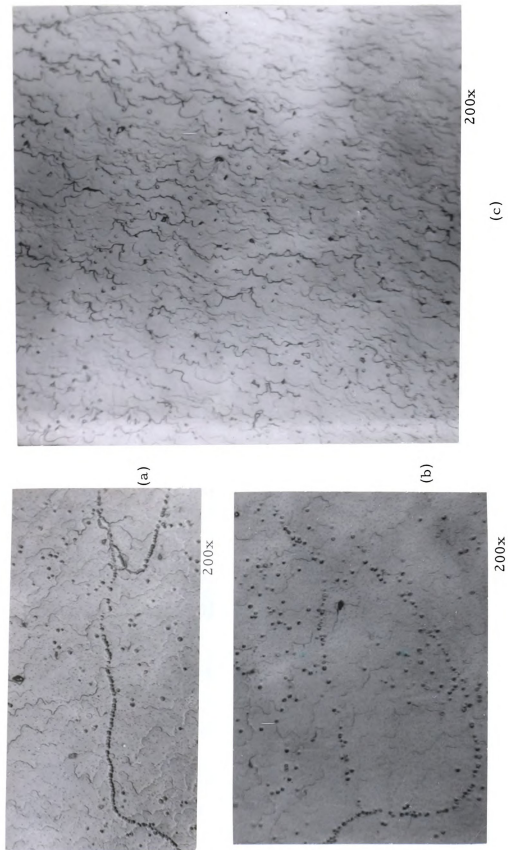
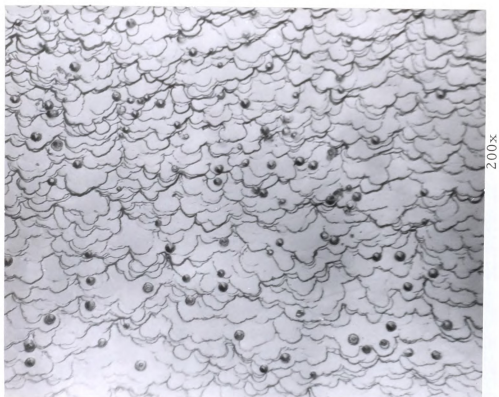
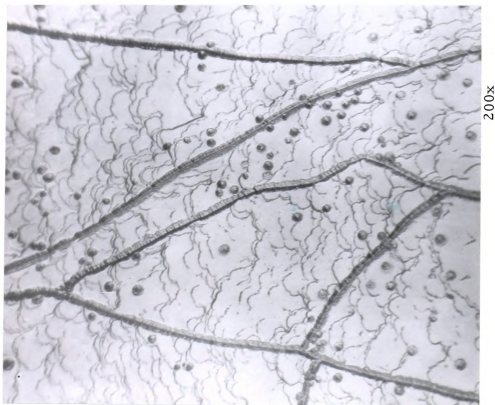


Fig. 5
(a), (b). Sub-grain boundary distribution
in a crystal grown by Czochralski
method.

(c). A region of low dislocation
density in a crystal grown by
Czochralski method.

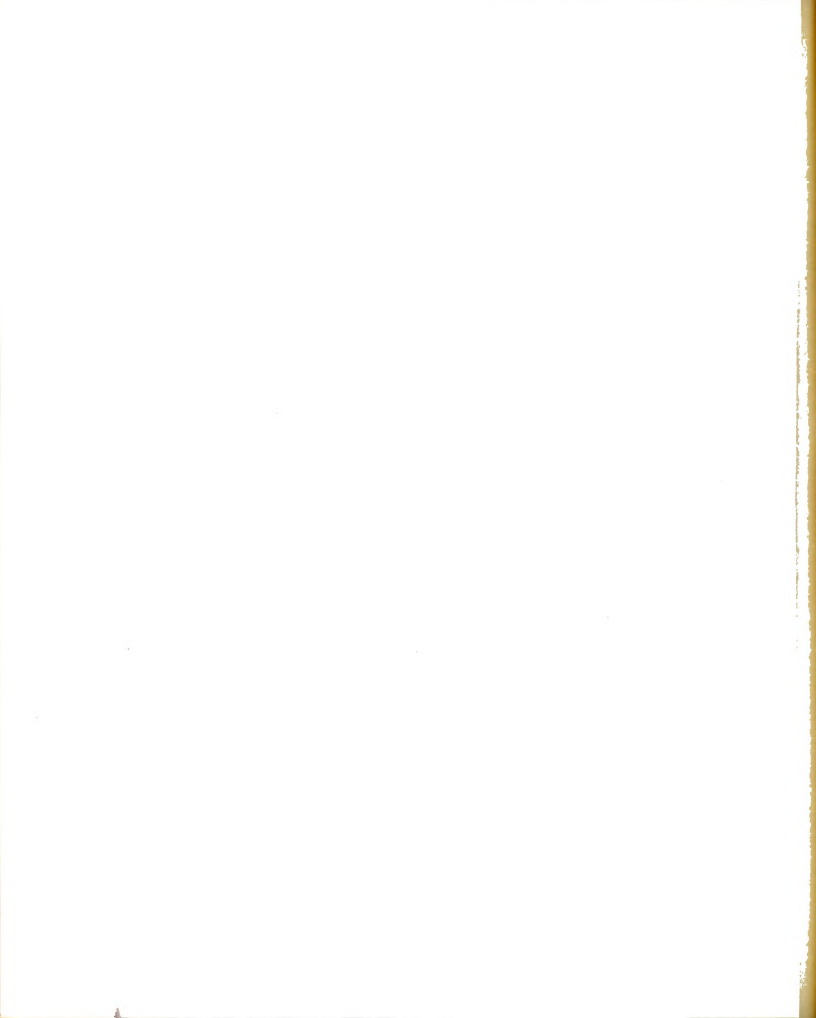


(b)



(a)

Fig. 6. Effect of off-centering on sub-boundary distribution:
(a) Before off-centering (b) After off-centering



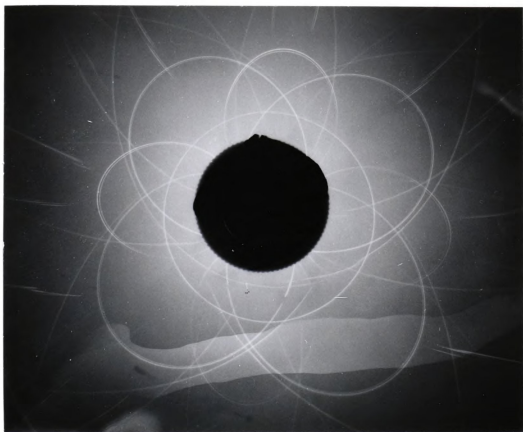


Fig. 7. Divergent beam X-ray picture of LiF crystal grown by Czochralski method (using off-centering principle).

Table 2. Typical data on Fatigue-Latent hardening experiments.

Crystal		Number of cycle									$\frac{\text{Final Y.S.}}{\text{Initial Y.S.}}$	
		I	II	III	IV	V	VI	VII	VIII	IX		
1	Y.S.	143	248	238								1.66
	./. ϵ direction	1.00 original	1.00 original	- latent								
2	Y.S.	1090	1220	1770	2180	3690						3.39
	./. ϵ direction	0.45 original	0.76 original	0.91 original	1.05 original	- latent						
3	Y.S.	69.5	48	440								6.33
	./. ϵ direction	1.10 original	1.17 soft	- latent								
4	Y.S.	258	425									1.65
	./. ϵ direction	1.71 original	- latent									
5	Y.S.	1590	2300	4450								2.80
	./. ϵ direction	2.00 original	2.10 original	- latent								
6	Y.S.	396	2350	4160								10.50
	./. ϵ direction	2.05 original	2.05 soft	- latent								



Crystal	Number of cycle									Final Y. S. Initial Y. S.	
	I	II	III	IV	V	VI	VII	VIII	IX		
7	Y. S. ./. ϵ direction original	86 2.03 soft	46 1.97 original	305 2.00 soft	37 1085 latent						12.60
8	Y. S. ./. ϵ direction original	455 3.46 latent	1680 - latent								3.70
9	Y. S. ./. ϵ direction original	1275 2.22 original	3220 3.36 original	5550 - latent							4.35
10	Y. S. ./. ϵ direction original	311 3.52 original	2530 3.92 original	4310 4.03 original	5800 4.27 original	1520 - latent					4.90
11	Y. S. ./. ϵ direction original	404 3.99 original	466 4.86 soft	4208 - latent							10.46
12	Y. S. ./. ϵ direction original	275 1.31 original	228 3.42 soft	385 10.88 original	318 4.46 soft	5480 - latent					19.95
13	Y. S. ./. ϵ direction original	185 3.70 original	364 1.50 soft	277 2.96 original	484 1.60 soft	462 4.50 original	726 1.29 soft	554 2.34 original	968 2.25 soft	5400 - latent	29.20

Note: Y. S. - Yield Stress in gm/mm² ϵ - plastic strain

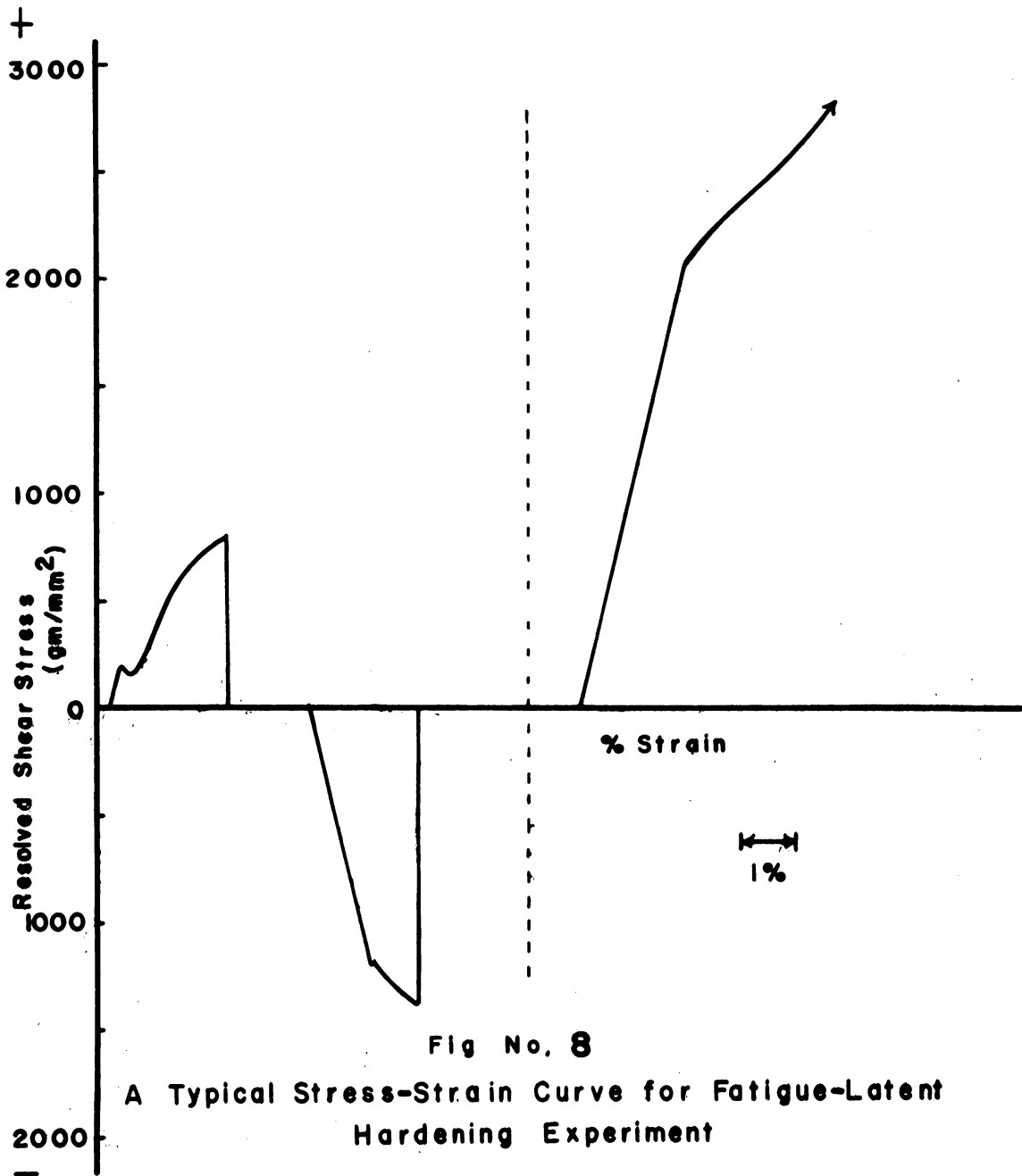


Fig No. 8

A Typical Stress-Strain Curve for Fatigue-Latent Hardening Experiment

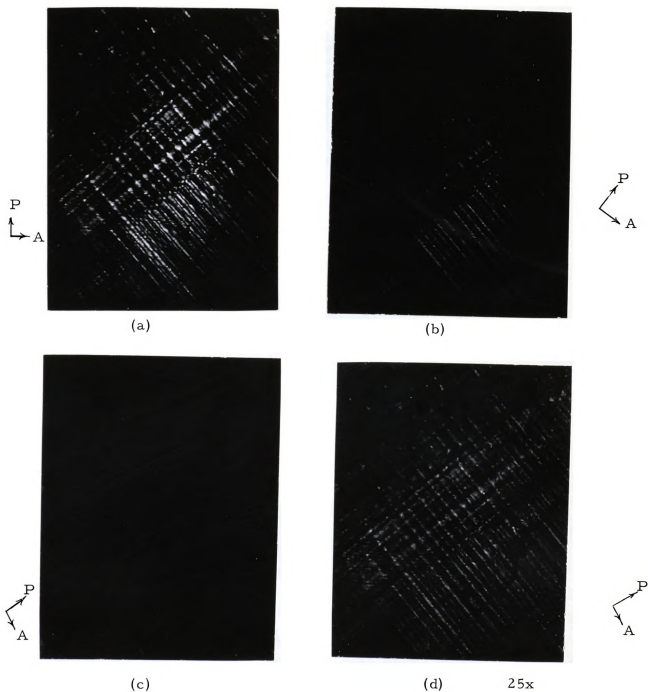
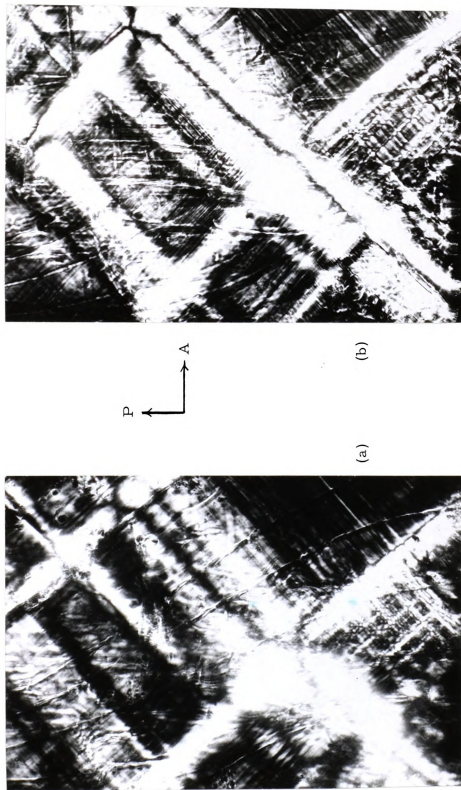


Fig. 9. Orthogonal slip bands on (100) surface as observed at various orientations of the slip vector with the direction of polarization in dark field:

- (a) Direction of polarization vertical,
- (b) Direction of polarization 30° to the vertical,
- (c) Direction of polarization 50° to the vertical,
- (d) Direction of polarization 70° to the vertical.



30x

Fig. 10. Slip band growth observed on (100) plane during unreversed cyclic loading
(a) After the first cycle, (b) After the second cycle.

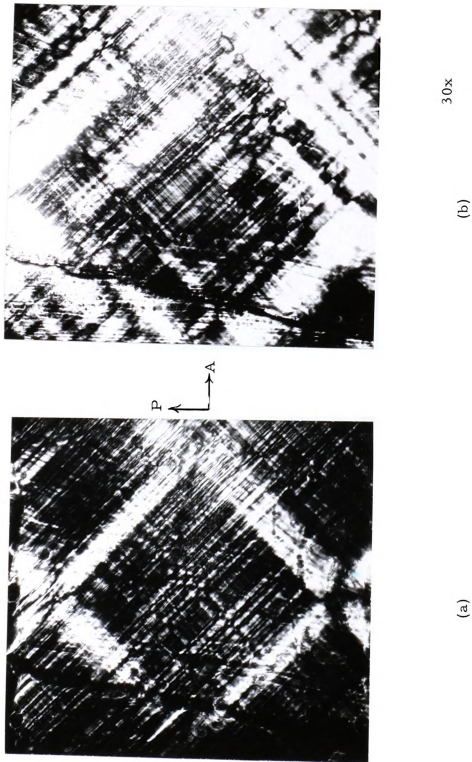
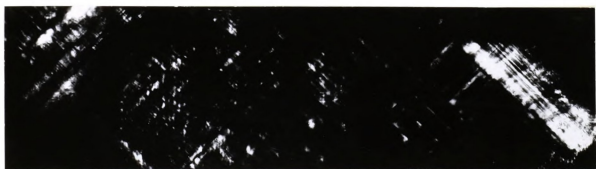
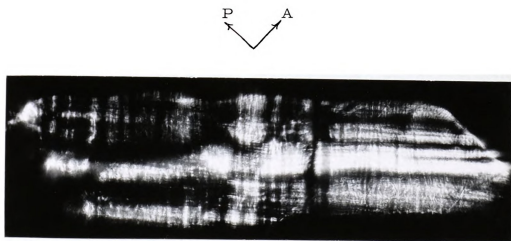


Fig. 11. Slip band growth observed on (100) plane during reversed cyclic loading
(a) After the first half of first cycle,
(b) After the second half of the first cycle with reversed shear in the same slip planes deformed in the first half cycle.



40x

Fig. 12. Slip distribution observed on a (100) plane of a crystal deformed in the latent direction.



15x

Fig. 13. Orthogonal slip bands on the (100) surface of a specimen prepared for the observation of damage in the (011) slip plane.

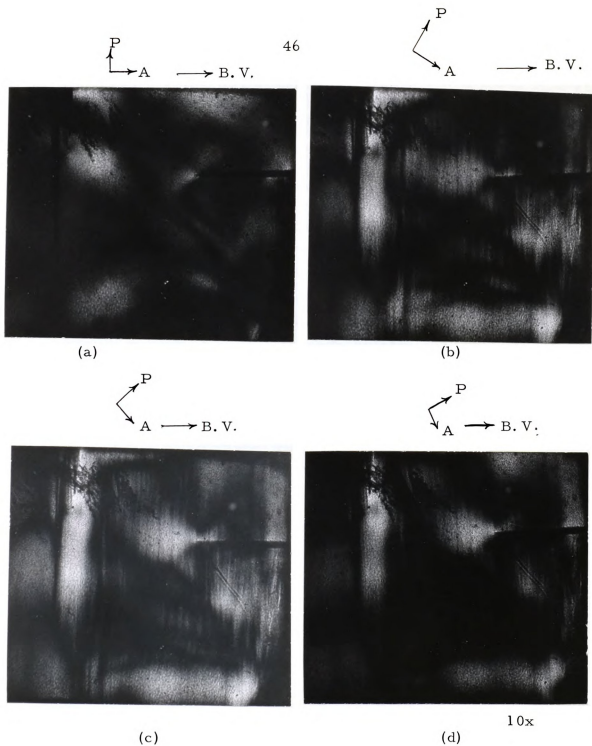


Fig. 14. Band structure observed in the slip plane of the specimen shown in figure 13, linearly polarized light dark field observations:

- (a) Direction of polarization vertical,
- (b) Direction of polarization 30° to the vertical,
- (c) Direction of polarization 45° to the vertical,
- (d) Direction of polarization 65° to the vertical.



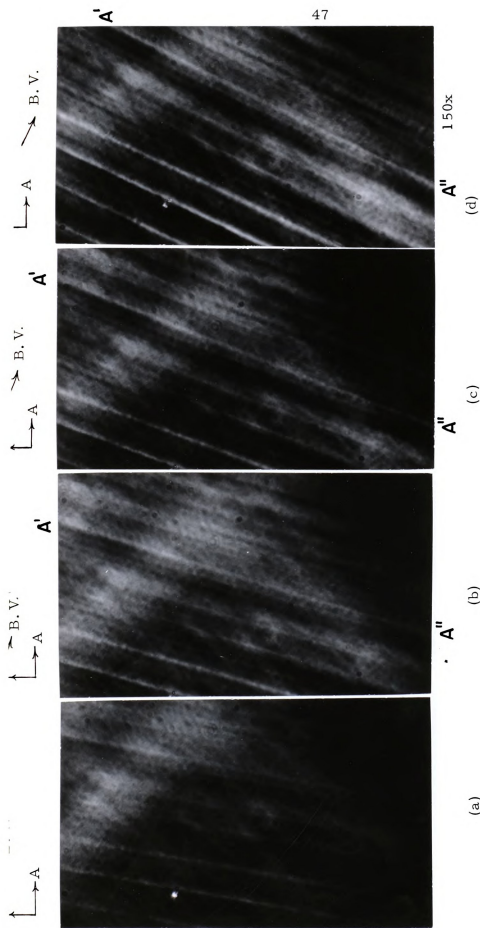


Fig. 15. Polarized light observation of the bands in the slip plane:

- (a) Bands making 10° to the direction of polarization,
 (b) Bands making 15° to the direction of polarization,
 (c) Bands making 20° to the direction of polarization,
 (d) Bands making 25° to the direction of polarization,

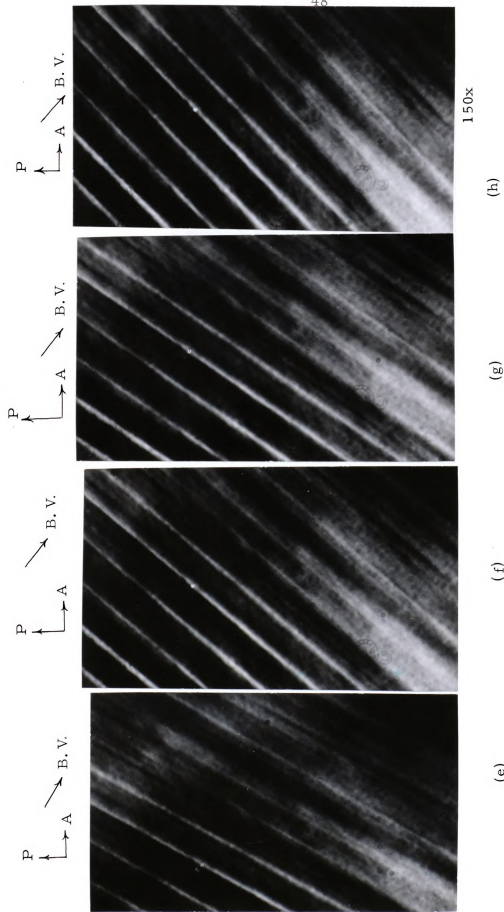


Fig. 15. continued

- (e) Bands making 30° to the direction of polarization,
- (f) Bands making 35° to the direction of polarization,
- (g) Bands making 40° to the direction of polarization,
- (h) Bands making 45° to the direction of polarization.



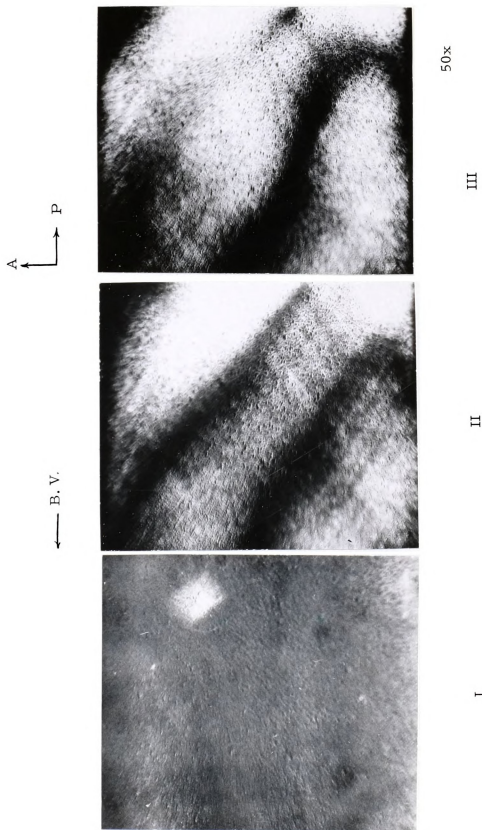


Fig. 16. Band structure at various stages of deformation in three-point bending; Burgers vector parallel to the direction of polarization.



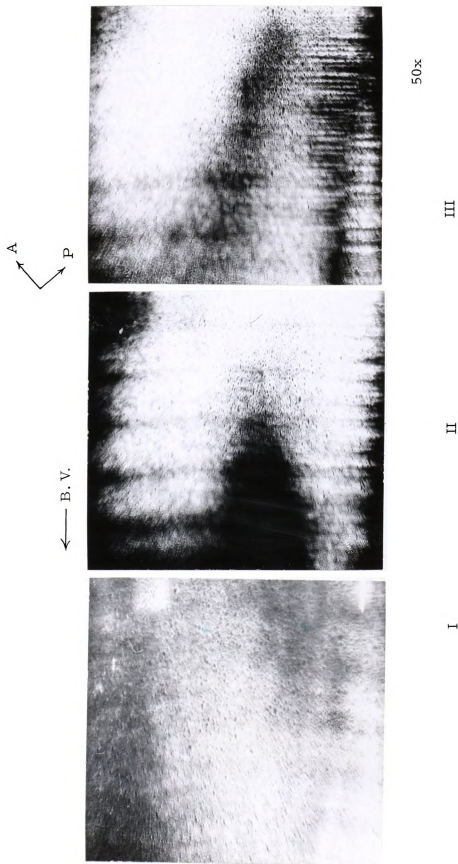
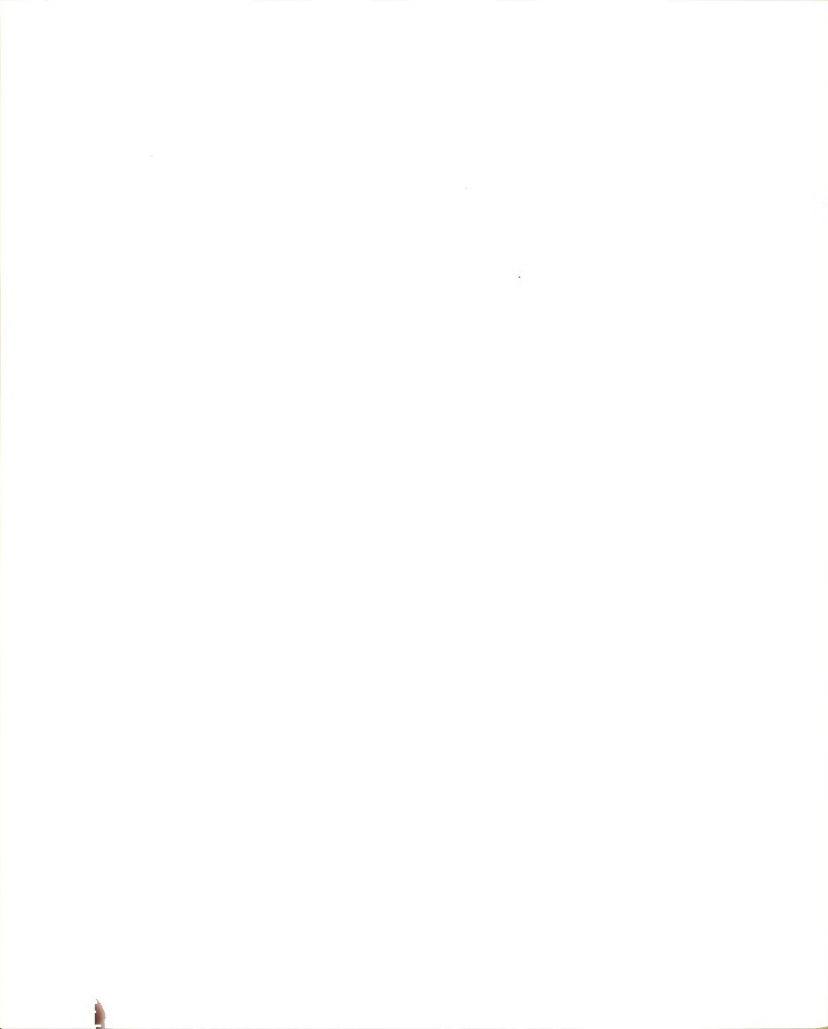


Fig. 17. Band structure at various stages of deformation in three-point bending; Burgers vector making 50° to the direction of polarization.



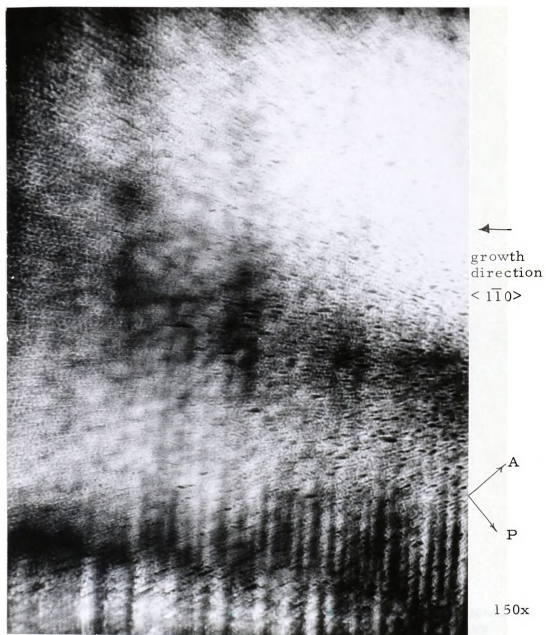
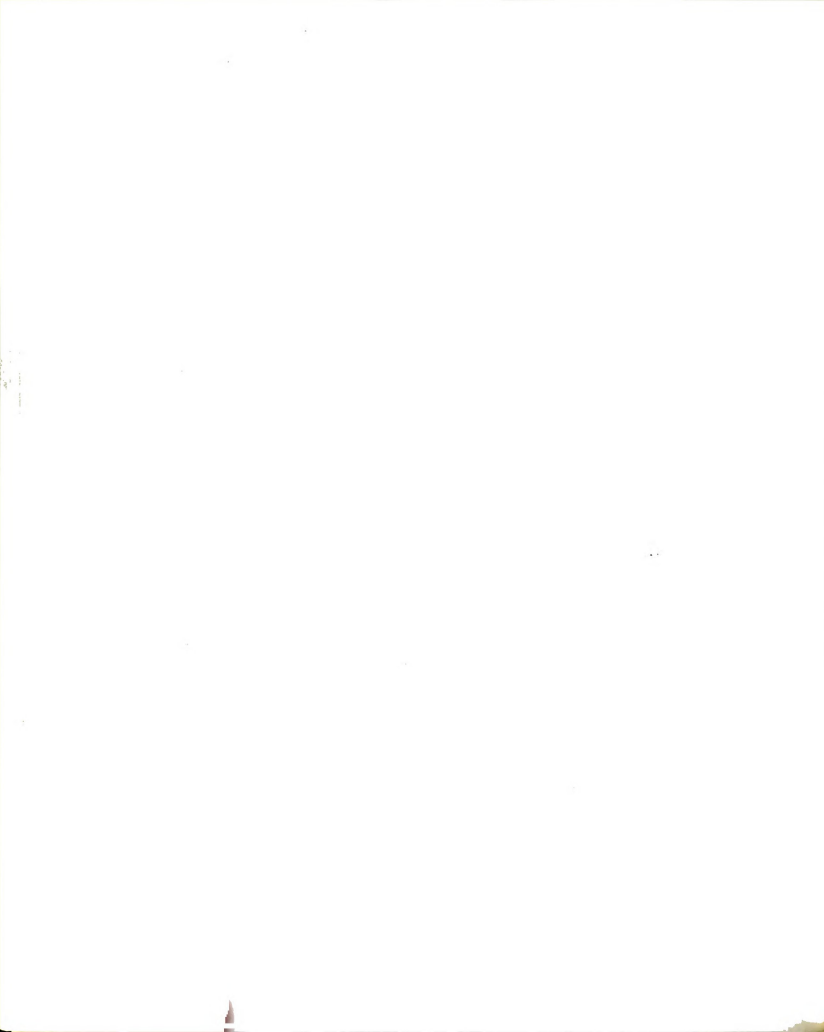


Fig. 18. Network observed in a lithium fluoride crystal.



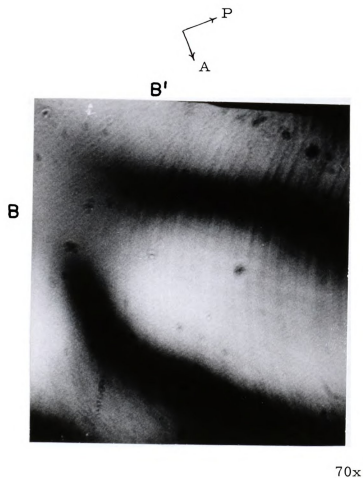
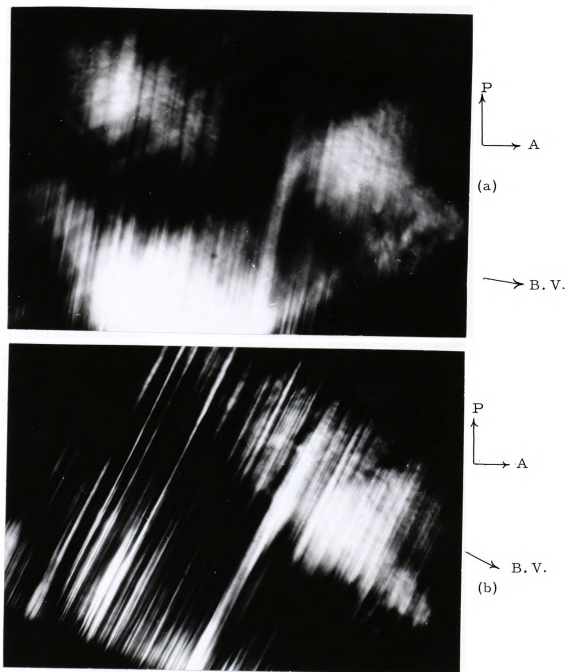


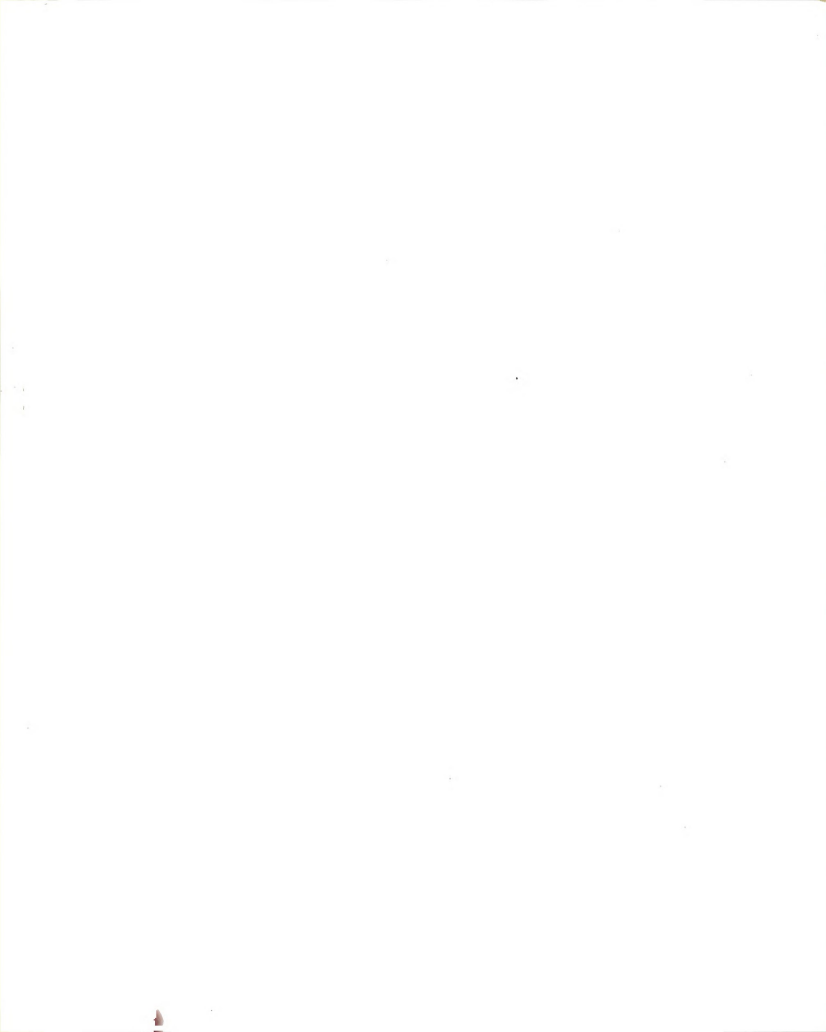
Fig. 19. Band structure observed along non-orthogonal slip plane intersections in a thick specimen deformed in three-point bending; Burgers vector making 20° to the direction of polarization.





30x

Fig. 20. Band structure in a thick sodium chloride specimen deformed in uniaxial compression; direction of polarization vertical. (a) and (b) are two different orientations of the Burgers vector with respect to the direction of polarization.



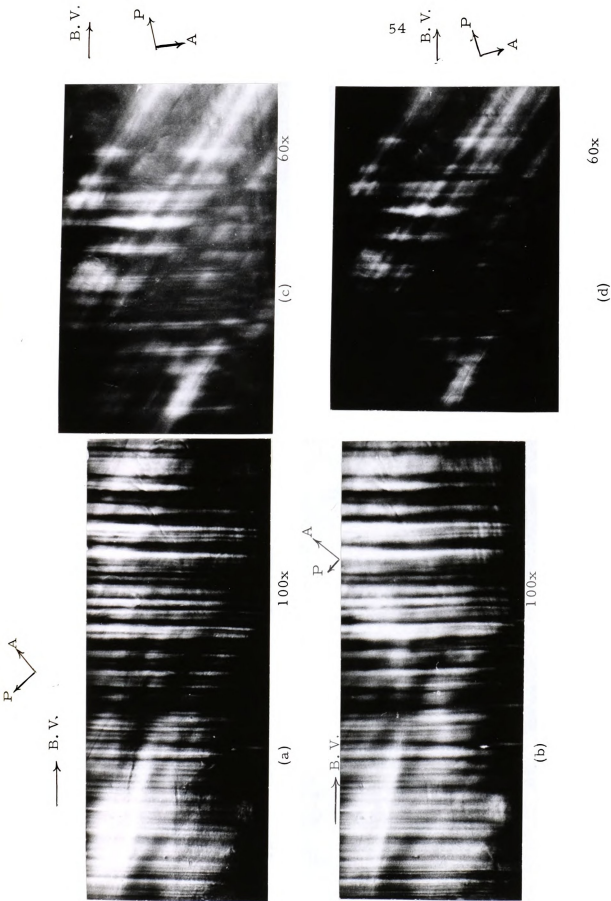
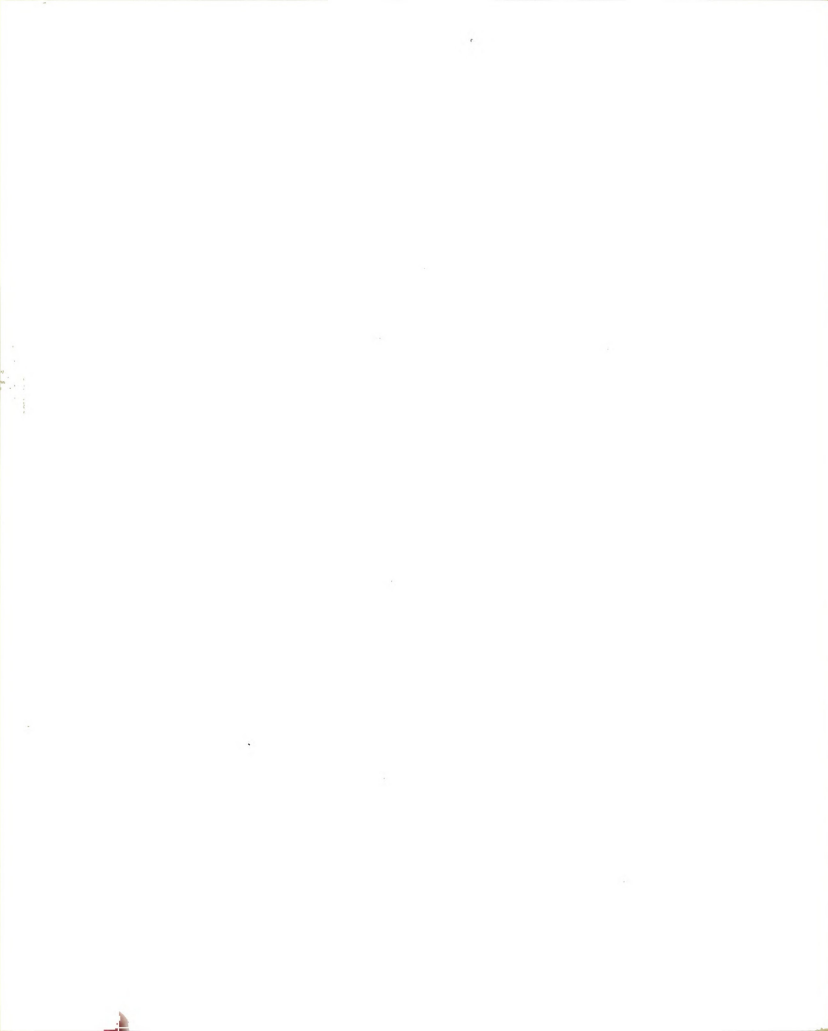


Fig. 21. Band structure in the sodium chloride specimen observed in figure 20 after thinning down.

(a) and (b) reveal loops in these bands,

(c) and (d) reveal the stress concentration caused by non-orthogonal slip band intersections.



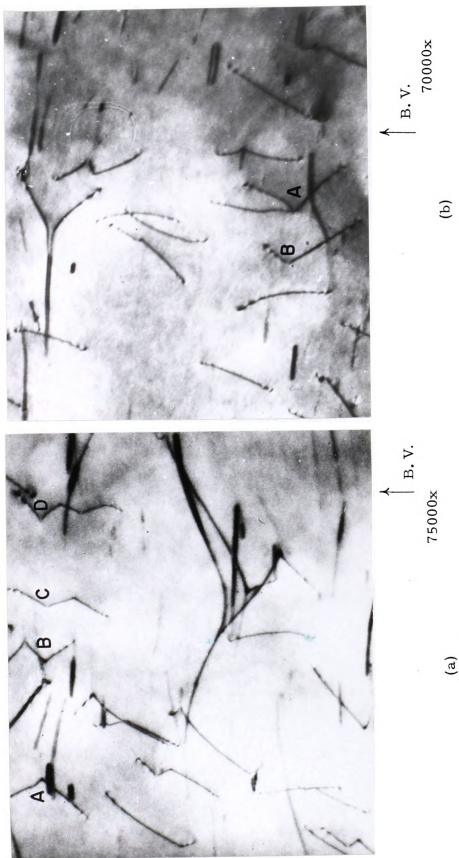


Fig. 22. Transmission electron micrographs of an MgO single crystal fatigued in cantilever bending at room temperature.



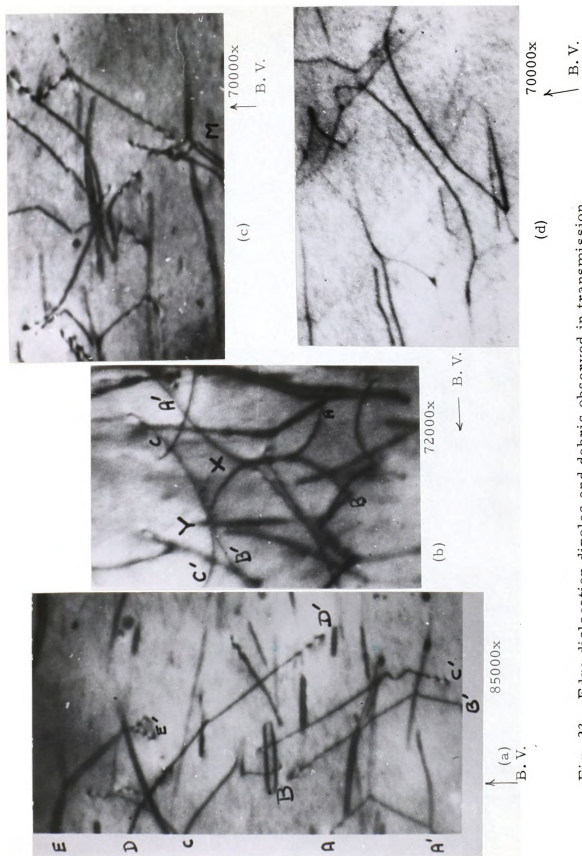


Fig. 23. Edge dislocation dipoles and debris observed in transmission electron micrographs of fatigued MgO specimens.

DISCUSSION

I. Crystal Growth

As it was shown in the previous chapter, sub-grain boundaries and possibly individual dislocations originated in the seed were effectively prevented from propagating into the growing crystal by using either the off-centering method or the necking technique. During the growth of a crystal, each dislocation line that intersects the liquid-solid interface must extend into the newly crystallized material. It has been experimentally observed that if the dislocation density is low enough to make dislocation interactions unimportant, each individual dislocation would propagate along a path normal to the liquid-solid interface. However, the precipitation of excess vacancies and the presence of stresses in the growing crystal due to thermal gradients or due to impurity segregation can cause the end of a dislocation to move away from this path.

These ideas were utilized in the off-centering method. Since both the crystal and the melt were rotated with respect to the same axis, the growing crystal had a tendency to align itself with the axis of rotation. The seed was placed in contact with the melt at a point away from the axis of rotation, and hence it developed a curved region before it grew along the axis of rotation. Most of the dislocations extending from the seed terminated at the crystal surface in the curved portion because of their



tendency to propagate along the direction normal to the solid-liquid interface. The sub-boundaries and the dislocations propagating from the seed were, therefore, practically eliminated.

The necking technique for reducing the number of dislocations propagating from the seed is based on the following observations. During fast growth dislocations tend to follow low index crystallographic paths in their slip plane, whereas during slow growth they tend to follow the temperature gradient. In the necking technique the crystals were grown at a fast rate for some time and then the growth rate was slowed down to produce crystals of the required size. If $[100]$ happens to be the growth direction, four of the six $\{110\}$ slip planes are at 45° to the growth direction and intersect the surface of the crystal. Most of the dislocations present in the seed will not propagate into the fast growing crystal because they tend to remain in the slip plane. In the necked section, the other two slip planes, which are parallel to the direction of growth, occupy only a very small area compared to the seed or the growing crystal. This also helps to reduce the number of dislocations extending from the seed into the growing crystal.

The dislocation density of the crystals grown was approximately 10^4 lines per square centimeter. It was not noticeably affected by the growth rate in the range 6 to 75 mm per hour employed. Washburn et al.^{73, 74} obtained crystals having 10^4 dislocations per square centimeter at a growth rate of 1 to 10 mm per hour. Improved growth conditions, such as the reduction of mechanical disturbances,



rotation of the crucible and the seed to give a planer interface and homogeneity, and water cooling the seed rod to maintain a longitudinal temperature gradient, helped to increase the growth rate up to 75 mm per hour in the present work.

Thermal stresses and vacancy condensation are other possible sources of dislocations. The vacancy condensation can produce dislocation loops, but it probably cannot account for all the grown-in dislocations observed in lithium fluoride crystals. Washburn has suggested that internal stresses must be reduced in order to avoid dislocation multiplication during growth. These internal stresses are due to non-linear thermal gradients, segregation of impurities which may cause local change in the lattice parameters, inclusion of foreign particles, etc. In the present work the impurity level should have been very low because the crystals had a yield stress as low as that of pure crystals. The major cause of the grown-in dislocations seems to be the non-linear thermal gradients. The longitudinal temperature gradient was fairly well controlled whereas the thermal gradient in the radial direction was not. Attempts were made to use an additional heating element just above the solid-liquid interface to make it planar. In spite of maintaining the temperature difference between the melt and this heating element at about 100°F , no appreciable difference in dislocation density could result. At smaller temperature differences it was not possible to grow the crystal because the temperature of the seed approached the melting point thereby making the longitudinal temperature gradient too small.



Attempts to grow crystals with large cross-sections (greater than 12 mm square) resulted in specimens with white inner cores. The core of such a specimen was made up of a large number of small crystallites. The region outside this core was a single crystal. The crystallites were formed far above the interface in a region of the crystal that had already grown. At the time of their formation the region outside the core had completely solidified and was shrinking while the core itself was still at a temperature near the melting point and susceptible to plastic deformation. The thermal stresses due to the shrinking of the outer region might have caused the formation of the crystallites. This effect would be severe in lithium fluoride because it is a poor thermal conductor.

The above observation suggests the reason why it has not been possible to reduce the dislocation density of lithium fluoride single crystals below 10^4 lines per square centimeter. Most of the dislocations are probably caused by the thermal stresses which exist even in small crystals due to the temperature gradient present, especially in lithium fluoride which has a poor thermal conductivity. In large crystals the thermal stresses are more pronounced. This may introduce a large number of dislocations which form the boundaries of the crystallites. In small crystals the effect is not so severe, but it has not been possible to eliminate the thermal stresses as well as dislocations completely with the present technique.



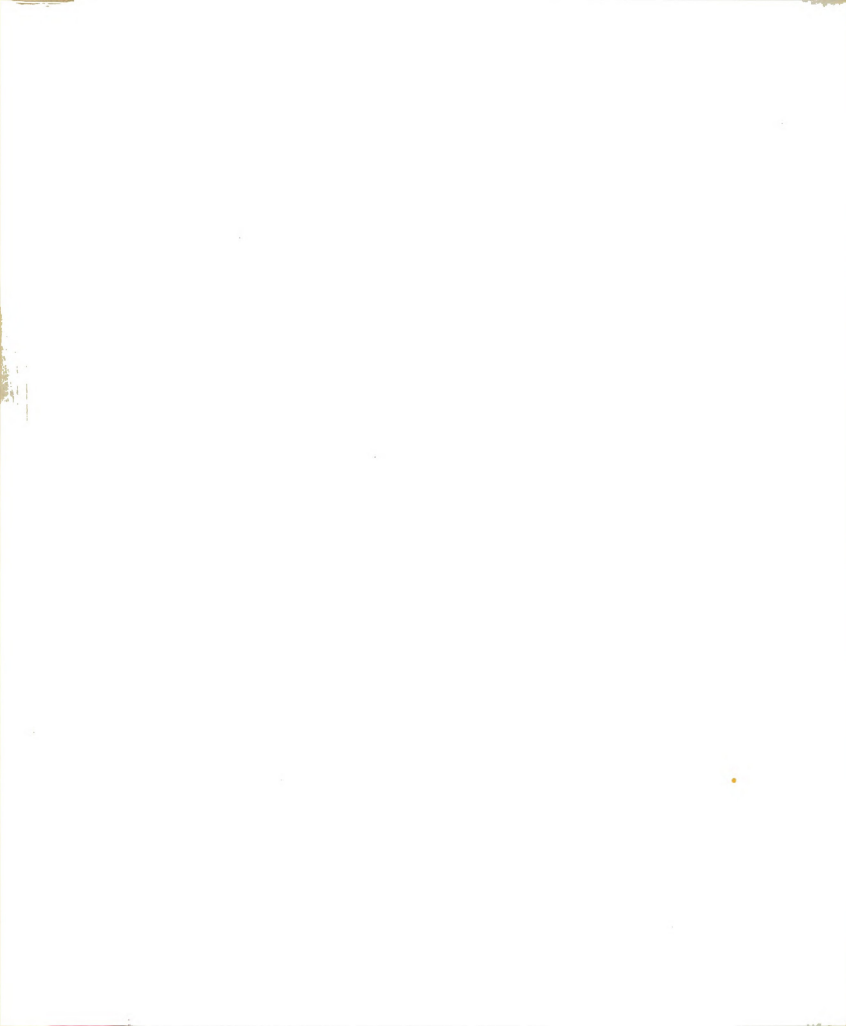
The crystals grown by Czochralski method conformed to crystallographic symmetry (inspite of the rotation of the melt and the seed either in the same direction or in opposite directions). The crystals grown in a $[100]$ direction had a fourfold symmetry and the four surfaces were $\{001\}$ planes. The crystals grown in a $[110]$ direction had a two fold symmetry and the planes having larger areas were $\{001\}$; the other two surfaces were $\{1\bar{1}0\}$. When the growth direction was $[111]$ the crystals had a threefold symmetry with $\{1\bar{1}0\}$ surfaces. This can be interpreted in terms of surface energy. Since $\{100\}$ planes have less surface energy than any other planes, they will have maximum area and predominate.⁷⁵ In $[100]$ crystals it is possible to have four $\{001\}$ planes parallel to the growth direction. These will form the bounding surfaces. In $[110]$ crystals it is possible to have only two $\{001\}$ surfaces along the growth direction. These will form the major portion of the surface area of the crystal. The other two bounding surfaces are $\{1\bar{1}0\}$ because they have the next lowest energy. In $[111]$ crystals there is no possibility of having $\{100\}$ surfaces. The $\{1\bar{1}0\}$ planes, which have the next lowest energy, are the only ones that can form the bounding surfaces.

II. Principles of Polarized Light Microscopy - Observations at Various Orientations of the Slip Vector with Respect to Direction of Polarization

In polarized light observations isoclinics, which appear as dark lines, show the loci of the points where the direction of one of the principal stresses is parallel to the axis of the polarizer and the direction of the other, to that of the analyzer. Isochromatics, which appear as bright lines, are due to principal stresses being unequal, and their intensities are proportional to the difference in the principal stresses. In plane polarized light dark field observations, both the isoclinics and isochromatics are present while circularly polarized light dark field observations give the isochromatics only. Therefore, by studying the fringe patterns consisting of isoclinics and isochromatics, it is possible in principle to follow the directions of the principal stresses from point to point as well as to obtain the difference in the magnitudes of the principal stresses.

In plane polarized light dark field observations the polarizer and the analyzer were rotated simultaneously through the same angles. As described previously there was complete extinction of the patterns only when the polarizer was either parallel or perpendicular to the orthogonal slip bands. Since these slip bands were otherwise present in the plane polarized as well as the circularly polarized light dark field observations, they were isochromatics.

For an interpretation of the photoelastic patterns resulting from a three-dimensional stress field the stress-optic law in three-



dimensions, which is connected with the concept of secondary principal stresses, should be applied. Secondary principal stresses for a given direction are defined as the principal stresses resulting from the stress components which lie in a plane normal to this direction.⁷⁶

There exists at the same point an infinite number of secondary principal stresses, depending on the choice of the direction through the given point, although for each direction, the pair of secondary stresses is unique. The stress-optic law in three-dimensions may be described by the following propositions:⁷⁶

- (a) A polarized beam of light on passing through a stressed medium is resolved into components along the secondary principal stress directions corresponding to the direction of the ray at the point of entrance.
- (b) The vibrations associated with the beam of light traveling through the stressed body are at each point parallel to the directions of the secondary principal stresses for the given ray.
- (c) If, however, the directions of the secondary principal stresses for the given ray rotate as the light advances, then the directions of vibration of the components of the light vector also rotate through the same angle.
- (d) When the secondary principal stresses remain constant between the point of entrance and the point of exit the retardation in wave lengths or fringes is given by

$$n = C t (p - q)$$

where C is the strain-optic coefficient

t is the actual distance traveled by the light and

p and q are the secondary principal stresses.

(e) If the directions of the secondary principal stresses remain constant and the magnitudes vary, then

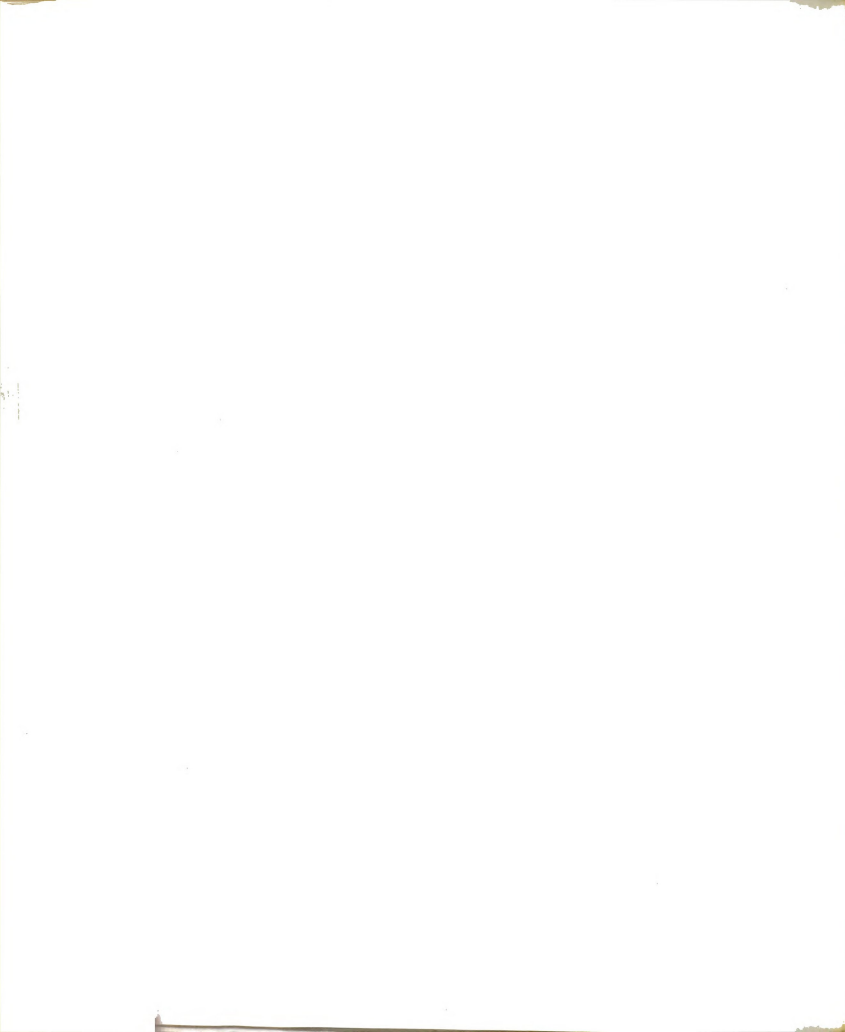
$$n = C \int_0^t (p - q) dt \quad .$$

When the directions of the secondary principal stresses rotate, the rotation tends to increase the retardation; the exact relationship between this rotation and its effect on the retardations is at present not fully established.

(f) Normal stresses parallel to the ray produce no photoelastic effects.

(g) Systems of shear stresses which are coplanar with the direction of the ray, and the components of which are parallel and perpendicular to the ray, produce no photoelastic effects.

There have been few attempts to interpret the observations in photoelastic experiments with regards to the stress birefringence of the dislocations and the orientation dependence of the intensity of the birefringence patterns. Nye was the first one to point out that the birefringence observed in the glide bands of deformed silver chloride crystals is the direct consequence of the presence of a majority of edge dislocations of one sign.⁷⁷ Such an array of edge dislocations of one sign results in a stress pattern which changes from compression to tension on crossing the slip plane. This stress pattern has been shown by Nye to be responsible for the birefringent band as seen under polarized light. Kear and Pratt found asymmetrically colored



birefringence bands in the interior of quenched sodium chloride crystals when a sensitive tinted plate was included in the optical system.⁷⁸ The asymmetry of the color on each side of the slip plane was shown to be associated with the presence of edge dislocations of a particular sign. Bond and Andrews made the first significant observation of the birefringence pattern around a single edge dislocation in silicon that it conformed to the stress pattern predicted by the theory of elasticity.⁷⁹

Bullough has calculated the expected intensity distribution in the immediate neighborhood of an edge dislocation in silicon for both plane polarized and circularly polarized infrared light based on the principal strains, and suggests that the birefringence patterns observed by Bond and Andrews are due to macrodislocations but not due to individual edge dislocations.⁸⁰ The principal strains associated with an edge dislocation are

$$e_{11}' = \frac{A}{r^2} [x - (1 - 2\nu) y]$$

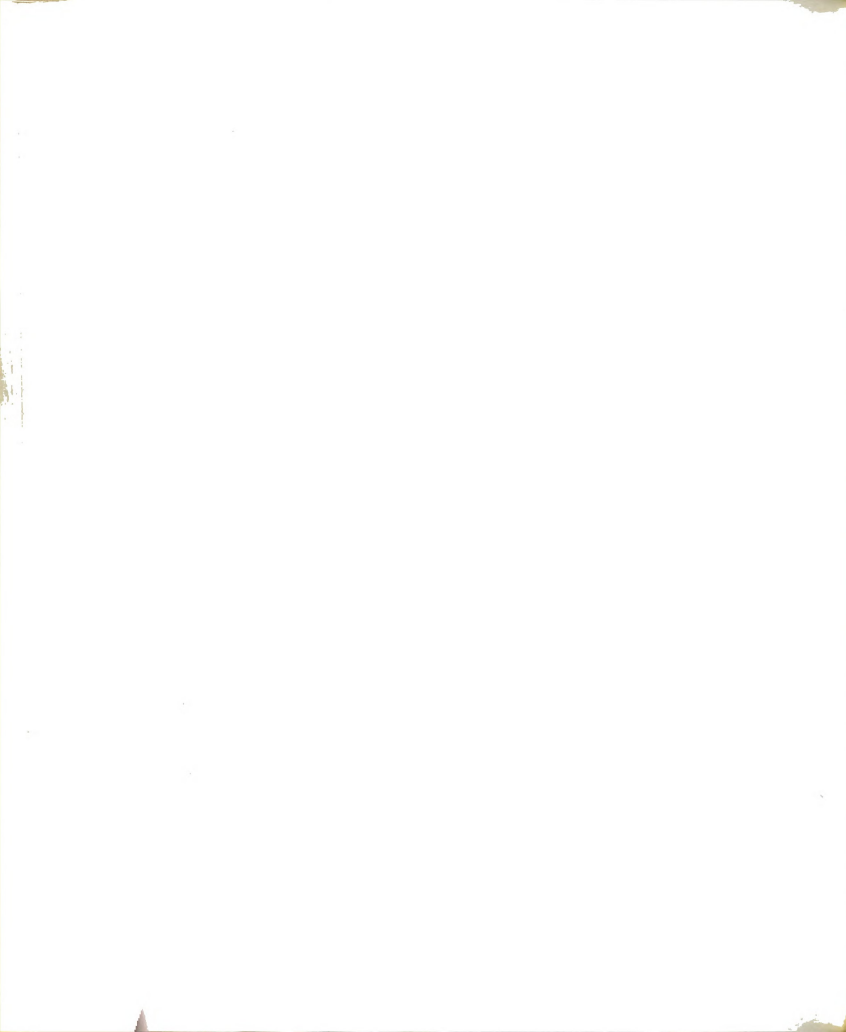
$$e_{22}' = \frac{A}{r^2} [x + (1 - 2\nu) y]$$

$$\theta = \frac{1}{2} \tan^{-1} \left(\frac{y^2 - x^2}{2xy} \right)$$

where θ is defined as the angle between the slip direction (X-axis) and the X' principal axis,

$$A = \frac{b}{4\pi(1 - \nu)}$$

ν is Poisson's ratio



and

$$r^2 = x^2 + y^2 \quad .$$

Using these values he has obtained an expression for the transmitted light intensity T as

$$T = \frac{4 a^2 A^2 \pi^2 t^2 C^2}{\lambda} \frac{x^2}{r^4} \sin^2 (2\theta + 2\beta)$$

where a is the amplitude of the incident plane polarized light
 t is the thickness of the specimen
 C is the mean strain-optic coefficient
 λ is the wave length of the incident light
 β is the angle between the polarizer and the slip direction.

He has also plotted the intensity distribution versus the orientation of the slip direction with respect to the polarizer.

Mendelson analyzed the birefringence due to the dislocations in the glide bands of sodium chloride single crystals.⁸¹ By considering a slip band as being consisted of a row of equally spaced edge dislocations he argues that the stress field between neighboring edge dislocations in the slip band is such that the principal directions are respectively parallel and perpendicular to the Burgers vector. The shear stresses on the planes parallel and perpendicular to the Burgers vector vanish completely midway between any two edge dislocations in an array of edge dislocations of the same sign. This is also true at the points lying directly above and below the dislocation

lines because the shear stresses on such surfaces all add up to zero except for those dislocations which are near the two ends of the array. At all other points the shear stresses on such surfaces almost cancel each other. This leads to the conclusion that one of the principal directions in the stress field of a row of edge dislocations of the same sign is parallel or nearly parallel and the other direction, perpendicular or nearly perpendicular to the slip vector. Therefore when the plane of polarization is parallel to one of these principal directions, most of the light does not go through the analyzer since the Neumann-Maxwell law states "light passing through the stress region is polarized parallel to the direction of the principal stresses in the plane of the wave front at that point." The component of the incident light beam in the other principal direction or the direction of the analyzer is zero and hence the intensity of the transmitted light beam is exceedingly low in such a case.

Based on these concepts of photoelasticity, the photoelastic observations made in this work may now be interpreted in the manner given below:

(i) Screw dislocations

For a single screw dislocation, the difference in the secondary principal stresses in $\{100\}$ and $\{110\}$ planes of observation vanishes resulting in zero intensity of the stress birefringence patterns.

(ii) Edge dislocations

The stress birefringes observed in $\{100\}$ and $\{110\}$ planes must be due to the stress field of edge dislocations as

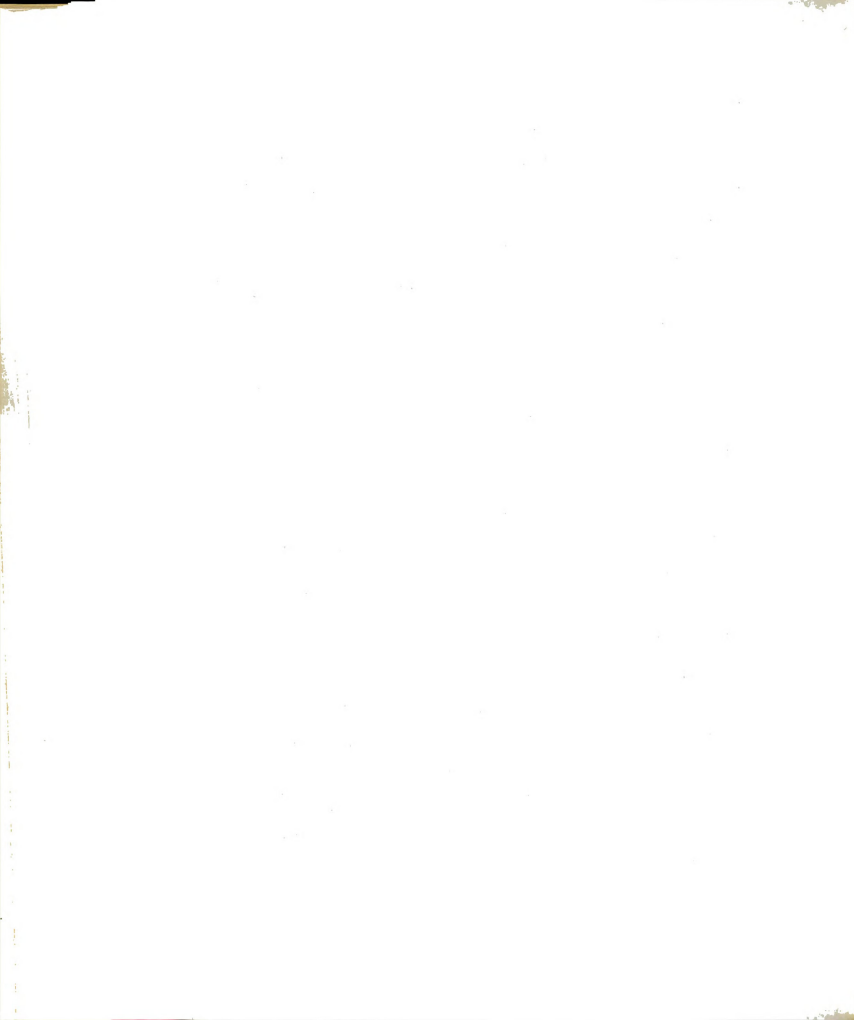
explained below:

(a) $\{100\}$ observations

Figures 9 (a), (b) and (d) show individual spots along the slip bands, whereas figure 9 (c) shows complete extinction of the pattern when the direction of polarization is parallel to the slip vector. One cannot interpret these spots as being due to individual dislocations since were it true, the pattern would not vanish when the direction of polarization is parallel to the slip vector according to Bullough's explanation.

For complete extinction of a point along the isochromatics, the principal directions of the stress field at that point should be parallel to the directions of the polarizer and the analyzer respectively. The present observations agree with the results obtained by Mendelson with plane polarized light in dark field in that there was complete extinction when the plane of polarization was either parallel or perpendicular to the slip vector. The slip bands observed by him were thick and intense, similar to those shown in figure 10.

In the light of Mendelson's explanation one could overcome the difficulty encountered in interpreting the extinction of the photoelastic patterns by Bullough's model. Accordingly each spot can be considered as being due to the stress field of an array of edge dislocations. However, the possibility of having such edge dislocations alone during deformation is very small. Thus the stress field causing the birefringence is probably due to the edge components of the arrays of dislocation loops in the slip plane as shown in figure 24.



(b) $\{110\}$ observations

In $\{110\}$ observations the stress field of the edge dislocation arrays has its two secondary principal directions respectively parallel and perpendicular to the Burgers vector, and therefore the maximum intensity of the stress birefringence patterns is observed when the plane of polarization is at 45° to the Burgers vector. There is complete extinction when the plane of polarization is either parallel or perpendicular to the Burgers vector.

(iii) Mixed dislocations

Mixed dislocations can be treated as being composed of edge and screw components whose contribution to the birefringence patterns varies with the orientation of the mixed dislocation with respect to the Burgers vector. Therefore one may consider the stress birefringence of mixed dislocations as being due to their edge components of reduced strengths only.

In $\{110\}$ observations stress birefringence patterns are seen to be consisted of loops usually lined up in a direction perpendicular to the Burgers vector. These patterns are probably caused by dislocation loops lying in the slip plane. Dislocation loops are in general made up of edge, screw and mixed parts. The stress field of the edge parts and that of the edge components of the mixed parts may give rise to patterns not inconsistent with the observed ones.



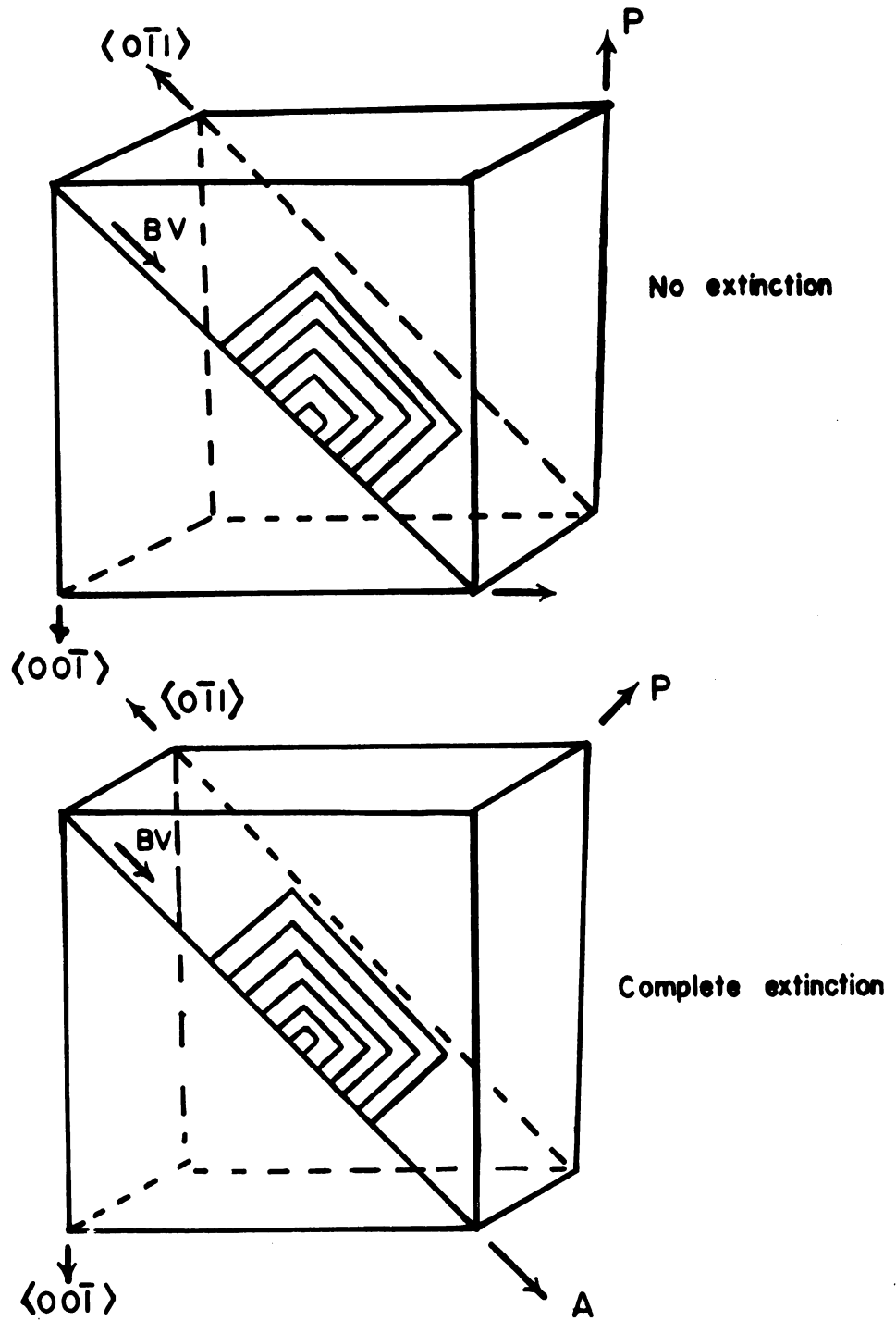


Fig. No. 24

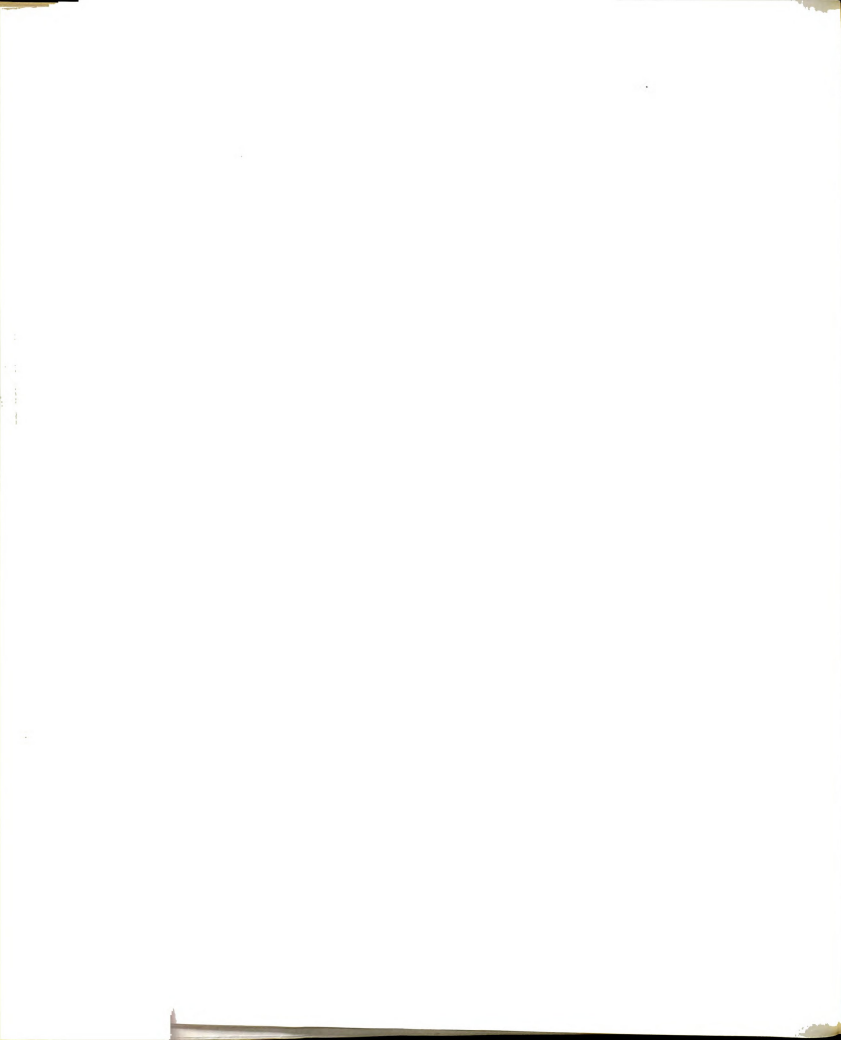
Dependence of contrast on the orientation of the slip vector with respect to the direction of polarization



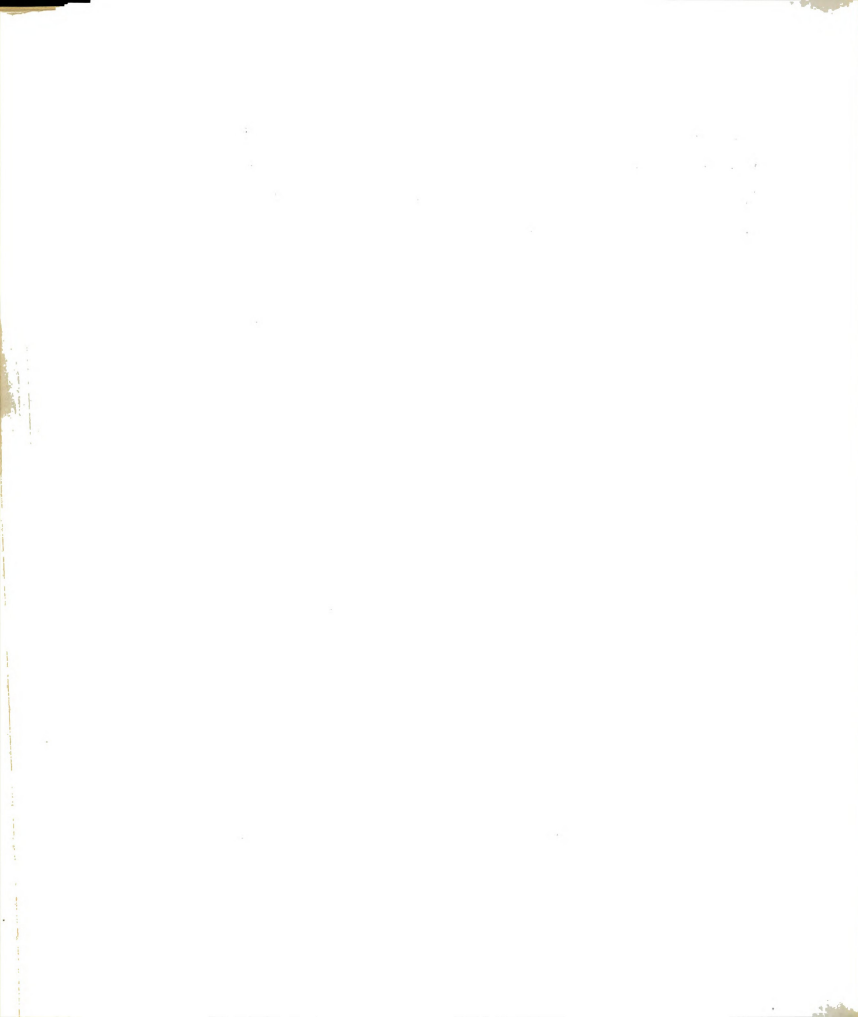
III. Slip Distribution and Work Hardening

It has been experimentally proved by Stokes, Johnston and Li that MgO specimens developing block slip, in which a single slip band expands laterally to fill the entire gage length, are extremely ductile.⁸² Bruneau and Pratt showed that specimens, which develop conjugate as well as non-conjugate slip intersections, work harden much more rapidly than specimens which develop conjugate slip bands alone.⁸³ Nabarro lists the order of increasing rate of shear hardening as (1) simple shear and kinking, (2) single slip, (3) double slip, and (4) quadruple slip.⁸⁴ The increase in work hardening in the specimens which develop non-conjugate slip is interpreted by the above authors in terms of interactions of individual dislocations moving in such non-conjugate slip planes that their Burgers vectors intersect at an angle of 60° . This intersection produces barriers which inhibit further movement of other dislocations.

The results of the present investigation agree in general with the above picture as far as the effects of the conjugate and the non-conjugate slip intersections on work hardening are concerned. However, it seems possible to interpret the work hardening in this type of materials by means of the band structure observed in the slip planes of the deformed bulk crystals rather than the interaction of individual dislocations. The high ductility and the low but finite work hardening of specimens deformed in single slip may be attributed to the formation of the band structure in a single slip system. The hardening in double slip, especially during a non-cyclic



loading, may be due to the interaction of dislocations moving in one slip plane with the band structure in the conjugate slip plane. In the case of non-conjugate slip, the dislocations moving in a slip plane have to cut through many bands which are present in the non-conjugate slip planes with difficulty, thereby causing a maximum work hardening.

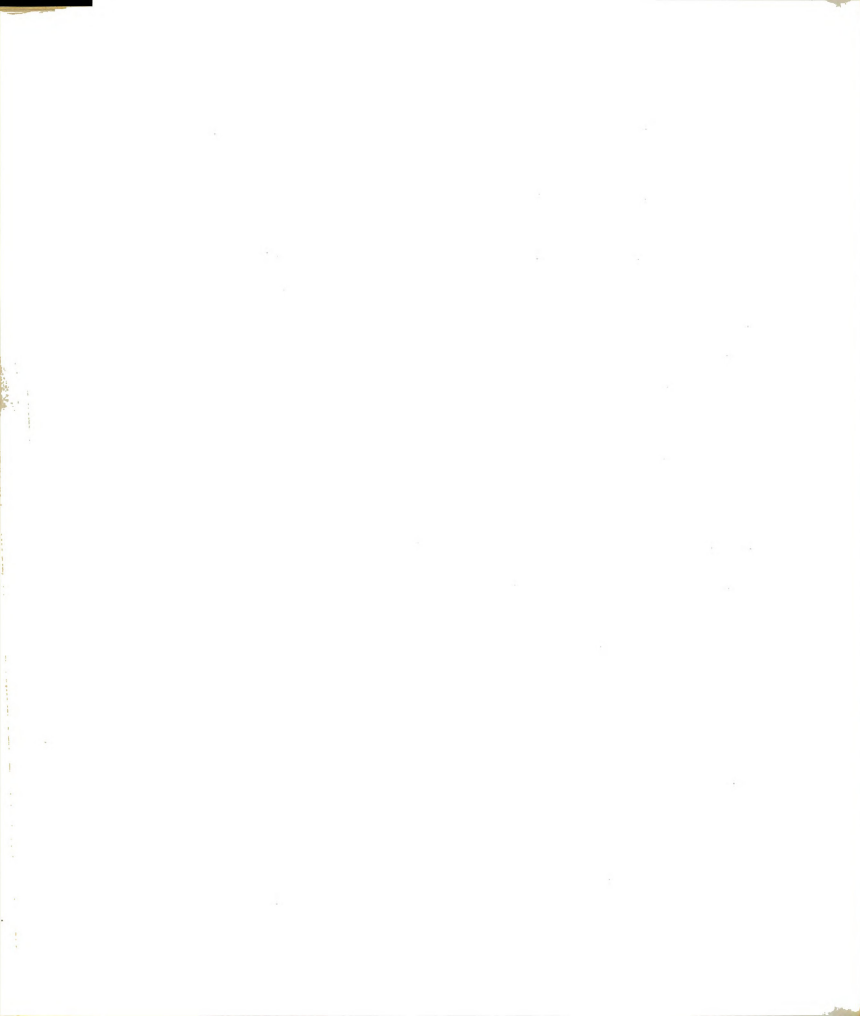


IV. Theory of Band Formation

The damage in the slip plane was made up of bands which were resolved as being consisted of overlapping loops. An interesting aspect of this band formation is that it is usually in a direction perpendicular to the Burgers vector. These bands are similar to the ones observed in zinc where they are classified as deformation bands.²⁴ It is to be discussed later in section (c) of this chapter that intersecting slip may create collinear sources which may contribute to the formation of the band structure. However, this mechanism cannot explain the band structure formation in zinc because the basal plane is the only active slip plane at a moderate stress level and room temperature. There should be a general mechanism of the band formation regardless of the intersecting slip. Extending the idea originated by Frank, Wei has proposed such a mechanism based on the interaction of dislocation loops originating from sources in neighboring atomic planes.²⁴ The following discussion is intended to justify such a mechanism from the interaction energy and force considerations.

(a) Assumptions

It is assumed that random dislocation networks which exist in crystals before deformation starts are the active sources. The grown-in edge dislocations in ionic crystals are pinned by precipitates. These precipitates have been observed in the electron microscopic study of magnesium oxide single crystals.^{28, 30} The pinning is so close that the grown-in edge dislocations cannot act as sources, whereas screw dislocations, which are not pinned by



the impurities in the crystal, act as the sources in the early stages of deformation.

(b) Single Slip

The sources distributed at random are most likely non-coplanar. Some of them may lie in nearby parallel planes. In a set of parallel slip planes in which dislocation loops are expanding due to the applied stress, the loops should have the same Burgers vector. When these expanding loops approach each other the interacting segments can be either edges or screws of the opposite signs or mixed segments whose components are of the opposite signs as shown in figure 25.

(i) Screw Interaction

The interaction force per unit length between two screw dislocations of opposite signs is an attractive force given by

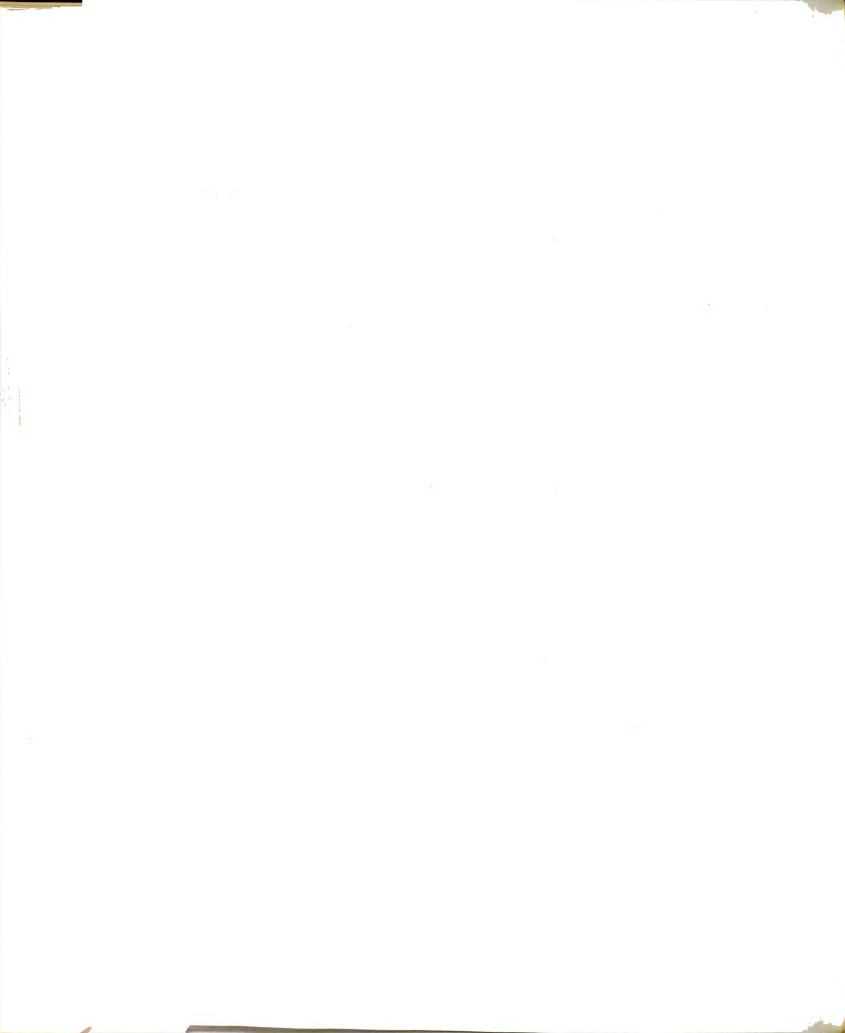
$$F_r = \frac{\mu b^2}{2 \pi r}$$

where r is the distance between the two dislocations,

μ is the shear modulus, and

b is the Burgers vector.

Since cross-slip is difficult in ionic crystals, this attractive force will cause the two screw components to arrange themselves parallel to one another in a plane perpendicular to the slip planes when the separation is a minimum. In the case of a large number of dislocation loops being generated from two neighboring sources and interacting in their screw components, all the screw components will line up in similarly parallel pairs of opposite signs resulting in the formation of a screw-lock. The early stage of the screw-lock



formation can be accomplished relatively easily by the movement of a few pairs. However, after a large number of pairs have been locked, any further addition of the pairs becomes difficult because it requires the movement and rearrangement of all the pairs locked already. The screw-lock becomes a barrier against which the subsequent dislocations may pile up thereby making the source inoperative and causing some degree of work hardening. It seems that screw-locking is a possible cause of band formation in materials that do not have easy cross-slip. It explains why the loops observed in these bands usually line-up in a direction perpendicular to the Burgers vector.

Dislocation Model and Simple Mathematical Analysis of Screw-Lock

A simple mathematical analysis of the screw-lock is presented in this section. This analysis gives only a qualitative or a semi-quantitative picture because of the following assumptions and approximations: (i) the distance between any two dislocations in each slip plane is constant, (ii) there is an equal number of dislocations N in each slip plane, (iii) second order effects are neglected enabling the use of the principle of superposition to calculate the strain energy and the total force for the system.

Formation of the Screw-lock — Strain Energy Considerations

The self energy of a single screw dislocation is given by the formula

$$U_S^s = \frac{\mu b^2}{4\pi} \left[\log_e \left(\frac{r_1}{r_0} \right) - 1 \right]$$



where r_1 is the radius of the surface free of stress
 r_0 is the radius of the dislocation core.

Consider an isolated region away from the free surface as shown in figure 26 (a), and assume that there is no interaction between the top and bottom rows before the screw-lock is formed. The total strain energy $U_{(i)}$ for this arrangement having N dislocations in each slip plane can be calculated by the following equation:

$$U_{(i)} = \frac{2 N \mu b^2}{4 \pi} \left[\log_e \left(\frac{r_1}{r_0} \right) - 1 \right] + 2 U_0$$

where U_0 is a term accounting for the interaction energy between those dislocations within the same slip plane whose spacing does not change during the formation of the screw-lock. The radius r_1 is very large compared with the dimensions of the screw-lock, and can, therefore, be treated as a constant. The difference between r_1 and r_0 is about seven orders so that small variations in r_1 will not affect the calculations appreciably.

Figure 26 (b) shows the dislocation distribution after the screw-lock is formed. In this arrangement, the interaction between dislocations in parallel slip planes cannot be neglected. This interaction energy, U_I^s , for a pair of unlike screw dislocations is given by

$$U_I^s = - \frac{\mu b^2}{2 \pi} \left[\log_e \left(\frac{r_1}{r} \right) - 1 \right]$$

where r is the distance between the dislocations. The total strain energy, $U_{(f)}$, of the screw-lock having N pairs of screw dislocations of opposite signs, becomes



$$U_{(f)} = \frac{2 N \mu b^2}{4\pi} \left[\log_e \left(\frac{r_1}{r_0} \right) - 1 \right] + 2 U_0 + N U_I^s + \Delta U_0$$

where ΔU_0 is the decrease in strain energy due to the interaction of the individual dislocations in the screw-lock with dislocations of the opposite sign in the neighboring pairs. $\Delta U_0 \rightarrow 2 U_0$ when the separation of the slip planes is very small compared to the distances between the neighboring dislocations in each slip plane. It approaches zero when the slip planes are separated by a large distance. The quantity $N U_I^s$ is negative which lowers the energy of the system thereby making the screw-lock configuration more stable. To estimate $N U_I^s$, let $N = 100$ and $\frac{r_1}{r} \approx 10^6$, one obtains $N U_I^s \approx 150$ ev per atomic plane threaded by the screw-lock having 100 pairs.

Stability of the Screw-lock

Once the screw-lock is formed it does not dislodge by itself because it requires an increase in energy to do so. To prove this, consider a screw-lock having N dislocations in each slip plane as shown in figure 27 (i). Let one pair move out leaving $(N-1)$ pairs in the screw-lock as shown in figure 27 (ii). These two configurations have $(N-1)$ common pairs whose self energy as well as interaction energy remain constant in the two cases. The difference in strain energy between these two configurations is the difference between the interaction energy of one extra pair A - B in configuration (i) and the interaction energy of A - D separated by a distance r_3 in configuration (ii). All other interaction energies are the same in the two cases.

The total strain energy $U_{(i)}$ of configuration (i) is



$$U_{(i)} = U' - \frac{\mu b^2}{2\pi} \left[\log_e \left(\frac{r_1}{r_2} \right) - 1 \right]$$

and that of configuration (ii) $U_{(ii)}$ is

$$U_{(ii)} = U' - \frac{\mu b^2}{2\pi} \left[\log_e \left(\frac{r_1}{r_3} \right) - 1 \right]$$

where U' is a constant which includes the self energy of $2N$ dislocations and the interaction energy of $(N-1)$ pairs within themselves and with A - B or A - D, r_2 is the distance between the two slip planes under consideration, r_3 is the distance between the dislocations A and D in configuration (ii).

Therefore the difference ΔU in total strain energy in both the configurations is given by

$$\begin{aligned} \Delta U &= U_{(ii)} - U_{(i)} \\ &= - \frac{\mu b^2}{2\pi} \left[\log_e \left(\frac{r_1}{r_3} \right) - \log_e \left(\frac{r_1}{r_2} \right) \right] \\ &= - \frac{\mu b^2}{2\pi} \log_e \left(\frac{r_2}{r_3} \right) \\ &= \frac{\mu b^2}{2\pi} \log_e \left(\frac{r_3}{r_2} \right) . \end{aligned}$$

Assuming $r_2 = 10 b$ and $r_3 = 1000 b$, this gives an increase in strain energy of approximately 4 ev per atomic plane threaded by the screw-lock. So the first configuration is stable, and once the screw-lock is formed it will not dislodge itself.



Forces associated with the formation of the screw-lock

Consider two rows of screw dislocations coming from two different sources lying in different slip planes near each other and separated by a distance y as shown in figure 28 (a). Each row has N dislocations uniformly separated by a distance x . Due to the applied shear stress τ , the top row is moving to the left and the bottom row is moving to the right which is designated as the positive direction. Only the forces acting in the X-direction will be responsible for the formation of the lock.

Consider figure 28 (b) in which two rows having N dislocations each overlap each other by N' number of dislocations. The force F_x acting on the leading dislocation of the bottom row is given by

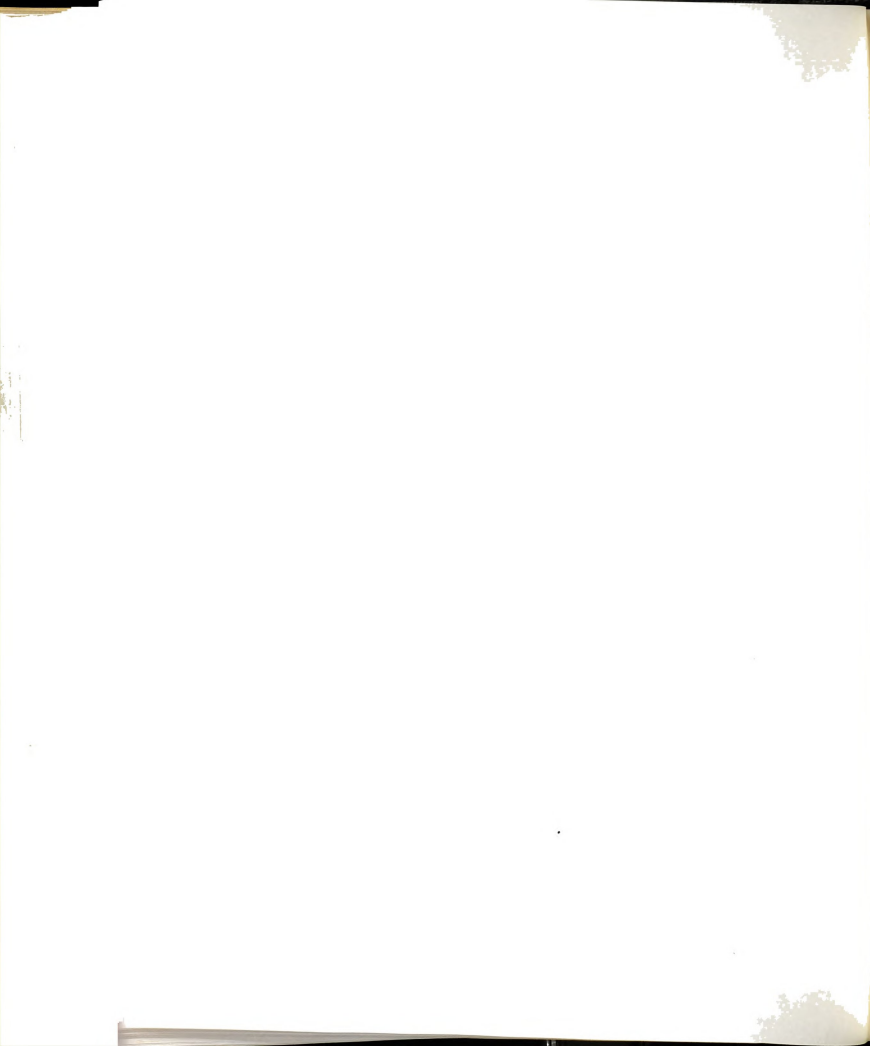
$$F_x = \frac{\mu b^2}{2\pi} \left\{ \left[- \sum_{n=1}^{N'-1} \frac{nx}{(nx)^2 + y^2} \right] + \left[\sum_{n=1}^{N-N'} \frac{nx}{(nx)^2 + y^2} \right] \right\} \\ + \frac{\mu b^2}{2\pi x} \left[\sum_{n=1}^{N-1} \frac{1}{n} \right] + \tau b$$

where $-\frac{\mu b^2}{2\pi} \sum_{n=1}^{N'-1} \frac{nx}{(nx)^2 + y^2}$

is the -X component of the attractive forces due to the dislocations to the left of the leading dislocation in the top row,

$+\frac{\mu b^2}{2\pi} \sum_{n=1}^{N-N'} \frac{nx}{(nx)^2 + y^2}$

is the +X component of the attractive forces due to the dislocations to the right of the leading dislocation in the top row,



$$\frac{\mu}{2\pi x} \frac{b^2}{\sum_{n=1}^{N-1} \frac{1}{n}}$$

is the +X component of the repulsive forces due to the dislocations lying to the left of the leading dislocation in the same slip plane, and τb is the force due to the applied stress.

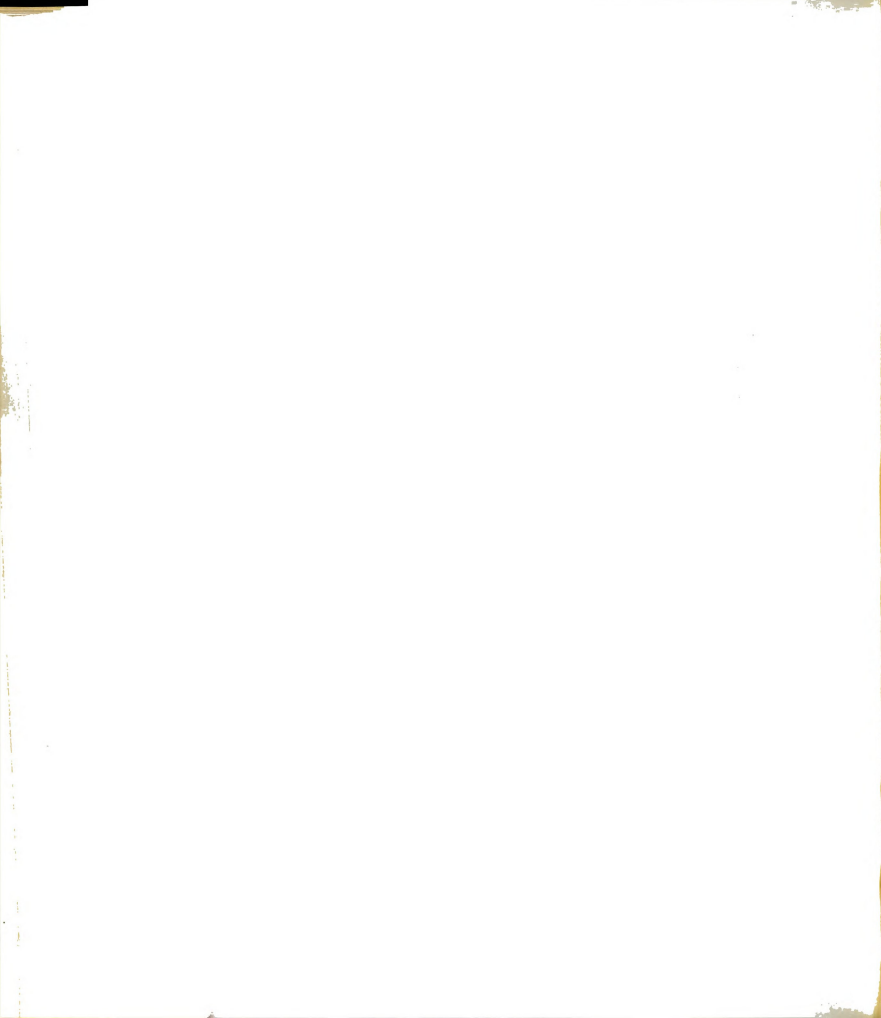
When the leading dislocation of the two rows approach each other as shown in figure 28 (a) the first component is zero, and all the remaining three are directed in the +X direction and, therefore, help the formation of a screw-lock. When the first pair in the screw-lock is formed

$$F_x = \frac{\mu b^2}{2\pi} \left[\sum_{n=1}^{N-1} \frac{nx}{(nx)^2 + y^2} \right] + \frac{\mu b^2}{2\pi x} \left[\sum_{n=1}^{N-1} \frac{1}{n} \right] + \tau b .$$

As the rows move passing each other further, the -X component of the attractive forces due to the dislocation to the left of the leading dislocation in the top row becomes appreciable and thus reduces the value of F_x . When the two rows overlap by $\frac{N}{2}$ dislocations in each row the positive and negative X-components of the attractive forces due respectively to the dislocations lying to the right and left cancel each other. After the leading dislocation crosses this point, the net X-component of the attractive forces will be in the -X direction and thus oppose the applied force and the +X component of the repulsive forces. However, the X-component of the net resultant force will be in the +X direction, facilitating the formation of as many pairs as possible before the leading dislocation stops.

Force Field Components in the Central Portion of the Screw-lock

Consider the central portion of the screw-lock consisting of three pairs of dislocations as shown in figure 29 (a) with no applied



force. Dislocation 1 experiences interaction forces due to dislocations 2 through 6. For any pair of screw dislocations the radial interaction force

$$F_r = \frac{\mu b^2}{2\pi r}$$

has components

$$F_x = \frac{\mu b^2 x}{2\pi (x^2 + y^2)}$$

$$F_y = \frac{\mu b^2 y}{2\pi (x^2 + y^2)} \quad .$$

The repulsive forces between dislocations 1 and 3 and 1 and 2 are of equal magnitude and opposite in sign. They will cancel each other. The X-components of the attractive forces between 1 and 4 and 1 and 6 are of equal magnitude and opposite in sign. They too will cancel each other. The attractive force between 1 and 5 does not have any components in the X-direction. Thus the dislocation 1, in the central portion of the screw-lock experiences no net resultant force in the X-direction due to the immediate neighboring pairs. The force due to interaction between this dislocation and the next pairs on either side or the pairs beyond will be very weak. Generalizing this idea, it can be said that most of the dislocations in the central portion, except the ones near the outer edges of the screw-lock, experience no or very little net force in the X-direction.

The resultant force F_y on dislocation 1 of a screw-lock having $(2N + 1)$ pairs of dislocations is

$$F_y = \frac{\mu y}{2\pi} \left\{ \frac{b^2}{y^2} + 2 \sum_{n=1}^N \frac{b^2}{(nx)^2 + y^2} \right\} \quad .$$



In the series $\sum_{n=1}^N \frac{b^2}{(nx)^2 + y^2}$ both x and y are greater than b and n is a finite number having integral values between 1 and N . The denominator $(nx)^2 + y^2$ is always greater than the numerator b^2 . Therefore, the series has a finite sum, and it converges fast. Assuming that $y = 10b$ and $x = 100b$, the error in considering the first term alone is less than three percent and the error in considering the first two terms is less than one percent. Thus for all practical purposes the first term will be sufficient to give the approximate force in the Y -direction.

The magnitude of F_y determines if cross-slip will take place. For ionic crystals the stress required for cross-slip through the secondary slip plane is ten to twelve times the stress required for primary slip. Knowing this one can determine a maximum value of y beyond which cross-slip will not take place. The maximum value so obtained is of the order of $10b$.

(ii) Edge Interaction

The interaction force field between two edge dislocations of opposite signs has the following components:

$$F_x = \frac{\mu b^2}{2\pi(1-\nu)} \frac{x(x^2 - y^2)}{(x^2 + y^2)^2}$$

$$F_y = \frac{\mu b^2}{2\pi(1-\nu)} \frac{y(3x^2 + y^2)}{(x^2 + y^2)^2}$$

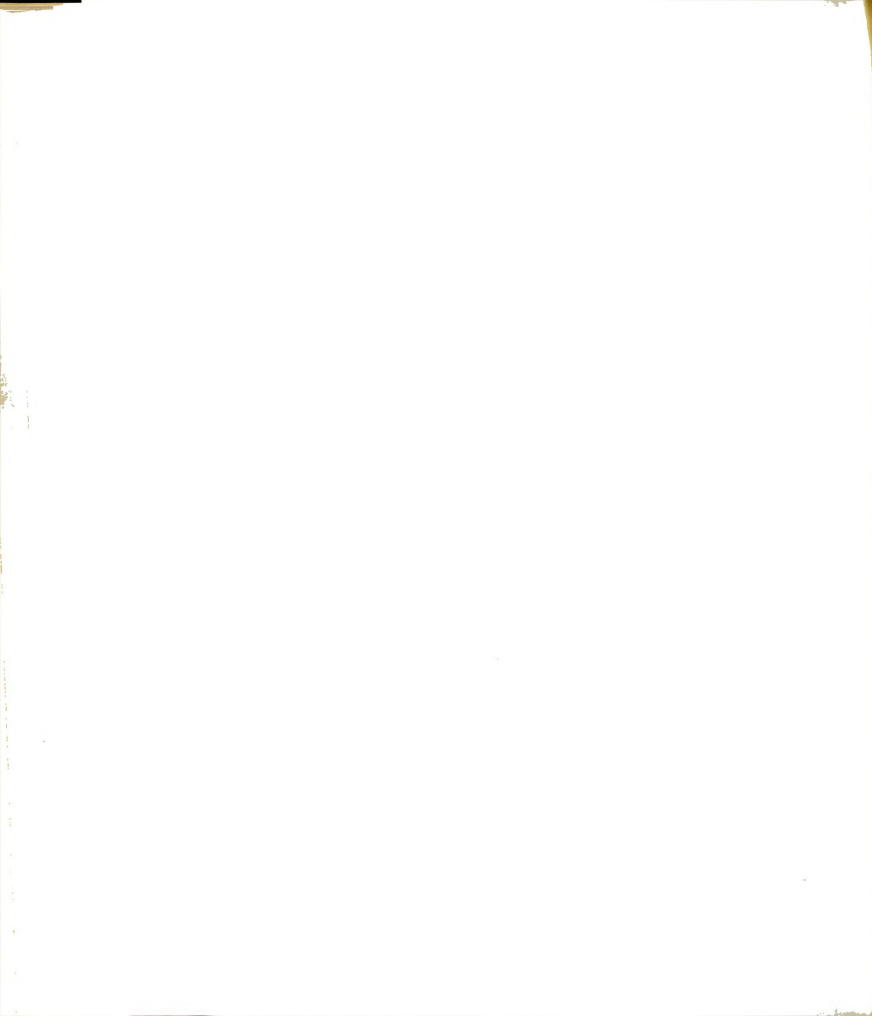
where x and y are the coordinates of one of the dislocations with respect to the other at the origin, with X -axis along the direction of the Burgers vector and Y -axis perpendicular to the slip plane. The



component F_x is attractive when $|x| > |y|$ and is repulsive when $|x| < |y|$. In the absence of applied stresses and dislocation climb the equilibrium configurations of these dislocations are at $|x| = |y|$ and at $x = 0$. Under an applied shear stress τ acting on the slip plane in the slip direction and for a particular value of the distance between the slip planes y , the value of x will depend on the applied stress τ . When τ is greater than $\mu b/8\pi(1-\nu)y$, the dislocations will cross over and move away from each other, otherwise, they will attain an equilibrium configuration when the repulsive force component becomes equal and opposite to the applied force resulting in a plus-minus pair.

In the early stage of deformation when the randomly distributed sources are operating, the sources will probably be in planes which are far apart. There will be no severe interaction between the individual dislocations due to their short range stress fields. If the approaching segments are edge components of opposite signs, they can cross over easily. However, when two arrays of edge dislocations in parallel planes approach each other this will not be the case because of their long range stress fields.

Consider the interaction of a positive and a negative edge dislocation arrays moving in slip planes separated by a large distance a . The stress field of a finite set of uniformly spaced horizontal edge dislocation array has the following stress components at distances comparable to its finite width $2L$.⁸⁵



$$\begin{aligned}
\sigma_{xx} &= -2 \tan^{-1} \left[\frac{2Ly}{x^2 + y^2 - L^2} \right] \\
&\quad - y \left[\frac{x-L}{(x-L)^2 + y^2} - \frac{x+L}{(x+L)^2 + y^2} \right] \\
\sigma_{yy} &= y \left[\frac{x-L}{(x-L)^2 + y^2} - \frac{x+L}{(x+L)^2 + y^2} \right] \\
\sigma_{zz} &= -2 \nu \tan^{-1} \left[\frac{2Ly}{x^2 + y^2 - L^2} \right] \\
\sigma_{xy} &= -\frac{1}{2} \log_e \left[\frac{(x-L)^2 + y^2}{(x+L)^2 + y^2} \right] \\
&\quad - \frac{y^2}{(x-L)^2 + y^2} + \frac{y^2}{(x+L)^2 + y^2} \\
\sigma_{yz} &= \sigma_{xz} = 0
\end{aligned}$$

in units of

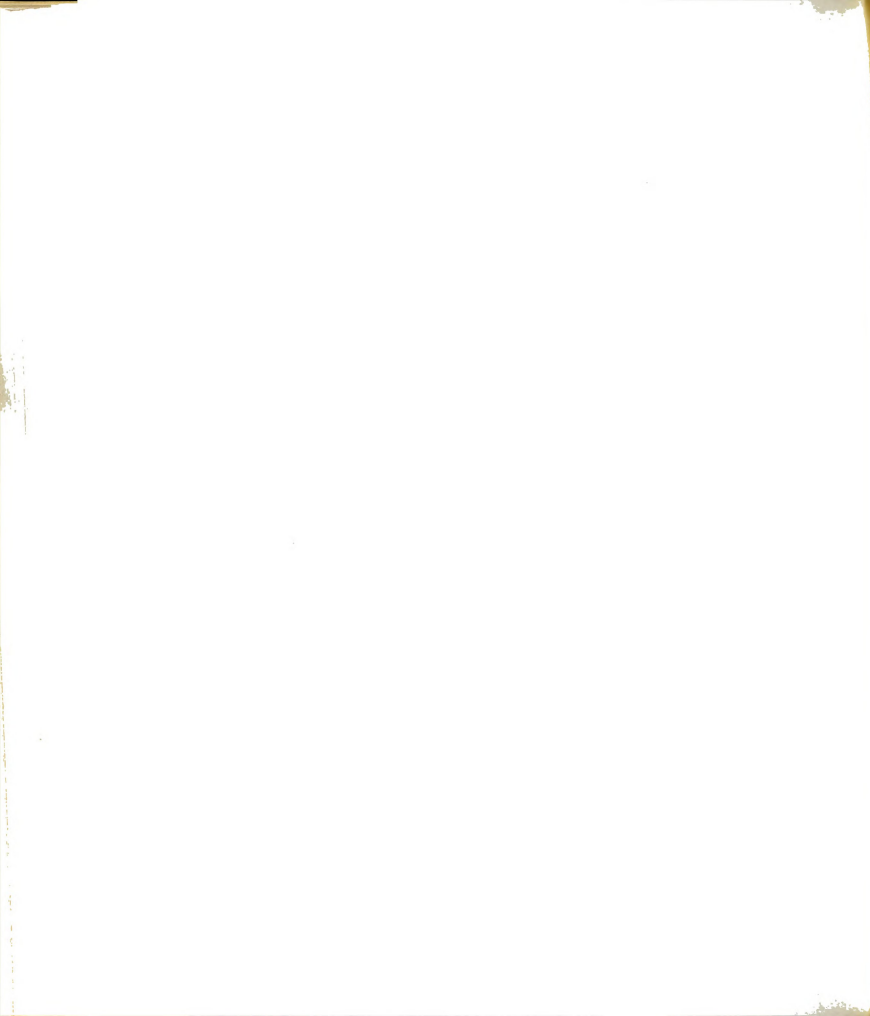
$$\frac{\mu b}{2\pi h (1 - \nu)}$$

where L is the half width of the array, viz, $L = \frac{Nh}{2}$

N is the total number of dislocations

h is the spacing between dislocations in the array.

At larger distances compared with the width of the array, the above stress components reduce to those of a single "super-dislocation" of strength Nb situated at the center of the array. In such a case their interaction can be considered as that of two super-dislocations of strength Nb each, which have long range stress fields instead of the short range stress fields of single



edge dislocations as discussed above. The minimum shear stress τ required to cross over will depend on the separation a of the two slip planes and is given by

$$\tau = \frac{\mu b'}{8\pi(1-\nu)a}$$

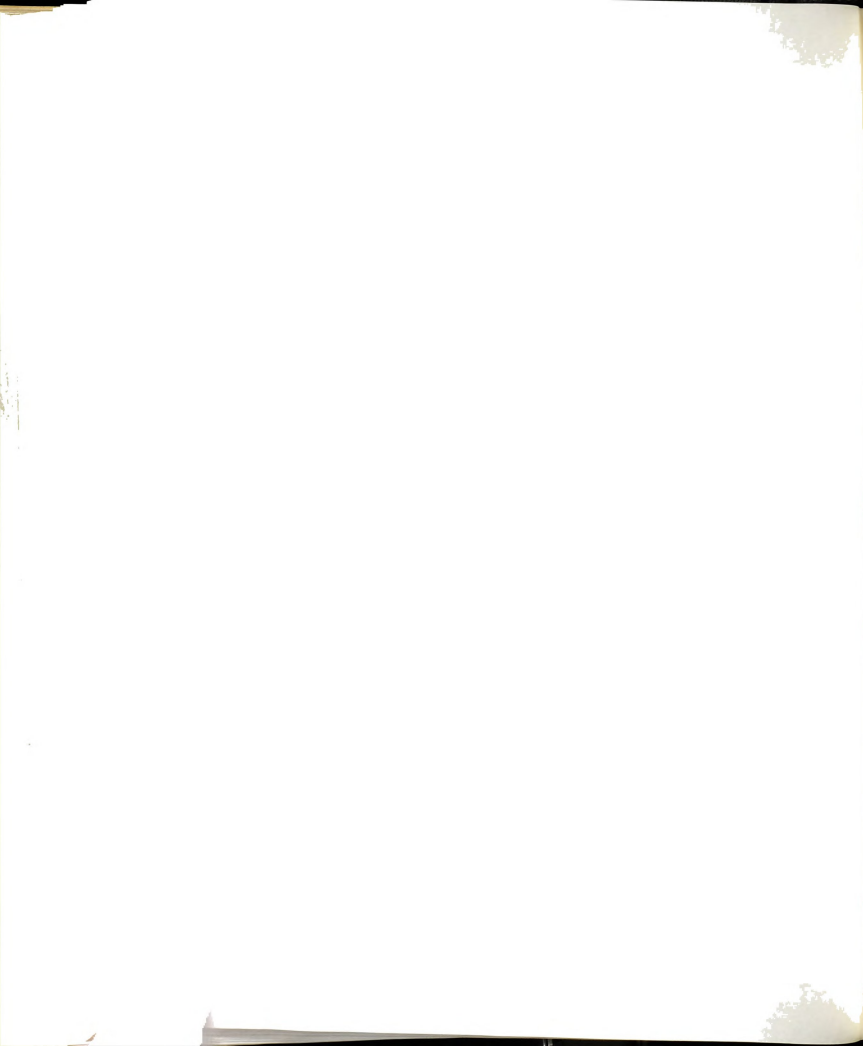
where

$$b' = Nb$$

When a is small the shear stress τ is very large and the cross over does not take place. The dislocations, then, reach an equilibrium configuration having a horizontal separation x as a function of a . In the absence of applied shear stresses and dislocation climb, the dislocation arrays would reach an equilibrium configuration when the line connecting their centers of gravity makes an angle of 45° with the slip plane.

As deformation proceeds, the dislocations moving in nearby planes will approach each other resulting in a configuration shown in figure 30 (b) which may be transformed into the configuration shown in figure 30 (c) by rearrangement of the dislocations through a climb process — a model for the deformation bands as suggested by Mott.

In the case of single edge dislocations moving in nearby slip planes the short range forces play a prominent role. For slip planes approximately 10^8 \AA apart the dislocations cannot pass over each other since the applied stress required is very high, being of the order of one hundredth of the theoretical shear strength. Therefore, they will form a plus-minus pair which is sometimes termed as debris.



For the interaction of two arrays of edge dislocations in nearby slip planes as shown in figure 31 (a), the plus-minus pair formed by the two leading dislocations as indicated above, acts as a barrier against which the rest of the dislocations pile up. The net force F_{x_A} acting on the leading dislocation A may be calculated by considering one array as a pile-up and the other having uniformly spaced dislocations with δ being the space between neighboring dislocations is

$$\begin{aligned}
 F_{x_A} &= (N - 1) \tau b \\
 &+ \frac{\mu b^2}{2\pi(1 - \nu)} \sum_{n=2}^N \frac{[(n-1)\delta + x] \{ [(n-1)\delta + x]^2 - y^2 \}}{\{ [(n-1)\delta + x]^2 + y^2 \}^2} \\
 &+ \tau b + \frac{\mu b^2}{2\pi(1 - \nu)} \frac{x(x^2 - y^2)}{(x^2 + y^2)^2}
 \end{aligned}$$

where the first term accounts for the stress concentration, the second term includes the interaction force components due to dislocations in the other plane with the dislocation A and the third term is the force due to the applied stress. If N is large, F_x may become a driving force sufficiently high enabling A to cross over.

The process may repeat, and after two dislocations have formed pairs as shown in figure 31 (b) the net force F_x acting on the second dislocation is



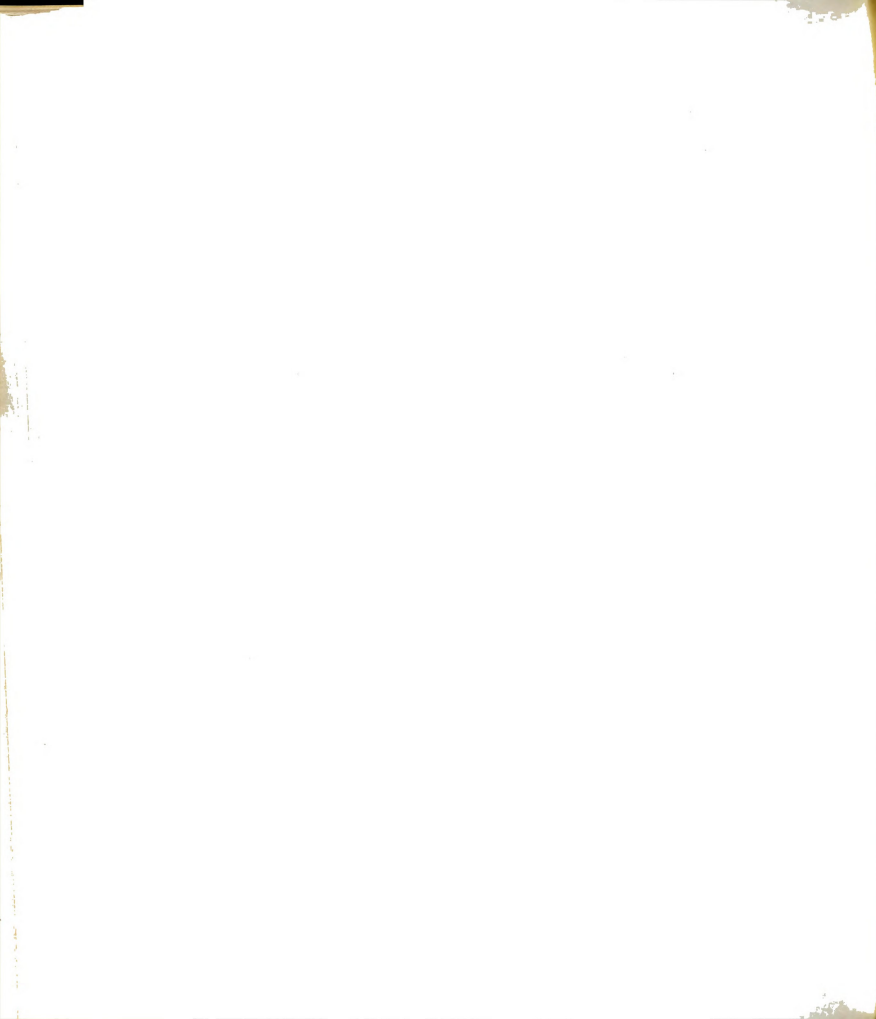
$$\begin{aligned}
F_{x_B} &= (N - 2) \tau b \\
&+ \frac{\mu b^2}{2\pi(1-\nu)} \sum_{n=3}^N \frac{[(n-1)\delta + x] \{ [(n-1)\delta + x]^2 - y^2 \}}{\{ [(n-1)\delta + x]^2 + y^2 \}^2} \\
&+ \tau b + \frac{\mu b^2}{2\pi(1-\nu)} \frac{x(x^2 - y^2)}{(x^2 + y^2)^2} .
\end{aligned}$$

The contribution due to interaction with the leading pair containing dislocation A is, however, negligible. If this process is repeated until N' pairs have formed, the net force acting on the N' th dislocation is

$$\begin{aligned}
F_{x_{N'}} &= (N - N') \tau b + \frac{\mu b^2}{2\pi(1-\nu)} \sum_{n=N'+1}^N \frac{[(n-1)\delta + x] \{ [(n-1)\delta + x]^2 - y^2 \}}{\{ [(n-1)\delta + x]^2 + y^2 \}^2} \\
&+ \tau b + \frac{\mu b^2}{2\pi(1-\nu)} \frac{x(x^2 - y^2)}{(x^2 + y^2)^2} .
\end{aligned}$$

It is evident from this expression that as N' increases $F_{x_{N'}}$ decreases, and eventually the two rows will stop against each other.

The above considerations lead to the conclusion that the leading dislocations, by forming one or more plus-minus pairs, hold the rest of the dislocations against each other resulting in a back stress. When a sufficient number of edge dislocations have piled up against the plus-minus pairs the back stress will build upto a level making the sources inoperative.



(iii) Interaction of Two Sets of Dislocation Loops on Parallel Slip Planes

When the expanding dislocation loops lying on parallel slip planes approach each other, the interacting segments can be either edges or screws of opposite signs or mixed as shown in figure 25. As discussed earlier, the interaction of the screw components will form the screw-lock which is a stable configuration and causes work hardening. The interaction of the edge components will lead to the formation of plus-minus pairs and dislocation pile-ups. The sources will soon become inoperative due to the back stress of the pile-ups. It can be shown that the interaction between mixed dislocations may also lead to the formation of screw-lock, because it has the lowest strain energy.

Consider two dislocation loops originated from two different sources lying in different slip planes, approach and interact with each other. For simplicity of discussion of the mechanism, assume the two loops are semi-circular of equal diameters and form either a mixed, an edge, or a screw dipole as shown in figures 32 (a), (b) or (c) respectively. The total dislocation length and the slipped area are the same in all three configurations. The dislocation segments other than the dipole segments are also of the same length irrespective of the type of dipole under consideration and will thus have approximately the same energy. Hence the difference in the strain energies of these configurations is due to the difference in the strain energy of the dipole segments only. The strain energy of the dipole segment depends on its orientation with respect to the

Burgers vector. It is sufficient, therefore, to consider the strain energy per unit length of the dipole as a function of its orientation because all the three dipoles have the same length.

The self energy per unit length of an edge dislocation is

$$U_S^e \approx \frac{\mu b^2}{4\pi(1-\nu)} \left[\log_e \left(\frac{r_1}{r_0} \right) - 1 \right]$$

and that of a screw dislocation is

$$U_S^s \approx \frac{\mu b^2}{4\pi} \left[\log_e \left(\frac{r_1}{r_0} \right) - 1 \right] .$$

The mixed dislocation can be treated as a superposition of an edge dislocation and a screw dislocation having their Burgers vector perpendicular to each other. The strength of the edge component is $b \sin \theta$ and that of the screw component is $b \cos \theta$, where θ is the angle between the dislocation line and the Burgers vector.

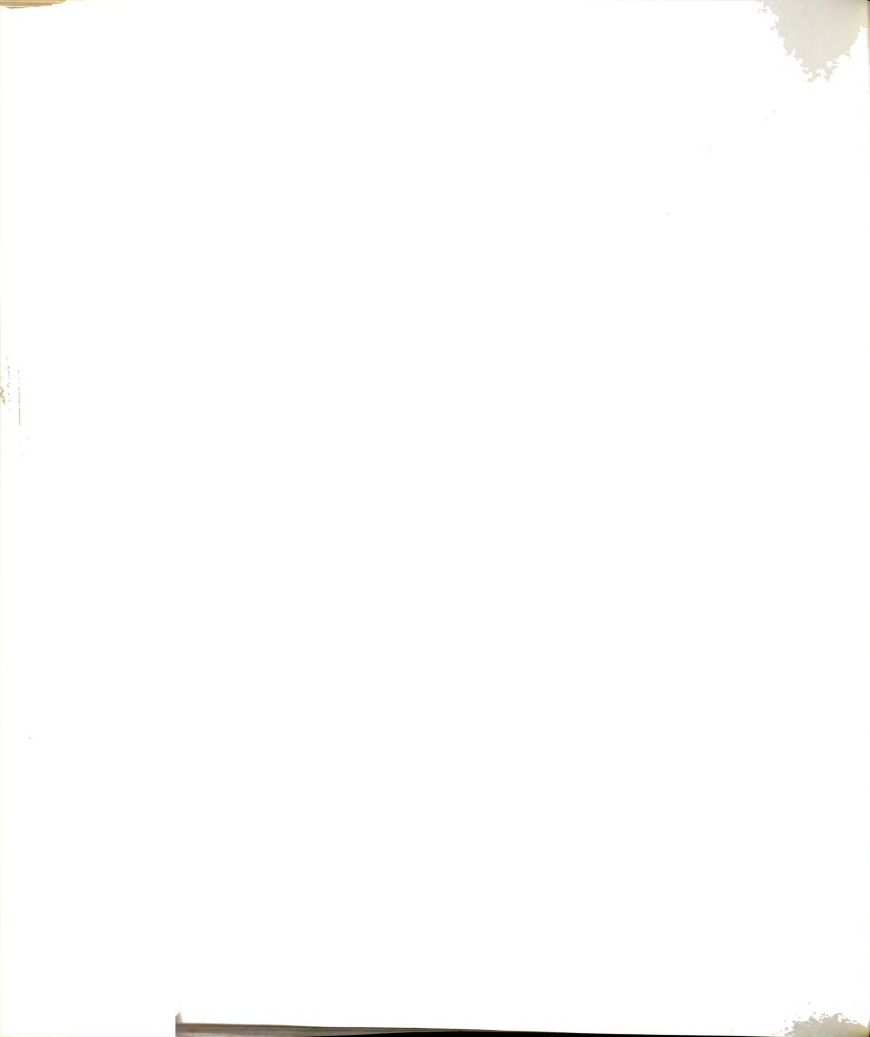
The self energy per unit length of the mixed dislocation is

$$\begin{aligned} U_S^m &\approx \frac{\mu b^2}{4\pi} \left[\log_e \left(\frac{r_1}{r_0} \right) - 1 \right] \left[\frac{\sin^2 \theta}{1-\nu} + \cos^2 \theta \right] \\ &= \frac{\mu b^2}{4\pi(1-\nu)} \left[\log_e \left(\frac{r_1}{r_0} \right) - 1 \right] [1 - \nu \cos^2 \theta] . \end{aligned}$$

The interaction energy per unit length between two edge dislocations is

$$U_I^e = - \frac{\mu b^2}{2\pi(1-\nu)} \left[\log_e \left(\frac{r_1}{r} \right) + \frac{1}{2} \cos 2\phi - 1 \right]$$

where r and ϕ are the polar coordinates of one of the dislocations with respect to the other at the origin.



For a stable configuration of the edge dipole ϕ is equal to 45° . The interaction energy per unit length of the edge dipole is thus

$$U_I^e = - \frac{\mu b^2}{2\pi(1-\nu)} \left[\log_e \left(\frac{r_1}{r} \right) - 1 \right] .$$

Similarly the interaction energy per unit length of the screw dipole is

$$U_I^s = - \frac{\mu b^2}{2\pi} \left[\log_e \left(\frac{r_1}{r} \right) - 1 \right] .$$

Therefore, the interaction energy per unit length of a mixed dipole is

$$\begin{aligned} U_I^m &= - \frac{\mu b^2}{2\pi} \left[\log_e \left(\frac{r_1}{r} \right) - 1 \right] \left[\frac{\sin^2 \theta}{(1-\nu)} + \cos^2 \theta \right] \\ &= - \frac{\mu b^2}{2\pi(1-\nu)} \left[\log_e \left(\frac{r_1}{r} \right) - 1 \right] \left[1 - \nu \cos^2 \theta \right] . \end{aligned}$$

The total energy of a mixed dipole is thus

$$\begin{aligned} U_T^m &= U_I^m + 2 U_S^m \\ &= \frac{\mu b^2}{2\pi(1-\nu)} \left[\log_e \left(\frac{r_1}{r_0} \right) - 1 \right] \left[1 - \nu \cos^2 \theta \right] \\ &\quad - \frac{\mu b^2}{2\pi(1-\nu)} \left[\log_e \left(\frac{r_1}{r} \right) - 1 \right] \left[1 - \nu \cos^2 \theta \right] \\ &= \frac{\mu b^2}{2\pi(1-\nu)} \left[\log_e \left(\frac{r}{r_0} \right) \right] \left[1 - \nu \cos^2 \theta \right] . \end{aligned}$$

When θ is zero, it gives the total energy of the screw dipole U_T^s and when θ is 90° , it gives the total energy of the edge dipole U_T^e . A plot of U_T^m versus θ as shown in figure 33 gives a monotonically increasing value of U_T^m as θ changes from 0° to 90° . Therefore, the screw dipole having $\theta = 0^\circ$ has the lowest energy and hence is



the most stable configuration. The slope of this curve gives the torque acting on the dipole and it is zero when the dipole is in either the edge or the screw orientation. It has a maximum value when the dipole is at an angle of 45° with the Burgers vector. This torque will cause a mixed dipole to reorient to the screw orientation and facilitate the formation of the screw-lock. The distance between the two dislocation segments of the edge dipole will be $\sqrt{2}$ times the distance between the two of the screw dipole. This leads to a small increase in the difference in strain energy between the two configurations.

This difference will be enhanced further when N dislocation loops generated from each of two neighboring sources in two parallel slip planes interact. When the interaction is of the screw type the total strain energy will be that of N screw dipoles and thus it will be N times the total energy of an individual screw dipole. For the edge type interaction, however, the total strain energy will be the energy of the first few edge dipoles plus the self energies of the dislocations held up against the edge dipoles. Interaction between dislocations of opposite signs always reduces the total energy thereby making the total energy of the screw type interaction lower than that of the edge type interaction where the lowering is due to one or a few dipoles only. This will make the difference between the total strain energy of the screw interaction and the edge interaction still greater. These arguments lead to the conclusion that the screw interaction is the most stable configuration and can, therefore, be called screw-lock. So the mixed components should reorient them-



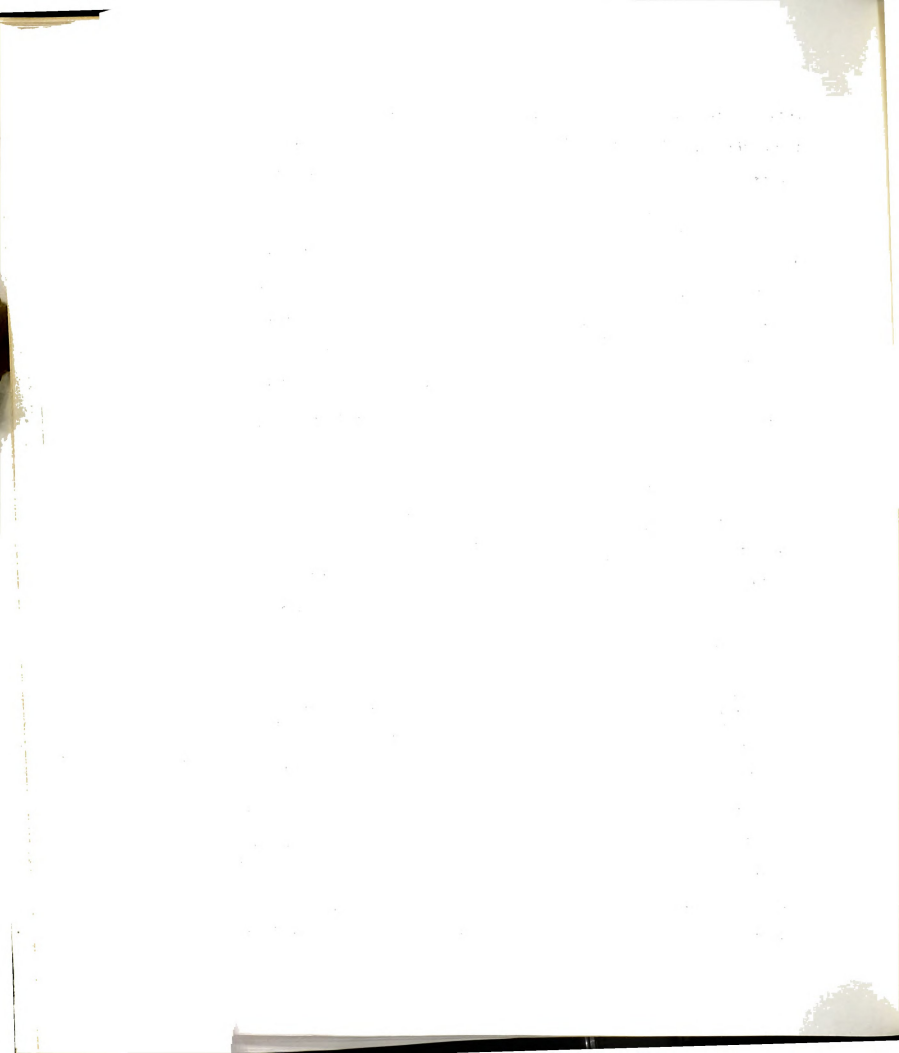
selves to form the screw-lock as long as the energy decrease due to reorientation is greater than the energy required to increase the dislocation length sufficiently to make this configuration possible.

(iv) Development of Deformation Bands

As discussed above, the interaction of dislocation loops generated from sources in neighboring parallel planes may give rise to screw-locks which, in turn, result in the formation of a band structure in a general direction perpendicular to the slip vector. The screw-lock formed in this manner should be the major factor contributing to the band formation in crystals which deform by a single slip system.

The lithium fluoride crystals had a grown-in dislocation density of about 2.5×10^4 dislocations per square centimeter. Assuming an even distribution, the distance between two neighboring sources should be approximately 60 microns. This should produce loops of approximately 60 microns diameter, which is of the same order of magnitude as the observed value of 20 microns.

The defect structure shown in figure 18 appears like three dimensional dislocation networks and it resembles the dislocation networks observed in sodium chloride crystals by the decoration techniques.³⁶ These networks are probably not resulted from deformation since in such a case dislocation loops usually arrange themselves along a direction perpendicular to the Burgers vector or along the non-conjugate slip intersections as has been observed throughout this investigation. This suggests that they are the grown-in three-dimensional dislocation networks. In addition the spacing



between the dislocations in this picture is of the same order as the spacing calculated by assuming a uniform distribution of the grown-in dislocations using the dislocation density data obtained by the etch-pit technique.

(c) Multiple Slip — Development of Deformation Bands Parallel to the Line of Intersection of the Slip Planes.

The mechanism of band formation discussed so far should have general applicability to most materials. It can be the controlling mechanism in materials with no intersecting primary slip planes such as zinc. However, for ionic crystals there seems to be acting at the same time an alternate mechanism as observed in lithium fluoride and discussed below. As shown in figure 19 the band structure may also be considered as being formed along the direction of the intersection of the primary slip planes.

Consider two intersecting conjugate slip planes A and B as shown in figure 34. In plane A there are two dislocation loops (I and II) expanding due to applied stress. The two loops may, however, be in nearby parallel planes. In the intersecting slip plane B a source is operating and is generating dislocation loops which intersect with the expanding loops in plane A. The loops I and II will thus acquire jogs which become larger and larger as more intersections take place. The jog acquired by loop I will be larger than that of loop II because it is intersected by more dislocations. These jogs act as pinning points and the segments in the planes A' and A'' may act as new sources of dislocations as shown in figure 34 (c) and (d). Loops generated from these sources may develop



into the observed band structure.

The sources will operate in parallel planes A' , A'' , etc. which, when viewed in a direction normal to these sets of planes, will appear to lie along the line of intersection of planes A and B . This line is perpendicular to the slip vector for the conjugate slip intersection. For non-conjugate slip planes the intersection line is inclined to the slip vector as seen in figure 19. From this point on the general mechanism of loop interaction discussed above takes over and screw-locks are formed in the case of conjugate slip plane intersections. In the case of non-conjugate slip plane intersections the interacting dislocations are mixed in nature. Since the dislocation loops are aligned before the interaction takes place, they would have to increase their lengths by a large proportion to form screw-locks. So the interacting dislocations may stay as mixed dipoles when the band structure is not fully developed.

The band formation in directions other than the one perpendicular to the slip vector was observed in one specimen only. This specimen was thick and had a complicated stress pattern. In a number of specimens where non-conjugate slip was present, no band structure was developed along the line of intersection. The bands shown in figure 19, which are due to non-conjugate slip intersection, have poor contrast compared to the bands observed along the line of intersection of the conjugate slip systems indicating that the general mechanism of band formation in a direction perpendicular to the slip vector is perhaps more important than the mechanism discussed here.



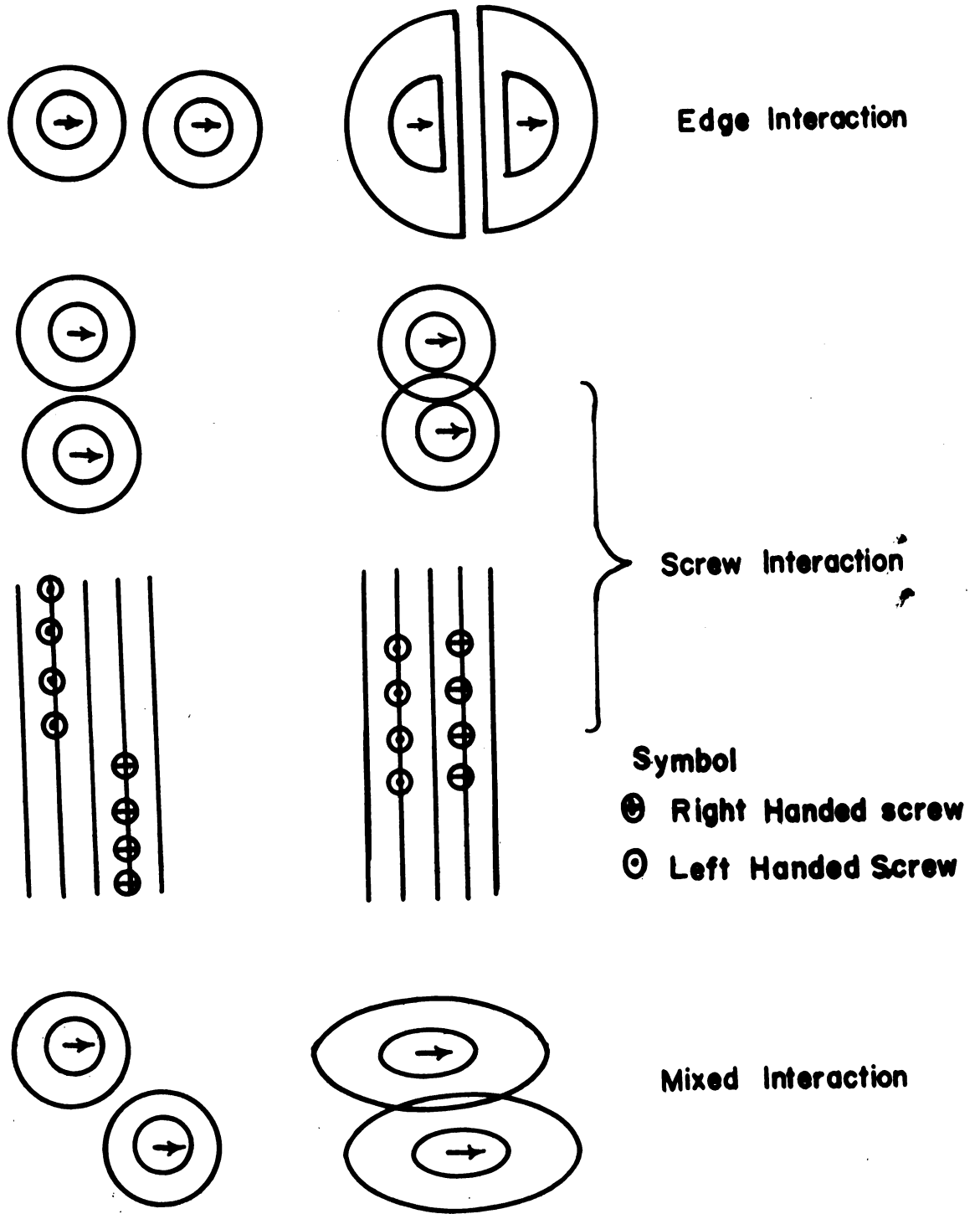


Fig. No. 25

General Mechanism of Band Formation



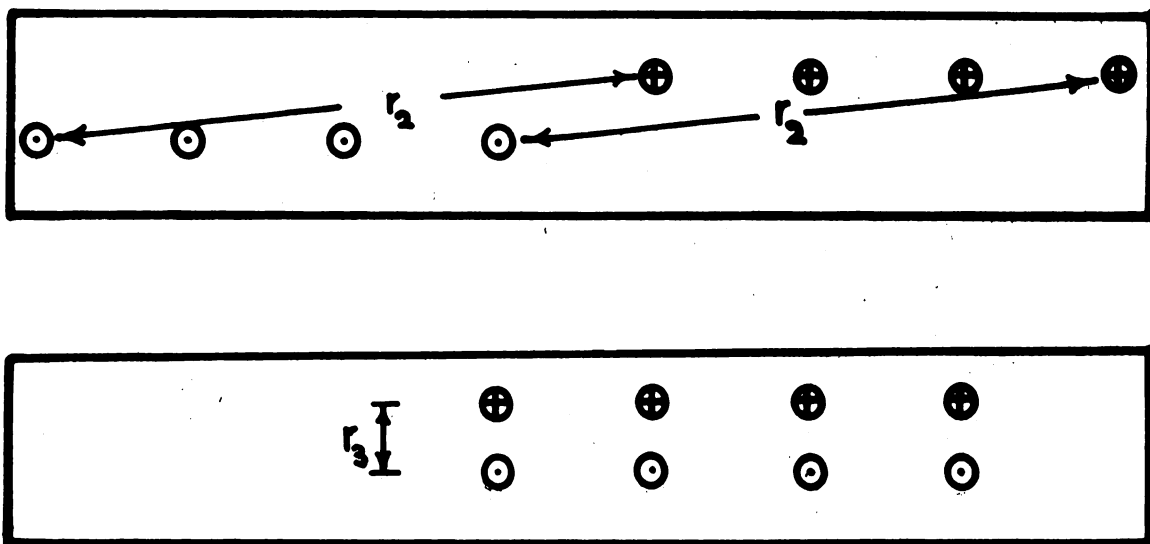
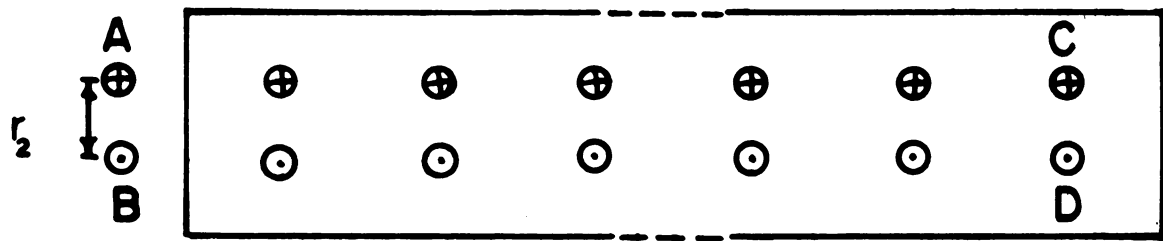


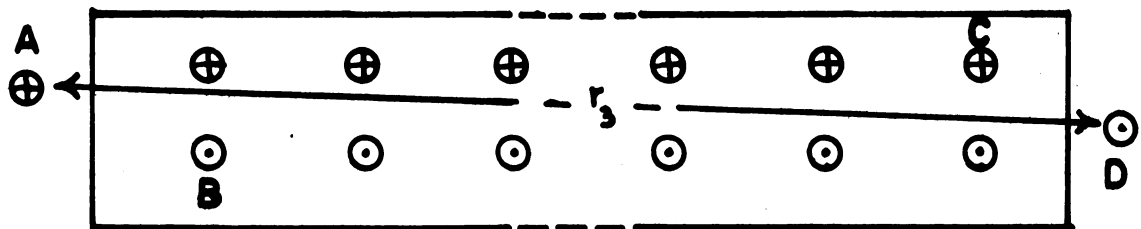
Fig. No. 26

Model for formation of Screw-Lock





(i)



(ii)

Fig. No. 27

Stability of Screw-lock



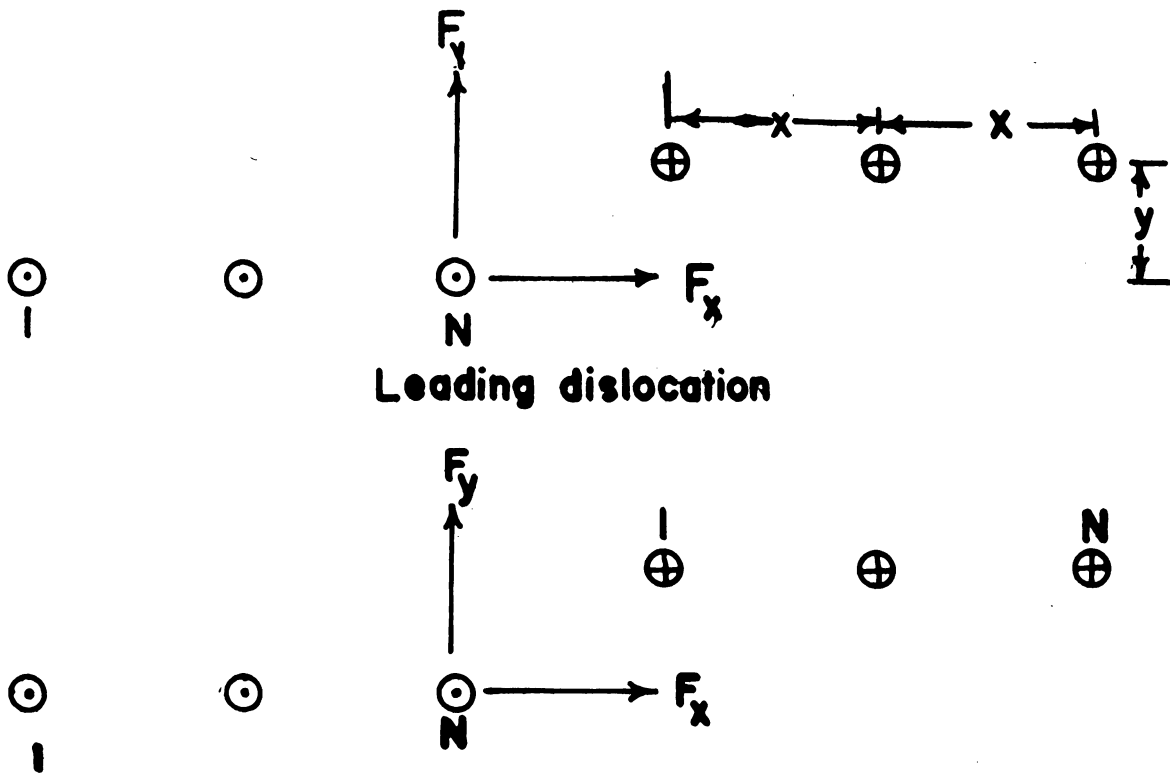
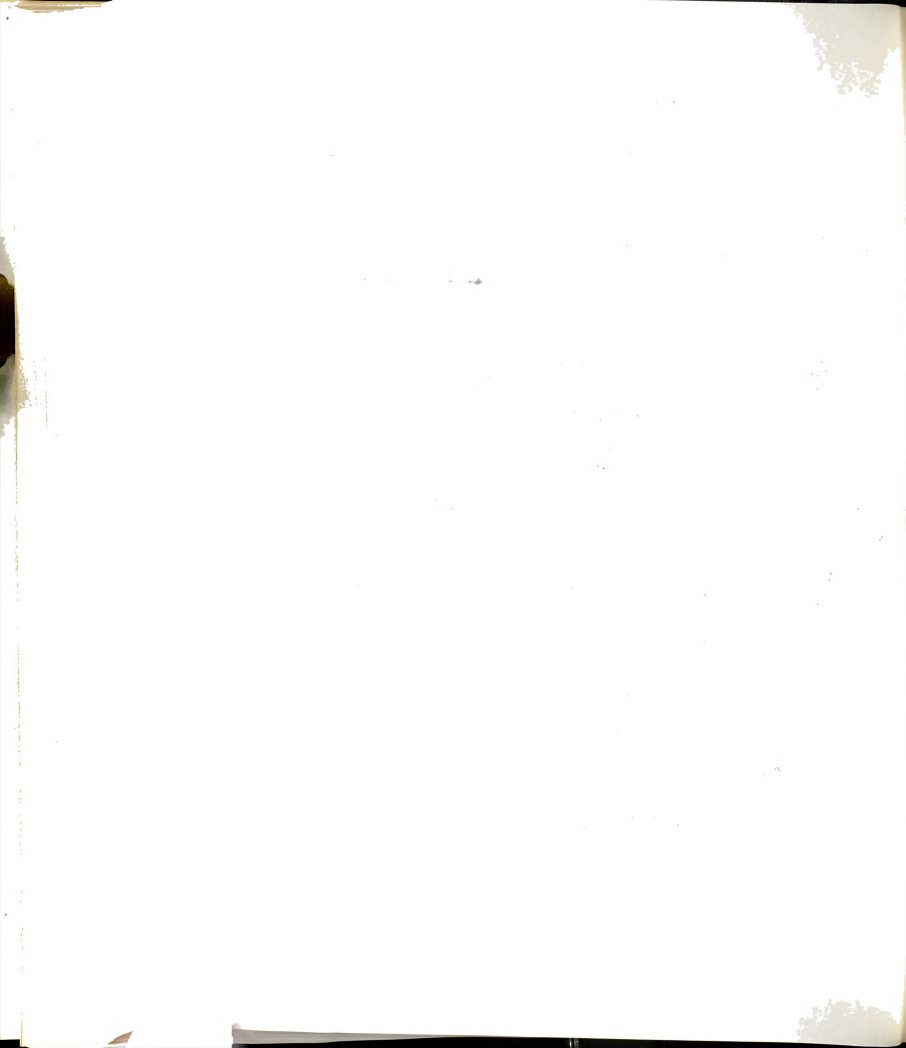


Fig. No. 28

**Forces associated with the formation of
Screw Lock**



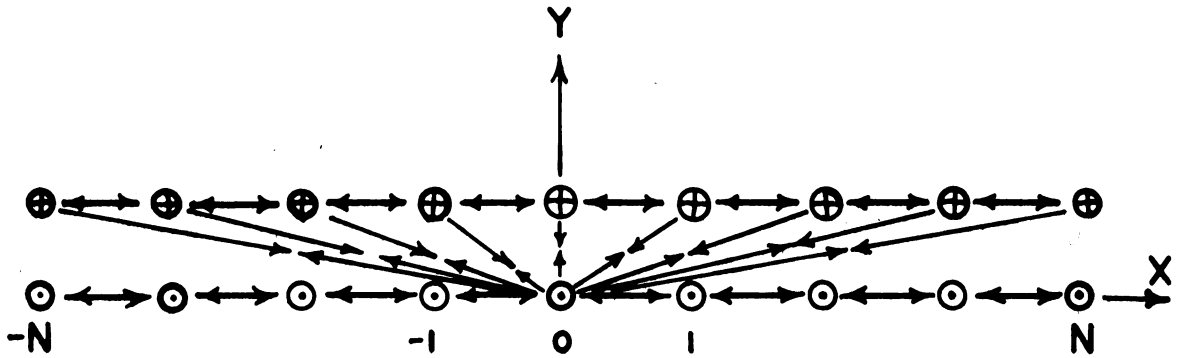
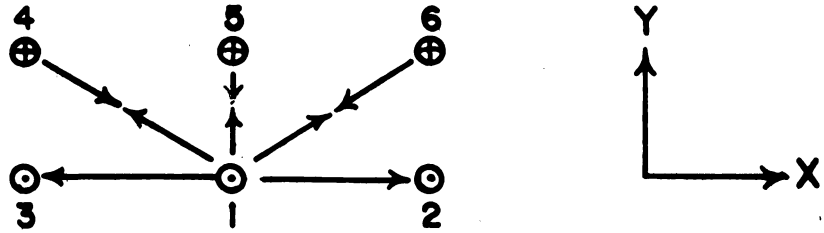


Fig. No. 29

Model for the Force Field at the central portion
of the Screw-Lock



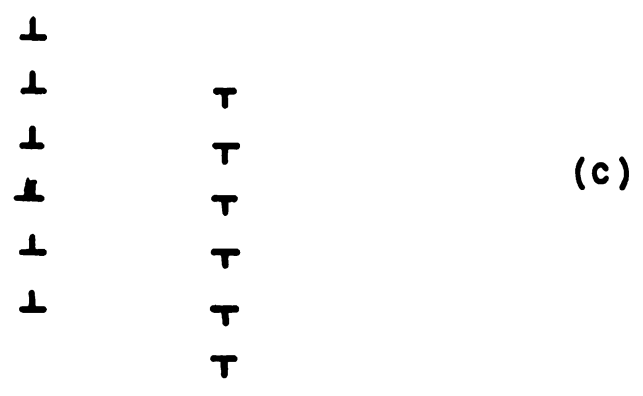
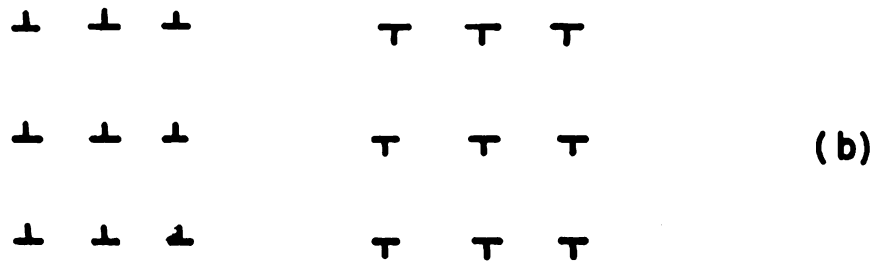
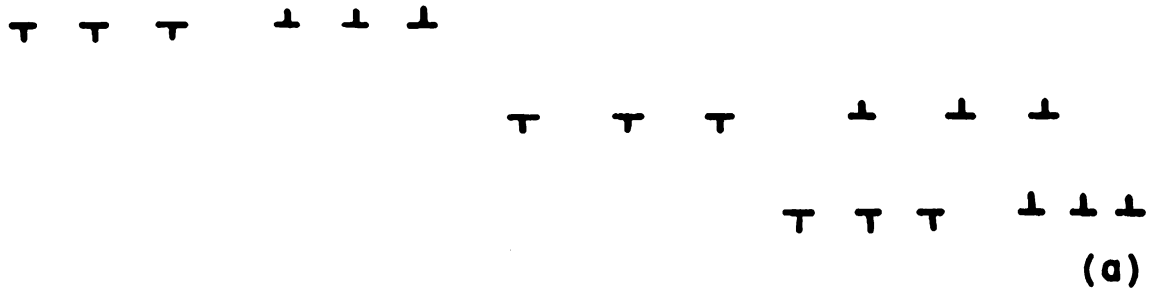


Fig. No. 30

Interaction of two rows of edge dislocations



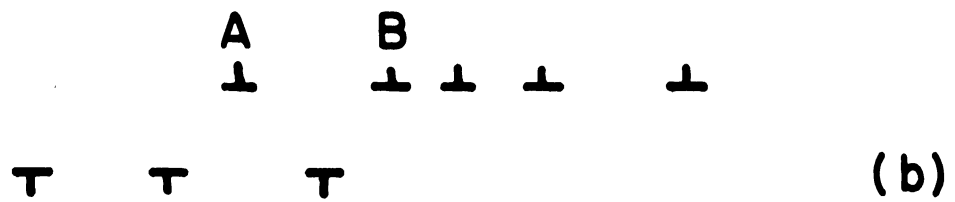
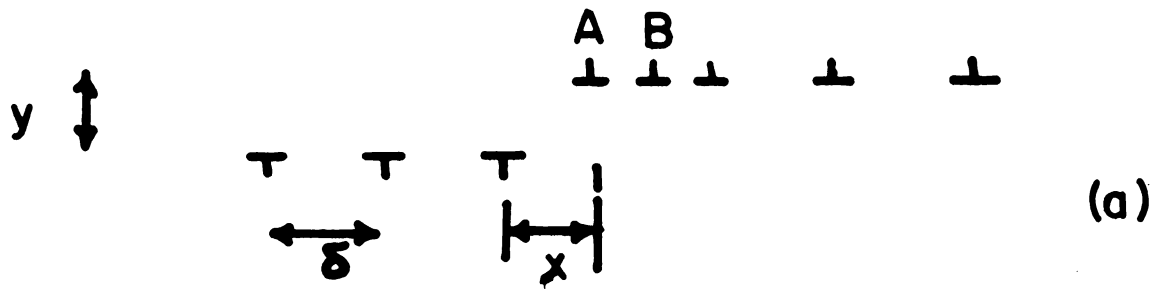


Fig. No. 31

Interaction of edge dislocation arrays present in nearby slip planes.



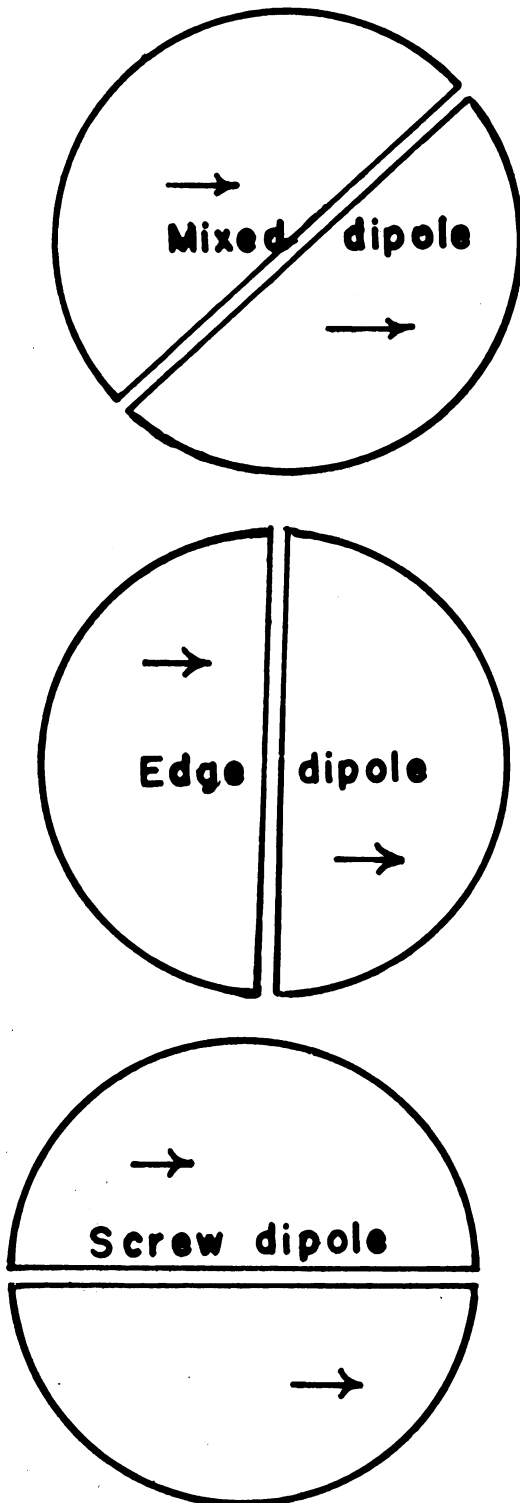


Fig. No. 32

**Stability of interacting
dislocation loops**



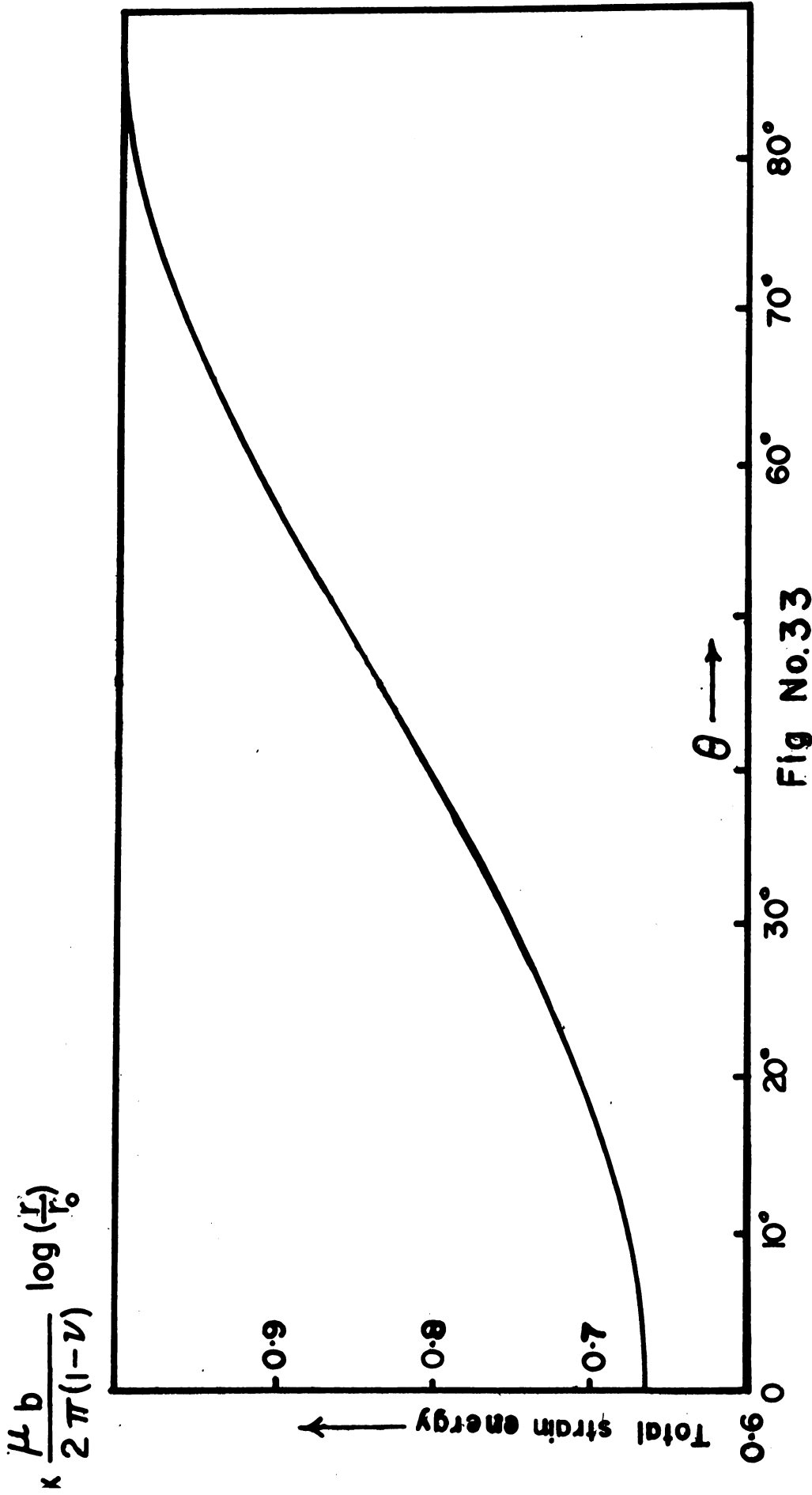


Fig No.33

Total Strain Energy of a Dipole of Unit Length Making Various Angles with The Burgers Vector



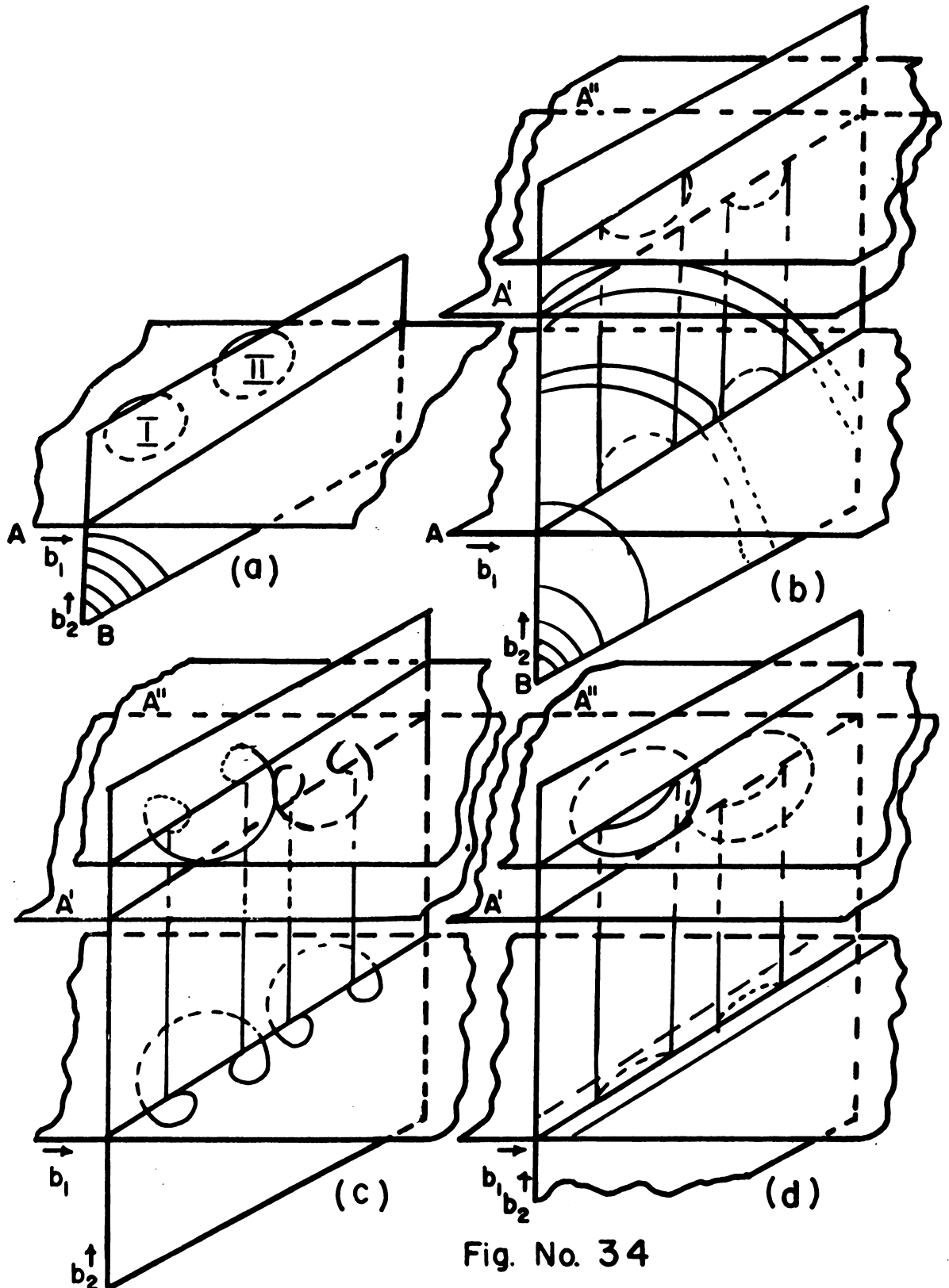


Fig. No. 34

Mechanism of Band Formation due to Intersecting Slip



V. Relation Between Deformation Structure and Work Hardening

The debris mechanism of hardening proposed by Gilman suggests that the debris left behind by moving dislocations can impede their motion.¹⁵ As dislocations move through longer distances, more and more debris is built up imposing greater resistance to dislocation motion and causing hardening. As observed in the present investigation and by other investigators, non-conjugate slip which manifests itself as latent hardening is by far more difficult to take place than the conjugate slip, and hence ionic crystals usually deform only in one set of conjugate slip planes when deformed in uniaxial stressing along the $\langle 001 \rangle$ direction. According to the debris mechanism, the debris should impede the motion of the dislocations irrespective of their motion being in the conjugate or non-conjugate slip planes. Thus it appears difficult to explain the latent hardening phenomenon and the fact that conjugate slip is preferred with the debris mechanism.

Furthermore, according to Gilman's interpretation the debris is presumably metastable, and as a result the material becomes harder and harder during cyclic stressing. For a particular total strain, irrespective of the type of fatigue procedure — tension-tension, tension-compression or compression-compression — the resultant damage in the slip plane should be the same since debris concentration should build up due to the motion of dislocations regardless of the method of testing.⁶⁴ In the present set of experiments fatigue and latent hardenings were coupled, and contrary to the predictions of Gilman's mechanism it was observed that hardening in the latent direction depended on whether the fatigue cycle was completely reversed or not.



All experimental observations of the debris so far have been limited either to thin foils by using electron transmission microscopy or to surfaces of bulk crystals by using the etch-pit technique.^{30, 35, 52, 86} It is uncertain that such observed debris represent the defect structure of the deformed bulk materials.

The following is a proposed model for work hardening based on the band structure formed in the slip planes. Since the specimens were deformed in the bulk form and the observations were made in specimens much thicker than those used for electron transmission microscopy, the band structure observed here is a bulk phenomenon. As the microscope was not focused on the surface and what was observed was a two-dimensional projection of the three-dimensional structure, it could not be a surface phenomenon. Besides, the deformation studies have shown that this kind of band formation was absent in thin specimens where there was no appreciable hardening either. Thus it seems that there is a close connection between the hardening of the bulk crystals and the band formation.

(a) Single Slip System

As deformation proceeds, more and more randomly distributed dislocation sources become active at various stress levels. Consider a number of sources operating at a certain stress level. The dislocation loops generated by these sources grow in size until their growth is stopped by the interaction with loops originated from other sources. This will lead to the formation of screw-locks and edge dipoles as discussed earlier. The initial phase of the formation



of screw-locks should be completed with relative ease. But as more dislocations are locked together, it becomes increasingly difficult for additional pairs to enter the locks. The locks thus act as barriers against which the dislocations pile up creating a back stress, and making the dislocation sources inoperative at this stress level. The material appears hardened. To make these sources active, the stress level has to be increased. New sources in different, undeformed regions and previously inoperative will become active. More screw-locks will be formed creating thus the band structure discussed earlier. This process continues until the active slip planes are filled with the band structure. The stress field associated with these bands resists the generation of new dislocations. This may be the major factor contributing to work hardening in the case of single slip.

The resulting hardening does not disappear upon removal of the applied stress because the screw-locks prevent the dislocations in the locks from dislocking. The debris left behind by the dislocation loops during their expansion will also prevent their contraction, but this may not be a major contributing factor in hardening.

(b) Conjugate Slip Systems

It has been observed, as shown in figure 9, that in the case of ionic crystals deformed under uniaxial stress along a $\langle 100 \rangle$ direction, deformation takes place only in one of the two possible sets of conjugate slip planes having the same resolved shear stress. Figure 35 illustrates the interaction of conjugate slip with the band



structure existing in a set of parallel slip planes. It can be seen that the band structure in these planes does not affect the motion of dislocations in the conjugate planes to any great extent because the bands are parallel to the intersecting slip planes. Conjugate slip is easy because it can proceed through the gaps existing between the bands in the intersecting planes without cutting through many dislocations. If a band structure develops in one of the planes in the early stage of plastic deformation, this band structure does not prevent its conjugate plane from becoming operative and hence acquiring a similar band structure. However, when the material is considerably deformed, both the slip planes will have a tightly packed band structure which should act as a barrier against further conjugate slip.

(c) Latent Hardening — Three or More Slip Systems

Latent hardening has been explained by Alden in terms of individual dislocation interactions.⁷¹ Since this is a bulk phenomenon, it would be more appropriate to explain this phenomenon by using the overall damage observed in the slip planes of deformed bulk crystals. When a crystal, deformed under uniaxial stress and having deformation bands in a set of conjugate slip planes, is stressed again uniaxially in a direction parallel to the slip planes having the band structure there is no resolved shear stress acting in these originally activated slip planes. New sets of slip planes, wherein the resolved shear stress reaches the critical value, should become operative. The intersection of this non-conjugate slip with the existing slip bands is



difficult as illustrated in figure 36 because it has to cut through the existing band structure in these slip planes. This necessitates a high stress for further deformation manifested as latent hardening. Figures 21 (c) and (d) show the high stress concentration at the intersections of non-conjugate slip with the band structure and explain why non-conjugate slip could not proceed easily.

(d) Fatigue Hardening

Materials which exhibit easy cross-slip characteristics such as f. c. c. metals often show fatigue softening and fatigue failure, whereas materials which do not cross slip easily show fatigue hardening and no fatigue failure.⁵⁵ When cross-slip is possible the screw components of the screw-lock may cross slip, and annihilate each other. This leaves a row of edge dislocations of one sign on one side and another row of opposite sign on the other side, a configuration on which Mott has based his discussion of deformation bands.² The screw-locks are probably absent in these materials and hence would not contribute to any hardening. In the materials such as LiF that do not cross slip easily, such annihilation is unimportant. The screw-locks will acquire more dislocation pairs as the cyclic stressing proceeds. New sources become operative, and new bands are formed as the stress level is increased. The material will be hardened by the formation of these bands.

The above mentioned results are in agreement with those predicated by Mott's mechanism of fatigue failure based on cross-slip.



Materials which do not cross slip easily are not hardened continuously in simple tension or compression. They have a definite fracture strength. It has been observed that the slip bands in fatigue test and in simple tension or compression test differ considerably.⁵³ Slip bands obtained in fatigue test are wide, whereas those obtained in simple tension or compression are narrow and intense. The dislocation density in the slip bands in the fatigue specimens was much lower than the density of dislocations in the slip bands in the tension or compression specimens. In the latter case a tightly packed band structure in these slip planes develops and may act as a barrier even for conjugate slip.

(e) Fatigue-Latent Hardening

The observed characteristics of the growth of the slip bands in the specimens subjected to reversed or unreversed cyclic stressing helps one to understand some specific features of fatigue-latent hardening. Specimens under reversed shear showed much greater hardening in the latent direction than those under unreversed shear. The slip band growth on $\{100\}$ surfaces caused by such cyclic stressing is shown in figures 10 and 11. Under unreversed shear very few new slip bands are formed in the second cycle. On the other hand, under reversed shear, new slip bands are formed in the second half cycle.

A dislocation loop will expand or contract, depending on the type of applied stress and the direction of its Burgers vector. In the case of cyclic stressing under unreversed shear dislocation loops



having parallel Burgers vectors in parallel slip planes multiply. Under reversed shear, during the second half cycle, slip takes place in different areas of the specimen where the dislocation loops have their Burgers vectors antiparallel to those of the operative dislocation loops in the first half cycle. Therefore, in the latter case dislocation loops with parallel and antiparallel Burgers vectors are present. Although the distribution of these loops may not be uniform within any individual slip plane, the overall distribution of both kinds of dislocation loops may be considered uniform for the whole specimen.

The structure obtained from such reversed cyclic stressing may act as a strong barrier to a dislocation moving in the non-conjugate slip plane during deformation in the latent direction. The whole specimen is interlaced with slip dislocations having parallel and antiparallel Burgers vectors, and slip in the latent systems becomes hard. On the other hand, the slip band distribution obtained from the unreversed cyclic stressing may not present difficulty of this kind. The dislocation loops have mainly parallel Burgers vectors. The presence of some unslipped regions allows to certain extent the propagation of non-conjugate slip during deformation in the latent direction.



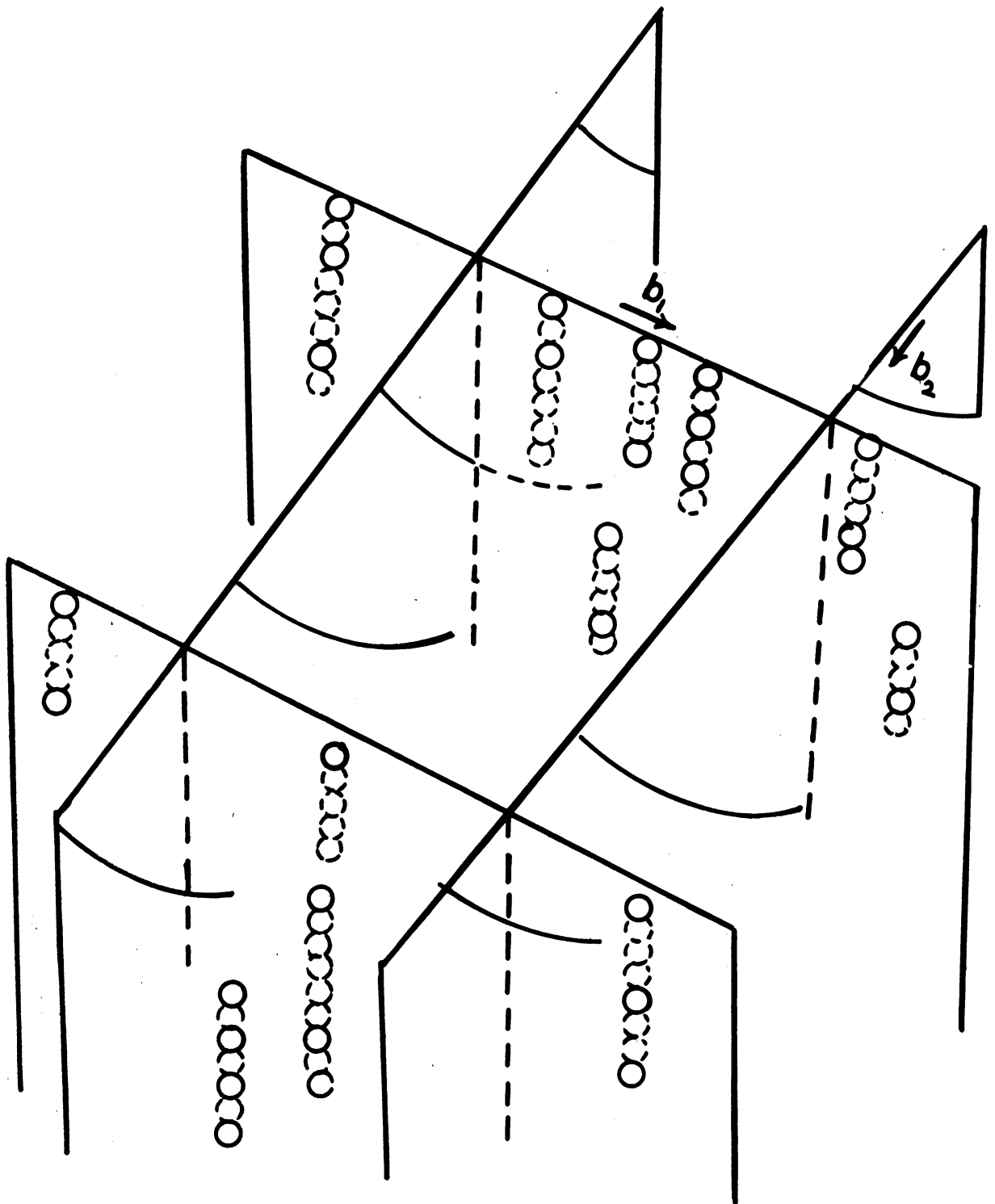


Fig No. 35

Conjugate Slip Intersection



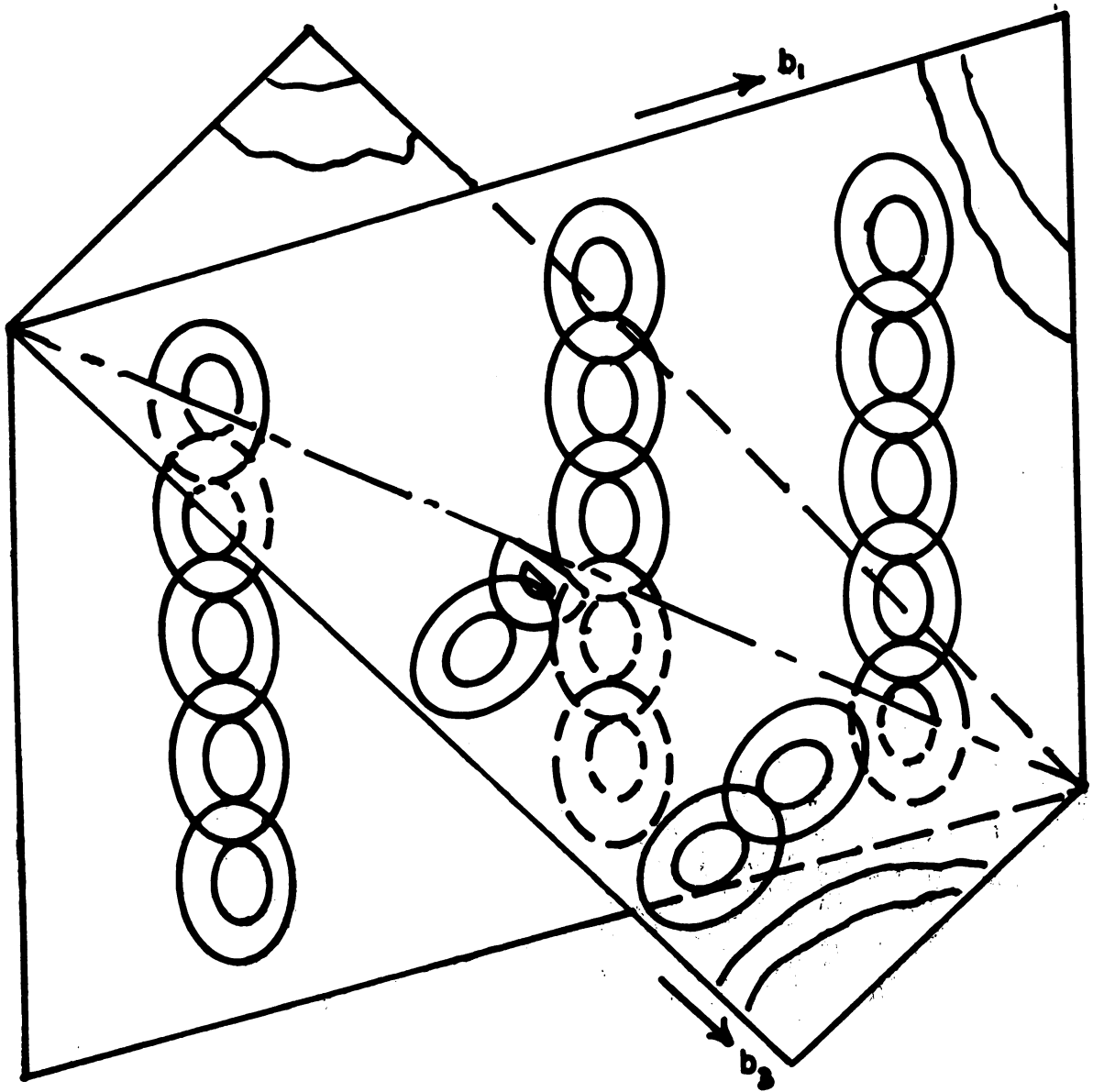


Fig. No. 36

Non Conjugate Slip Intersection



CONCLUSIONS

1. By using the Czochralski method and off-centering and necking techniques it was possible to grow at rates as high as 75 mm/hr oriented LiF single crystals which were substantially free from subboundaries with a dislocation density of approximately $10^4/\text{cm}^2$. Pseudo Kossel patterns of the crystals taken with a divergent X-ray beam generated from a micro focus unit revealed no subboundaries with disorientations higher than one minute of arc.
2. The results of fatigue experiments with cleaved LiF specimens showed that the yield strength in the latent direction increased by a factor of five compared with the initial yield strength after the crystals had been deformed by repeatedly unidirectional loading to a total strain of 16%, whereas a complete reversal of the resolved shear stresses acting on the initial slip systems during each successive loading resulted in a thirty fold increase in the yield strength in the latent direction for 20% total initial strain.
3. A band-like structure consisted of overlapping loops aligned in a direction perpendicular to the slip direction was observed with polarized light in the slip planes of specimens cut from the deformed crystals. Similar bands were occasionally observed to lie parallel to the line of intersection of slip planes also.
4. The experimental results also showed that the difference in the work hardening behaviors of the initial conjugate slip systems and



the latent slip systems appeared to have its origin in the relative orientation of the bands with respect to the intersecting slip planes whether the bands were parallel to the line of intersection of the slip planes or oblique.

5. A theory of formation of the bands was developed based on the interaction of dislocation loops in nearby parallel slip planes showing such bands were in a low energy state and hence stable.



REFERENCES

1. G. I. Taylor, 'The Mechanism of Plastic Deformation of Crystals,' Proc. Roy. Soc., 145, p 362, 1934.
2. N. F. Mott, 'A Theory of Work Hardening of Metal Crystals,' Phil. Mag., 43, p 1151, 1952.
3. N. F. Mott, 'A Theory of Work Hardening of Metals II; Flow without Slip Lines, Recovery and Creep,' Phil. Mag., 44, p 742, 1953.
4. A. H. Cottrell, 'Theory of Dislocations,' Prog. in Met. Phys., 4, p 205, 1953.
5. J. Friedel, 'Discussion on Work Hardening and Fatigue in Metals,' Proc. Roy. Soc., A 242, p 147, 1957.
6. J. S. Koehler, 'The Nature of Work Hardening,' Phys. Rev., 86, p 52, 1952.
7. J. Friedel, 'On the Linear Hardening Rate of Face Centered Cubic Single Crystals,' Phil. Mag., 46, p 1169, 1955.
8. A. Seeger, 'The Mechanism of Glide and Work Hardening in Face Centered Cubic and Hexagonal Close-packed Metals,' Dislocations and Mechanical Properties of Crystals, John Wiley, p 243, 1956.
9. A. Seeger, S. Mader and H. Kronmuller, 'Theory of Work Hardening of FCC and HCP Single Crystals,' Electron Microscopy and Strength of Crystals, Inter. Sci., p 665, 1963.
10. A. Seeger, J. Diehl, S. Mader and H. Rebstock, 'Work Hardening and Work Softening of Face Centered Cubic Metal Crystals,' Phil. Mag., 2, p 323, 1957.
11. N. F. Mott, 'Work Hardening of Metals,' Trans. AIME, 218, p 962, 1960.
12. Z. S. Basinski, 'Thermally Activated Glide in Face-centered Cubic Metals and its Application to the Theory of Strain Hardening,' Phil. Mag., 4, p 393, 1959.
13. S. K. Mitra and J. E. Dorn, 'On the Nature of Strain Hardening in Face-centered Cubic Metals,' Trans. AIME, 224, p 1062, 1962.



14. Kuhlman Wilsdorf, 'A New Theory of Work Hardening,' Trans. AIME, 224, p 1047, 1962.
15. J. J. Gilman, 'Debris Mechanism of Strain Hardening,' J. Appl. Phys., 33, p 2703, 1962.
16. F. R. N. Nabarro, Z. S. Basinski and D. B. Holt, 'The Plasticity of Pure Single Crystals,' Adv. in Phys., (Phil. Mag. Suppl.), 13, p 193, 1964.
17. N. F. Mott, 'The Mechanical Properties of Metals,' Proc. Phys. Soc., B, 64, p 729, 1951.
18. Doris Kuhlman, 'On the Theory of Plastic Deformation,' Proc. Phys. Soc. Lond., A, 62, p 140, 1951.
19. C. S. Barrett and L. H. Levenson, 'Structure of Iron after Drawing, Swaging and Elongating in Tension,' Trans. AIME, 135, p 327, 1939.
20. C. S. Barrett and L. H. Levenson, 'The Structure of Aluminum after Compression,' Trans. AIME, 137, p 112, 1940.
21. P. Gay and R. W. K. Honeycombe, 'X-ray Asterisms from Deformed { Aluminum } Crystals,' Proc. Phys. Soc., A 64, p 844, 1951.
22. R. W. Cahn, 'Slip and Polygonization in Aluminum,' J. Inst. Metals, 79, p 129, 1951.
23. N. K. Chen and C. H. Mathewson, 'Structural Studies of Plastic Deformation in Aluminum Single Crystals,' J. Metals, 3, p 653, 1951.
24. C. T. Wei, 'X-ray Study of the Plastic Deformation in Zinc Single Crystals,' Acta. Met., 5, p 435, 1957.
25. A. H. Cottrell, 'Dislocations and Plastic Flow in Crystals,' Clarendon Press, p 112, 1953.
26. J. J. Gilman, 'Plastic Anisotropy of Lithium Fluoride and Other Rock-salt Type Crystals,' Acta. Met., 7, p 608, 1959.
27. C. O. Hulse, S. M. Copley and J. A. Pask, 'Effect of Crystal Orientation on the Plastic Deformation of MgO,' J. Am. Ceram. Soc., 46, p 317, 1963.
28. J. Washburn, 'Sodium Chloride Structure,' Electron Microscopy and Strength of Crystals, Inter. Sci., p 301, 1963.
29. D. H. Bowen and F. J. P. Clarke, 'Impurity Precipitates in MgO,' Phil. Mag., 8, p 1257, 1963.



30. W. Elkington, G. Thomas and J. Washburn, 'Damage Produced by Moving Dislocations in MgO,' J. Am. Ceram. Soc., 46, p. 307, 1963.
31. J. J. Gilman, 'Nucleation of Dislocation Loops by Cracks in Crystals,' Trans. AIME, 209, p 449, 1957.
32. J. J. Gilman, C. Knudsen and W. P. Walsh, 'Cleavage Cracks and Dislocations in LiF Crystals,' J. Appl. Physics, 29, p 601, 1958.
33. J. J. Gilman and W. G. Johnston, 'Observation of Dislocation Glide and Climb in LiF Crystals,' J. Appl. Phys., 27, p 1018, 1956.
34. J. J. Gilman, W. G. Johnston and G. W. Sears, 'Dislocation Etch-pit Formation in LiF,' J. Appl. Phys., 29, p 747, 1958.
35. J. Washburn, G. W. Groves, A. Kelley and G. K. Williamson, 'Electron Microscopic Observations of Deformed MgO,' Phil. Mag., 5, p 991, 1960.
36. S. Amelinckx, 'The Direct Observation of Dislocation Patterns in Transparent Crystals,' Dislocations and Mechanical Properties of Crystals, John Wiley, p 3, 1956.
37. J. B. Newkirk, 'The Observation of Dislocations and Other Imperfections by X-ray Extinction Contrast,' Trans. AIME, 215, p 483, 1959.
38. B. H. Kear, A. Taylor and P. L. Pratt, 'Some Dislocation Interactions in Simple Ionic Crystals,' Phil. Mag., 4, p 665, 1959.
39. F. J. P. Clarke, R. A. J. Sambell and H. G. Tattersall, 'Mechanism of Microcrack Growth in MgO Crystals,' Phil. Mag., 7, p 393, 1962.
40. H. G. Tattersall and F. J. P. Clarke, 'Slip Distribution and Fracture in MgO,' Phil. Mag., 7, p 1977, 1962.
41. W. L. Phillips, Jr., 'Elevated Temperature Properties of Lithium Fluoride and Magnesium Oxide Single Crystals,' Trans. AIME, 218, p 939, 1960.
42. E. Schmidt and W. Boas, 'Plasticity of Crystals,' Hughes, p 227, 1950.
43. D. Hoover and J. Washburn, 'Tensile Behavior of LiF,' J. Appl. Phys., 33, p 11, 1962.



44. J. J. Gilman and W. G. Johnston, 'The Origin and Growth of Glide Bands in LiF Crystals,' *Dislocations and Mechanical Properties of Crystals*, John Wiley, p 116, 1956.
45. J. J. Gilman and W. G. Johnston, 'Dislocations in LiF Crystals,' *Solid State Physics*, 13, p 148, 1962.
46. T. L. Johnston, C. H. Li and R. J. Stokes, 'The Strength of Ionic Solids,' *Strengthening Mechanisms in Solids*, ASM, p 341, 1962.
47. W. G. Johnston, 'Effect of Impurities on the Flow Stress of LiF Crystals,' *J. Appl. Physics*, 33, p 2050, 1962.
48. J. J. Gilman, 'Dislocation Sources in Crystals,' *J. Appl. Phys.*, 30, p 1584, 1959.
49. W. G. Johnston and J. J. Gilman, 'Dislocation Multiplication in LiF Crystals,' *J. Appl. Phys.*, 31, p 632, 1960.
50. J. Washburn, 'Strain Hardening,' *Strengthening Mechanisms in Solids*, ASM, p 51, 1962.
51. R. E. Keith and J. J. Gilman, 'Progress Report on Dislocation Behavior in LiF Crystals During Cyclic Loading,' *ASTM Spec. Tech. Pub.*, STP 237, p 3, 1959.
52. K. N. Subramanian and J. Washburn, 'Fatigue Deformation of MgO,' *J. Appl. Phys.*, 34, p 3394, 1963.
53. K. N. Subramanian, 'Fatigue Damage in Magnesium Oxide,' *M. S. Thesis*, Univ. of Calif., Berkeley, 1962.
54. T. Broom and R. K. Ham, 'The Hardening and Softening of Metals by Cyclic Stressing,' *Proc. Roy. Soc. Lond.*, A 242, p 166, 1957.
55. A. J. McEvily, Jr. and E. S. Machlin, 'Critical Experiments on the Nature of Fatigue in Crystalline Materials,' *Fracture*, John Wiley, p 450, 1959.
56. T. H. Alden, 'Dynamic Recovery and Fatigue in Some Brittle Materials,' *Acta. Met.*, 11, p 791, 1963.
57. T. H. Alden, 'The Determination of the S-N Curve from Cyclic Hardening Data,' *Trans. AIME*, 224, p 1287, 1962.
58. D. M. Fegredo and G. B. Greenough, 'The Fatigue Properties of Zinc,' *J. Inst. of Metals*, 87, p 1, 1958-59.



59. J. T. McGrath and R. C. A. Thurston, 'The Effect of Cross-slip on the Fatigue Behavior of Cu and Cu-Zn Alloys,' Trans. AIME, 227, p 645, 1963.
60. N. F. Mott, 'Work Hardening and the Initiation and Spread of Fatigue Cracks,' Proc. Roy. Soc. Lond., A 242, p 145, 1957.
61. N. F. Mott, 'The Theory of the Origin of Fatigue Cracks,' Acta. Met, 6, p 195, 1958.
62. A. H. Cottrell and D. Hull, 'Extrusion and Intrusion by Cyclic Slip in Copper,' Proc. Roy. Soc. Lond., A 242, p 211, 1957.
63. I. Coronet and A. E. Gorum, 'The Observation of Fatigue Process in MgO Single Crystals,' Trans. AIME, 218, p 480, 1960.
64. A. J. McEvily, Jr. and E. S. Machlin, 'The Effect of Cyclic Loading on MgO Single Crystals,' Trans. AIME, 221, p 1086, 1961.
65. T. H. Alden, 'The Strain Hardening of MgO Single Crystals,' Trans. AIME, 227, p 1103, 1963.
66. T. H. Alden, 'High Strength MgO,' Applied Physics Letters, 2, p 107, 1963.
67. T. H. Alden, 'The Strain Hardening of Zinc Single Crystals in Alternate Tension and Compression,' Acta. Met., 10, p 653, 1962.
68. T. H. Alden, 'The Hardening of Cadmium Crystals by Cyclic Strain,' Acta. Met., 11, p 65, 1963.
69. C. E. Feltner, 'Cyclic Stress-induced Ductility in Cadmium,' Trans. AIME, 227, p 798, 1963.
70. A.S.M. Metals Handbook, p 6, 1948.
71. T. H. Alden, 'Extreme Latent Hardening in Compressed LiF,' Acta. Met., 11, p 1103, 1963.
72. E. H. Edwards and J. Washburn, 'Strain Hardening of Latent Slip Systems in Zinc Crystals,' Trans. AIME, 200, p 1239, 1954.
73. J. Washburn, 'Formation of Dislocation Sub-structures,' Growth and Perfection of Crystals, John Wiley, p 342, 1958.
74. J. Washburn and J. Nadeau, 'On the Formation of Dislocation Sub-structure during Growth of a Crystal from its Melt,' Acta. Met., 6, p 665, 1958.



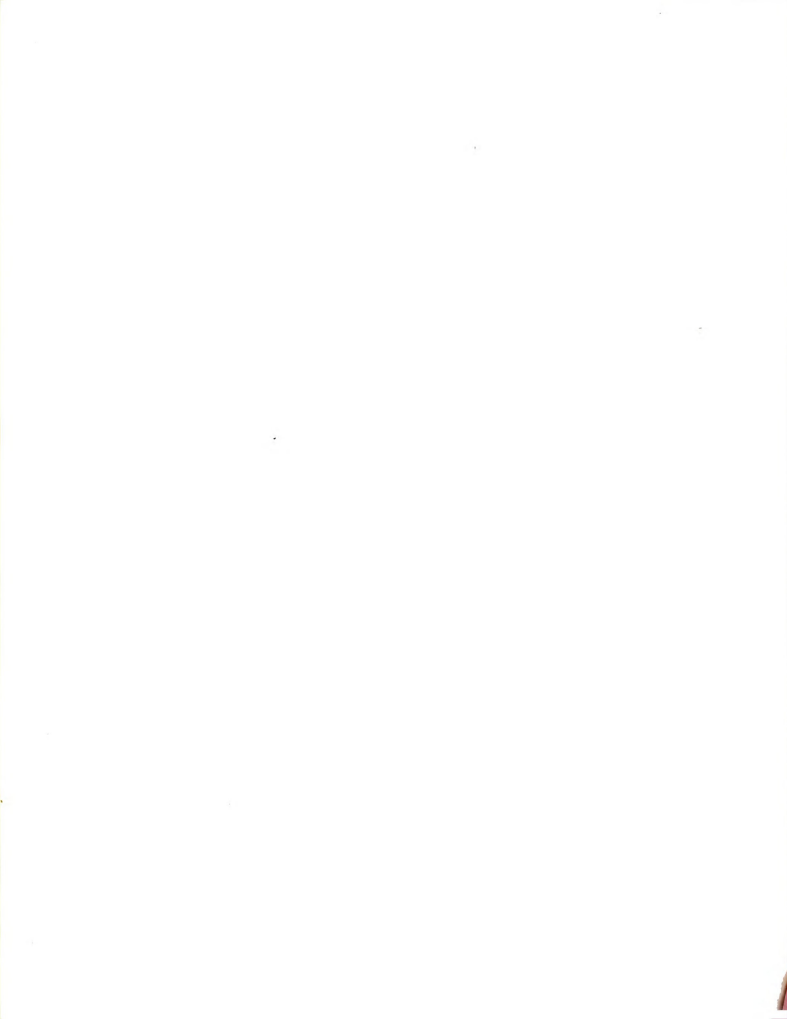
75. F. Van Zeggeren and G. C. Benson, 'Calculation of the Surface Energies of Alkali Halide Crystals,' J. of Chem. Physics, 26, p 1077, 1957.
76. M. M. Frocht, Photoelasticity, Vol. II, John Wiley, p 333-338, 1948.
77. J. F. Nye, 'Plastic Deformation of Silver Chloride I – Internal stresses and the Glide Mechanism (and their relationship to Similar Phenomena in Metals), Proc. Roy. Soc. (London), A 198, p 190, 1949.
78. B. K. Kear and P. L. Pratt, 'Quenching Stresses and Strains in Ionic Crystals,' Acta. Met., 6, p 457, 1958.
79. W. L. Bond and J. Andrus, Phys. Rev., 101, p 1211, 1956.
80. R. Bullough, 'Birefringence Caused by Edge Dislocations in Silicon,' Phys. Rev., 110, 620, 1958.
81. S. Mendelson, 'Birefringence Due to Dislocations in Glide Bands of Rocksalt Single Crystals,' J. Appl. Phys., 32, p 1999, 1961.
82. R. J. Stokes, T. L. Johnston and C. H. Li, 'Effect of Slip Distribution on the Fracture Behavior of MgO Single Crystals,' Phil. Mag., 6, p 9, 1961.
83. A. A. Bruneau and P. L. Pratt, 'The Bending Deformation of MgO,' Phil. Mag., 7, p 1871, 1962.
84. F. R. N. Nabarro, 'Deformation of NaCl Crystals,' Dislocations and Mechanical Properties of Crystals, John Wiley, p 235, 1956.
85. J. C. M. Li, 'Theory of Strengthening by Dislocation Groupings,' Electron Microscopy and Strength of Crystals, p 713, Inter. Sci., 1963.
86. J. J. Gilman, 'The Mechanism of Surface Effects in Crystal Plasticity,' Phil. Mag., 6, p 159, 1961.











MICHIGAN STATE UNIVERSITY LIBRARIES



3 1293 03146 1720